




Sea level variability and coastal inundation over the northeastern Mediterranean Sea

Yannis Androulidakis, Christos Makris, Zisis Mallios & Yannis Krestenitis



To cite this article: Yannis Androulidakis, Christos Makris, Zisis Mallios & Yannis Krestenitis (2023): Sea level variability and coastal inundation over the northeastern Mediterranean Sea, Coastal Engineering Journal, DOI: [10.1080/21664250.2023.2246286](https://doi.org/10.1080/21664250.2023.2246286)

To link to this article: <https://doi.org/10.1080/21664250.2023.2246286>

 [View supplementary material](#) 

 [Published online: 21 Aug 2023.](#)

 [Submit your article to this journal](#) 

 [View related articles](#) 

 [View Crossmark data](#) 

Sea level variability and coastal inundation over the northeastern Mediterranean Sea

Yannis Androulidakis^{a,b}, Christos Makris^a, Zisis Mallios^a and Yannis Krestenitis^a

^aLaboratory of Maritime Engineering and Maritime Works, School of Civil Engineering, Aristotle University of Thessaloniki, Thessaloniki, Greece; ^bLaboratory of Physical and Chemical Oceanography, Department of Marine Sciences, University of the Aegean, Mytilene, Greece

ABSTRACT

Sea level is a key element of global-scale climatic changes with significant coastal impacts. The northeastern Mediterranean Sea (Aegean, Ionian, and Cretan Seas: AICS) consists of extended low-lying coastal zones exposed to coastal inundation due to seawater level increases. The variability of the Sea Level Anomaly (SLA) in the AICS has been evaluated with the use of satellite-derived observations from 1993 to 2021. The general SLA trend over the AICS domain was 3.6 mm/year, which is higher than that of the overall Mediterranean Sea. The coastal inundation variability along the AICS coastline, specifically in 20 characteristic study areas, was investigated based on the long-term satellite-derived sea level observations, high-resolution land elevation data, and numerical simulations, conducted with a coastal inundation (CoastFLOOD) model. The coastal zones were categorized based on the frequency of occurrence and percentage coverage of flooding incidents during the 29-year period, while the interannual trends and the seasonality of inundated littoral and inland areas also showed intense spatial variation. High flooding levels occurred at coastal areas of either extended low-lying areas and/or high sea level elevations. The coastal zones were categorized based on a heuristic Coastal Inundation Hazard Index (CIHI: 1–5 ranking) that was determined by the occurrence frequency of severe floods (temporal component) and their impact area (spatial component). Our study findings provide vital information about the coastal inundation conditions and the respective hazard level of the AICS, useful to support enhanced coastal zone management for the improvement of coastal protection and decisions about coastal hazards' mitigation.

ARTICLE HISTORY

Received 4 May 2023
Accepted 5 August 2023
Published online

KEYWORDS

Seawater level; interannual variability; remote sensing; Climate change; coastal flooding; coastal zone hazards

1. Introduction

Sea level is a key element of global scale climatic changes with potentially significant coastal impacts (Cazenave et al. 2014), especially on the low-lying areas of the Mediterranean Sea, which is one of the most vulnerable regions to Sea Level Rise (SLR) worldwide (Adloff et al. 2015; Calafat, Chambers, and Tsimplis 2012; Church et al. 2013; Diffenbaugh and Giorgi 2012; Gualdi et al. 2013). The increase of the sea level is one of the most crucial drivers of natural hazards (floods, encroachment, erosion, etc.) putting intense pressure on the coastal zone (Bosom and Jiménez 2010; Nicholls 2002; Vousdoukas et al. 2017). The impact might become more intense during the 21st century, depending on the prevailing future climatic scenario (Neumann et al. 2015; Vitousek et al. 2017). The sea level variability controls a) the inundation levels of the coastal zone, depending on the local topographic characteristics (Calafat et al. 2022; Denamiel and Vilibić 2022; Ferrarin et al. 2021), b) the shoreline retreat, coastal erosion, and land loss (Enríquez et al. 2019; Jiménez et al. 2017; Monioudi et al. 2017; Sharaan and Udo 2020; Spencer et al. 2016),

and c) the salinity levels in estuaries and freshwater aquifers (Bijlsma et al. 1996; Krvavica and Ružić 2020; Shalem et al. 2015). The efficient assessment of the coastal zone risk under flooding conditions (Satta et al. 2017; Vousdoukas et al. 2016) is strongly associated to the accurate estimation of the sea level temporal and spatial variability and the respective past, current and future trends (Bevacqua et al. 2019; Hallegate et al. 2013; Lionello et al. 2021).

The water level characteristics are associated with three main environmental factors: a) the steric effect due to thermal and salinity changes (Adloff et al. 2015; Carillo et al. 2012), b) the addition of water mass (e.g. glacier ice melting and changes in ground water storage) (Galassi and Spada 2014; Jordà and Gomis 2013), and c) the atmospheric component (e.g. storm surge formation) (Androulidakis et al. 2015; Jordà and Gomis 2013; Jordà et al. 2012; Levitus et al. 2012; Makris et al. 2023; Marcos, Tsimplis, and Shaw 2009; Šepić et al. 2012, 2015). The North Atlantic Oscillation (NAO; Hurrell 1995) impact on the weather conditions varies between the eastern and western parts of the Mediterranean Sea (Lionello 2012) altering the

respective influence on the sea level variability that is linked primarily to atmospheric pressure changes and secondarily to local wind field changes (Tsimplis et al. 2013). The extreme positive Sea Level Anomaly (SLA) that occurred in 2010 was mainly associated to the negative phase of the NAO (Haddad, Hassani, and Taibi 2013; Landerer and Volkov 2013) causing about 12 cm of basin rise in the Aegean Sea (Tsimplis et al. 2013) and the broader eastern Mediterranean (Mohamed and Skliris 2022). The meteorologically induced component of the sea level (storm surge), which is associated to the Sea Level Pressure (SLP) and winds, reveals strong spatial variability, with stronger inverse barometer effect in the Aegean Sea compared to the Adriatic and Ionian Seas, where storm surges are mainly determined by the wind state (Androulidakis et al. 2015, 2023; Denamiel, Tojčić, and Vilibić 2021; Denamiel and Vilibić 2022; Krestenitis et al. 2011; Makris et al. 2016, 2023). The Mediterranean cyclogenesis can be categorized (Flaounas et al. 2022) to (i) cyclones formed over the Atlantic ocean and intrude into the basin (61–85% of total tracks; Neu et al. 2013), (ii) to Medicanes that form in western and central Mediterranean (weak frequency but strong magnitude; Cavicchia, von Storch, and Gualdi 2014), (iii) to north African cyclones that form over the deserts, (iv) explosive cyclones or weather bombs that form over northern areas (Kouroutzoglou et al. 2011), (v) Vb cyclones that affect mainly the western basin (Messmer, Gómez-Navarro, and Raible 2015), and (vi) secondary cyclones that form in the periphery of existing cyclones (Ziv et al. (2015). The AICS domain is mainly affected by the first and the second type that

may cause intensive coastal flooding due to storm surges (Androulidakis et al. 2023).

In the Mediterranean Sea, the recorded strong positive mean sea level trends, associated to climate change impacts, have been confirmed by long-term tide-gauge measurements (e.g. Adloff et al. 2018; Dieng et al. 2021; Marcos and Tsimplis 2008; Tsimplis et al. 2013) and especially by remote sensing data during the satellite altimetry era after 1993 (e.g. Bonaduce et al. 2016; Fenoglio-Marc 2002; Mohamed et al. 2019; Vigo, Garcia, and Chao 2005). Zanchettin et al. (2021) investigated both historic and future trends of Sea Level Rise (SLR) in Venice (Italy) finding an average shift of about $+2.76 \pm 1.75$ mm/year, between 1993 and 2019, estimated with tide-gauge data after the removal of the contribution of calculated land subsidence. The Mediterranean Sea is characterized by strong regional variability with large differences between the sub-basins, showing stronger interannual trends in the central region, in the Adriatic and along the Tunisian coasts (Bonaduce et al. 2016; Cid et al. 2016; Međugorac et al. 2018). Mohamed and Skliris (2022), using satellite-derived SLA gridded data, showed that the total sea level trend between 1993 to 2019 is around 3.1 ± 0.61 mm/year over the eastern Mediterranean domain. Herein, we expand the results of Mohamed and Skliris (2022) using the same satellite product, extended to 2021 (29-years) and focused on the Aegean, Ionian and Cretan Seas (AICS), which are divided to seven sub-regions (Figure 1a), following the categorization introduced by Androulidakis and Krestenitis (2022). The AICS domain includes various urban settlements,

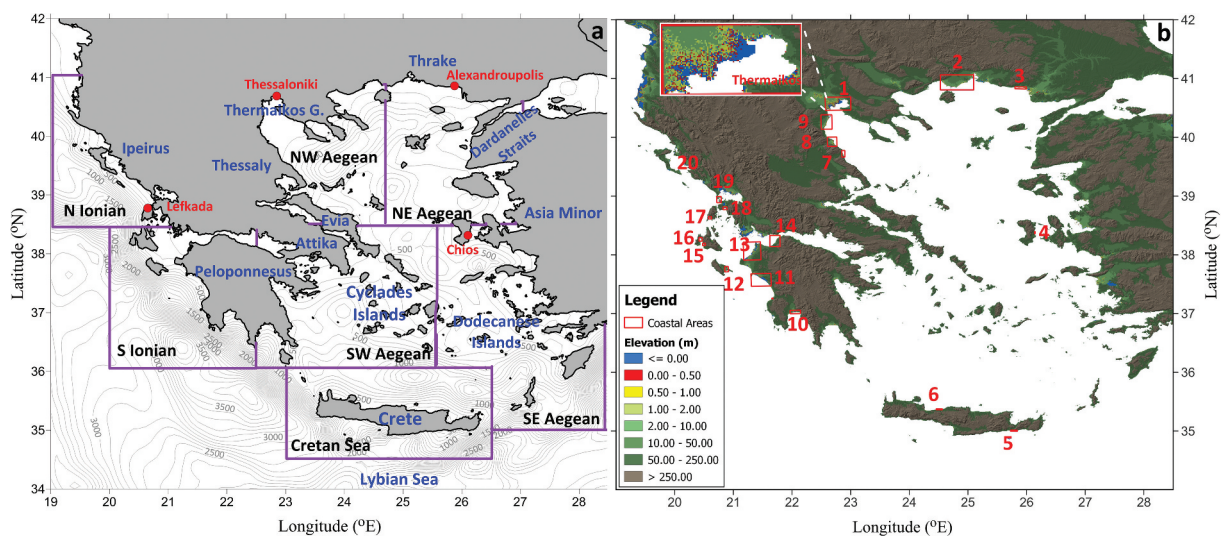


Figure 1. (a) Bathymetry of the study area divided into seven subregions: northwestern (NW) Aegean, northeastern (NE) Aegean, southwestern (SW) Aegean, southeastern (SE) Aegean, the Cretan Sea, northern (N) Ionian, and southern (S) Ionian Sea. The main topographic characteristics and the locations of the four tide-gauges (red dots) are marked. (b) land elevation (m) map, derived from the 25 m copernicus DEM, showing the 20 study coastal areas: Thermaikos Gulf (1), Nestos (2), Alexandroupolis (3), Chios (4), Ierapetra (Crete; 5), Rethymno (Crete; 6), Pineios (7), Agiokampos (8), Katerini (9), Kalamata (10), Katakolo (11), Laganas (Zakynthos; 12), Manolada (13), Patra (14), Argostoli (Kefalonia; 15), Livadi (Kefalonia; 16), Vassiliki (Lefkada; 17), Palairos (18), Preveza (19), Igoumenitsa (20).

environmentally protected areas, extensive touristic infrastructure containing a large number of recreational areas with sandy beaches, and many regions for several other activities (e.g. aquaculture, fisheries, navigational transportation, seaport commerce, athletics, etc.). The ultimate goal is to derive the coastal interannual SLA characteristics that will be used as boundary conditions (input) in the high-resolution coastal inundation assessment of characteristic low-lying areas (Figure 1b), located along the AICS coastline.

The worldwide socioeconomic and environmental impacts of SLR are significant. Desmet et al. (2021) have estimated the possible projected spatial shifts in economic activity until 2200 due to future SLR scenarios, including the reduction of global real Gross Domestic Product (GDP) and significant displacements of population from coastal localities. As a countermeasure, many researchers have introduced several approaches for an Integrated Coastal Zone Management (ICZM). For example, Clemente et al. (2022) have proposed a simplified risk assessment model for coastal built environments in terms of potential damages, direct and tangible, economic losses based on the Copernicus "Coastal Zones" database and exposure estimates by damage scenarios due to extremes of SLR in Italian littorals. The evaluation of estimations for future (projected) SLR is supported by a vast literature. For instance, Jeon et al. (2021) investigated sea level fingerprints and their relation to regional sea level changes, based on measured mass results from the Gravity Recovery And Climate Experiment (GRACE) and Argo float data (measuring thermal expansion), agreeing well with satellite altimetry. The most prominent natural hazard induced by episodic or long-term SLR is coastal flooding (short-term severe events) and/or coastal inundation (more long-term or perpetual situations) of low-lying littoral floodplains with various significant implications (Alvarado-Aguilar, Jiménez, and Nicholls 2012; Aucelli et al. 2017; Krestenitis et al. 2011; Nicholls and Hoozemans 1996; Refaat and Eldeberky 2016; Reimann et al. 2018; Rizzo et al. 2022; Shaltout, Tonbol, and Omstedt 2015; Snoussi, Ouchani, and Niazi 2008; Vandelli et al. 2022; Wolff et al. 2018). Favaretto et al. (2021) characterized storm events (by sea level variability and mean sea level rise) for the sake of coastal flood hazard assessment in north-central Mediterranean exposed littorals (Adriatic Sea; Venetian lagoon). Except from robustly defining the sea level components, Kulp and Strauss (2016, 2019) discussed the necessity to minimize errors in Digital Elevation Models (DEM) to avoid underestimations of coastal vulnerability due to sea level-induced flooding. Kulp and Strauss (2017) traced the rapid escalation of exposure of populations and infrastructure to coastal flooding in US municipalities due to rising sea levels,

assessed by LiDAR elevation data. Hauer et al. (2021) also assessed the exposure of US population to coastal flooding due to SLR, showcasing how the choice of zone results in differential spatiotemporal exposure estimates.

The scope of the study is to evaluate the interannual and spatial variability of the sea level over the AICS region and evaluate the respective impact on the coastal inundation characteristics along the topographically complex Greek coastline for 29 years (1993–2021). The main motivation is to assess the state and severity of coastal hazards, related to sea level increases, over the AICS. Coastal inundation estimations and trend analysis for the last three decades are based on the observed sea level increasing trends associated to changes in climatic patterns. The SLA differences among the seven AICS sub-regions are investigated based on a continuous long-term satellite dataset that covers the study region. The derived information will be used to estimate the inundation variability during the same 29-year period over the Greek coastal zone with the use of numerical simulations with CoastFLOOD model (Androulidakis et al. 2023; Makris et al. 2022, 2023; Skoulikaris et al. 2021) and an updated high-resolution dataset of land elevation derived from a DEM that covers the entire Greek coastline. We identified twenty (20) low-lying coastal areas (Figure 1b; based on the Copernicus DEM of 25 m resolution) that have been impacted by intense flooding events in the past and expand the analysis with the use of the finest available land elevation data (5 m) at the 20 study areas.

2. Methodology

2.1. Sea level observations

The altimeter satellite SLA data (sea surface height above the mean sea level), computed with respect to a twenty-year (1993–2012) mean, has been collected from the Copernicus Marine Service (CMEMS; <https://data.marine.copernicus.eu/>; accessed in June 2023; Landerer and Volkov 2013; Pujol and Larnicol 2005) to investigate the sea level variability over the AICS region and provide the boundary conditions of the coastal flooding simulations (see Section 2.4) covering a 29-year period (1/1/1993–31/12/2021). The DT-2021 European product (SEALEVEL_EUR_PHY_L4_MY_008_068), used in the study, has a spatial resolution of 1/8° (approximately 13 km), and it is provided in a daily step, while the initial coverage of the dataset extends over all European Seas. The Level L4 gridded data are produced by merging observations of Topex/Poseidon, ERS1/2, Jason 1-2-3, Sentinel (3A/B and 6A), HaiYang-2A/B, Saral[–DP]/AltiKa, Cryosat-2, ENVISAT, and GFO altimetry missions. These satellite-derived SLA fields have been previously used to evaluate the sea level variability in the Mediterranean Sea

(e.g. Bonaduce et al. 2016; Landerer and Volkov 2013; Mohamed and Skliris 2022; Mohamed et al. 2019). Pujol et al. (2023) validated the recent version of the gridded L4 SLA product against independent SARAL-DP/Altika along-track measurements. The error is around 4 cm in the Mediterranean Sea and increased in high variability areas (e.g. Gulf Stream; >6 cm). Moreover, further comparisons with tide gauges showed that the improved altimeter product DT-2021, used herein, is characterized by the reduction of variance of the differences between altimetry and field measurements ranges between 0.2% to more than 5% of the tide gauge signal. The average results of different missions are used to calculate the SLA L4 interpolated fields of the SEALEVEL_EUR_PHY_L4_MY_008_068 product; the daily mapping SLA error is also provided in the product for every grid point (see Supplementary material). All standard geophysical and environmental corrections have been applied to this product, including the Dynamic Atmospheric Correction (DAC; Landerer and Volkov 2013) to improve the representation of high-frequency (<20 days) atmospheric forcing considering both pressure and wind effects. More information and quality control of the SLA dataset can be found in the product user manual (Pujol et al. 2023; <https://catalogue.marine.copernicus.eu/documents/QUID/CMEMS-SL-QUID-008-032-068.pdf>, accessed in June 2023).

In this study, we perform an additional evaluation of the satellite altimetry product with field observations, covering 11 continuous years (2002–2012), derived from in situ measurements by four tide gauges of the Hellenic Navy Hydrographic Service (HNHS; <https://www.hnhs.gr/en/>, accessed in June 2023) in the Aegean and Ionian seas (Thessaloniki, Alexandroupolis, Chios, Lefkada; Figure 1a). To compare the satellite altimetry product with tide gauge datasets, the respective altimetry grid point that covers the location of each station was used. Moreover, the tide gauge sea level timeseries were also corrected based on the DAC product provided by AVISO (<ftp.aviso.altimetry.fr>, accessed in June 2023), following the methodology presented by Mohamed and Skliris (2022). Daily and monthly averages were derived from the original hourly field data and were compared to the respective daily and mean monthly timeseries derived from the satellite gridded fields (Section 3.1).

2.2. Digital elevation model data

Two sources of land elevation were used to detect and describe the low-lying coastal areas along the AICS coastline, serving also as the topography input in the inundation estimations and simulations (Section 2.4). The first dataset was derived from the EU-DEM v1.1, which covers the entire European domain with a 25 m spatial resolution, including the AICS region (Figure 1b). The EU-DEM v1.1. is distributed by the

Copernicus Land Monitoring Service (CLMS; <https://land.copernicus.eu/>, accessed in June 2023). We have used the EU-DEM v1.1 data to select 20 characteristic low-land study areas along the AICS coastal zone (Figure 1b) based also on the flooding events of these areas as reported in scientific literature and mass-media press (see Section 2.6). The second dataset of coastal elevation has higher resolution (5 m) and was derived by the available geospatial data from the DEM of the official Greek service for comprehensive recording of real estate and property's metes-and-bounds, i.e. the Hellenic Cadastre (<https://www.ktimatologio.gr/en>, accessed in June 2023). This high-resolution dataset was used to investigate the variability of the inundation levels over the 20 coastal areas that have been affected by intense flooding events in the last 3 decades. The geometric accuracy of the DEM is less than 0.70 m, while its absolute accuracy is less than 1.37 m with a 95% confidence level (Chrisafinos and Kavvadas 2016). This DEM product is highly efficient to perform numerical simulations of flooding over the Greek coastal zone (Xafoulis et al. 2023). Maps of land elevation of the 20 study areas, derived from the high-resolution DEM, are provided (together with respective flood cover maps; Section 4) as supplementary material (Figures S2–S20).

2.3. Atmospheric conditions

The prevailing meteorological conditions during the 29-year period were evaluated based on the ERA5 reanalysis dataset produced by the European Centre for Medium-Range Weather Forecasts (ECMWF). The hourly data have a spatial resolution of 0.25° and are freely distributed by Copernicus Climate Change Service (<https://cds.climate.copernicus.eu>, accessed in June 2023). The SLP fields and the two (zonal and meridional) components of the wind at 10 m height are used to investigate the effects of the atmospheric forcing on the variability of the SLA over the AICS domain.

2.4. Numerical simulations of coastal inundation

Herein, we implement modeling of coastal inundation induced by a slowly varying component of the near-shore sea level with CoastFLOOD (Makris et al. 2022, 2023). CoastFLOOD is an Aristotle University of Thessaloniki (AUTH) in-house numerical model, applied in littoral inundation hydrodynamic studies focused on local-scale selected areas of the Greek coastal zone (Androulidakis et al. 2023; Makris et al. 2022, 2023; Skoulikaris et al. 2021). These study coastal regions may include a) urban areas with engineered waterfronts, ports and coastal structures, road, highway and railway networks, b) rural areas with agricultural farmlands, natural or wild vegetated fields, forests,

bare lands, stony element lands, pastures and grasslands, and c) coastal water bodies such as estuaries, lagoons, torrents, river deltas, and natural beaches. The model is fed by the SLA dataset (Section 2.1) as hydraulic load boundary conditions (i.e. floodwater level) on the study areas' coastlines represented by the marginal dry cell of the computational domain during Still Water Level (SWL) conditions. Hence, it provides estimations of possible extended flooding of lowland coastal areas, rural plains, farmlands, urban sites, engineered spaces, deltaic regions, natural beaches, and estuaries along littoral stretches due to sea level increase, e.g. storm surges/tides (Androulidakis et al. 2023; Makris et al. 2023). Two (realistic and idealized) types of numerical simulations were developed to derive i) daily realistic estimations of coastal inundation covering the 29-year period, based on the satellite-derived SLA levels at each study area (jobs: 20 areas x 10,592 days), and ii) estimations of the extreme floods, based on four idealized scenarios of SLA (0.5, 1.0, 1.5 and 2.0 m; jobs: 4 scenarios x 20 areas) along the coastline boundary of each study area. The extreme values are based on crude thresholds of extreme storm surge levels or storm tides (surge + highest astronomical tides) as derived by Makris et al (2016) and Galiatsatou et al (2019, 2023). and Total Water Level (TWL) as defined by Galiatsatou et al (2019, 2021). along the Greek coastline. Detailed information (conceptual approach, equations, grid discretization techniques, numerical schemes, etc.) about CoastFLOOD model are thoroughly presented by Makris et al. (2023a), who also discuss the benefits and limitations of specific model applications in coastal lowlands; a concise summary is provided in the Appendix.

2.5. Statistical methods

The magnitude of the interannual trends was evaluated based on the Sen's Slope estimation (Sen 1968) that provides the annual change of the variable under investigation. This slope corresponds to the median of all the slopes calculated between each pair of points (x_i, x_j) in the series:

$$\text{Sen's Slope} = \text{Median} \left\{ \frac{x_j - x_i}{j - i} : i < j \right\} \quad (1)$$

Sen's Slope is considered efficient to detect the linear relationship as it is not affected by outliers in the data (Ray et al. 2021). The significance, which represents the threshold for which the hypothesis that there is not trend is accepted, is determined based on the computation of the p_{value} . A significance level of $\alpha = 1\%$ was used in a two-tailed test, in which the null hypothesis is that there is no monotonic trend in the time series ($H_0: \tau = 0; p_{\text{value}} > \alpha$), and the alternative hypothesis is that there is a significant monotonic trend in the time series ($H_A: \tau \neq 0; p_{\text{value}} < \alpha$). Here, the Sen's Slopes and the

respective p_{values} were computed with the XLSTAT version 2018.1 for the timeseries and with the MATLAB toolbox "Mann-Kendall Taub with Sen's Method (version 1.15.0.2; Burkey 2023)" to produce horizontal maps. The detection of abrupt changes during specific points in the long-term timeseries was also assessed with XLSTAT toolbox, based on the Pettitt's homogeneity test (Pettitt 1979). This test detects shifts in the average and calculates their significance in a hypothesis test. The null hypothesis is that the data are homogeneous, as against the alternative hypothesis that there is a datum at which there is a change in the data. The empirical significance level (p_{value} ; significance level of 1%) was performed to test the hypothesis of a shift in the mean in the dataset. If a shift exists ($p_{\text{value}} < 0.01$), the difference between the two means, before (μ_1) and after (μ_2) the shift, is also computed. Pettitt's test is a widespread non-parametric method to detect inhomogeneity, the change point in a time series (Bickici Arikan and Kahya 2019). The Pettitt's test was mainly applied in this study to detect the changes of flooding levels during the 29-year period.

The correlation between timeseries was tested with the computation of the Pearson product-moment correlation coefficient (Pearson 1903); it is a value that varies between -1 and 1 measuring the strength and direction of the relationship between two timeseries. The statistical significance of the correlations was also derived based on the Mann-Kendall (Kendall 1975; Mann 1945) correlation test (p_{value}); if p_{value} is lower than a conventional value (e.g. 5%; $p_{\text{value}} < 0.05$), the correlation coefficient is statistically significant. The Willmott Skill Score (WSS) or Index of Agreement (Willmott, Robeson, and Matsuura 2012) is also used to evaluate the agreement between two timeseries; the higher the WSS (with ≤ 1 as a limit), the better match is reached between the timeseries. Another metric to define the potential need for bias-correction of satellite-derived timeseries, compared to field observations, is the Hit-Rate-of-Percentiles (HRP) index (Makris et al. 2016; Schoetter et al. 2012). It calculates the differences between sorted percentiles of two timeseries, then defined as the sum of all categorical fractions (viz., differences compared to an allowed deviation, usually the standard deviation of observed timeseries). In general, if HRP index is greater than 0.95, then bias correction of derived SLA is not necessary.

The characteristics of SLA over each AICS sub-region was also analyzed based on the development of heat maps. A heat map depicts values for a main variable of interest across two axis variables as a grid of colored squares. The axis variables are divided into ranges like a bar chart or histogram, and each cell's color indicates the value of the main variable in the corresponding cell range. It shows the relationships and potential patterns' similarities

between two variables (e.g. SLA over each year and over each sub-region) one plotted on each axis. By observing how cell colors change across each axis (e.g. years in x-axis and sub-regions in y-axis), one can observe if there are any patterns in value for one of both variables (e.g. sampling of years and areas with similar patterns of SLA). Clustering of the heat maps is also applied to create dendrograms for both rows and columns. The dendrogram is a tree-structured graph used in heat maps to visualize the result of a hierarchical clustering calculation. Herein, the heat maps were derived with the use of the XLSTAT toolbox to investigate both inter-annual and seasonal variability of SLA.

2.6. Case study areas

The twenty (20) selected case study areas (and the aquatic basins they belong to), located along the AICS coastal zone, are presented in Figure 1b. These are generally established lowland coastal areas, based on the EU-DEM v1.1, that are well-known to be prone to flooding events. We chose them based on a series of recorded coastal inundation events due to storm surge (and/or compound flooding) in AICS littoral regions, which were reported rather either in scientific literature (Androulidakis et al. 2023; Diakakis, Deligiannakis, and Mavroulis 2011; Ferrarin et al. 2023; Ghionis et al. 2015; Kombiadou et al. 2012; Kontogianni et al. 2012; Krestenitis et al. 2011; Makris et al. 2023; Martzikos et al. 2021; Monioudi et al. 2016; Poulos et al. 2022; Skoulikaris et al. 2021; Stavropoulos et al. 2020; Tragaki, Gallousi, and Karymbalis 2018; Tsoukala et al. 2016) or in journal press, mass and social media. A list of such indicative events and the respective weather characteristics is provided in Table S1 (included as Supplementary Material). The extent of each study area was selected to include its most important environmental and socioeconomic features such as the coastal urban infrastructure, seaport facilities, environmentally protected areas (lagoons, wetlands, watersheds, etc.), sandy beaches, touristic facilities, holiday residencies, lowland agricultural areas, natural bare lands in the coastal plain, etc. For example, Area 1 (Thermaikos Gulf) includes Thessaloniki city at its northern coasts, which is the second largest city of Greece, touristic regions and recreational beaches in the east, river deltas and extensive agricultural farmlands along the west coasts. The 20 study areas are representative of the entire AICS coastal zone with respect to topographical, environmental, and social characteristics.

3. Interannual trends and spatial variability of Sea level Anomaly

Initially, we evaluated the satellite-derived SLA observations against field observations at 4 coastal areas

(Section 3.1). The distribution of the SLA over the 7 sub-regions of the AICS (Figure 1a) was examined to detect the interannual trends (Section 3.2) and seasonal cycles (Section 3.3), highlighting the differences between the AICS sub-regions. Finally, the contribution of the two main atmospheric components (SLP and winds) on the SLA variability of each sub-region was also investigated to evaluate the spatial variability of air pressure and wind states over the AICS domain (Section 3.4).

3.1. Comparison between satellite and tide-gauge observations

The daily variability of the SLA at four locations of the AICS domain, derived from both satellite and tide-gauge observations during an 11-year period, is presented in Figure 2. The Pearson correlation coefficients in most of the stations are higher than 0.80 (Table 1) and they are statistically significant based on the MK correlation test ($p_{\text{values}} < 0.01$: statistical significance level 99%). The respective monthly averages show even higher correlation in Thessaloniki and Chios areas ($R_p > 0.90$). The agreement between the two datasets is good in terms of percentiles too, showing quite high HRP-index (> 0.99), reaching 1.00 in the Ionian Sea (Lefkada; Figure 2d), a region with significantly high storm surge frequency, especially due to severe tropical-like atmospheric cyclones (e.g. Medicanes; Androulidakis et al. 2023; Lagouvardos et al. 2022). These values signify that there is no imperative need for bias-correction of the SLA timeseries, at least for the present scope of feeding a large-scale coastal inundation model for flood hazard mapping. The Root Mean Square Error (RMSE) is between 2 to 5.5 cm given the difficulty to achieve agreement in point-to-point values' comparisons between gridded SLA values and *in situ* measurements. The ratio between RMSE and maximum SLA is less than 20% supporting the efficiency of the satellite-derived data to measure the high sea level peaks in the coastal zone. The WSS are significantly high, reaching close to unity (> 0.90) in most of the cases (Table 1). The maximum SLA values (> 0.40 m) were well recorded by both techniques, especially during the extended winter months (December – March) of 2009–2010 and 2010–2011, which were periods with high SLA values in the eastern Mediterranean Sea under negative NAO phase conditions (Bonaduce et al. 2016; Mohamed and Skliris 2022; Tsimplis et al. 2013). Differences between tide gauge measurements and satellite observations can also be related with the vertical land motion of coastal areas affected by geodynamic processes and landscape evolution due to tectonic movements, eustatic factors, etc. For example, in the coasts of central Ionian there is a slow land subsidence rate ≤ 2 mm/year (Anzidei et al. 2014). This may result to approximately 2 cm per

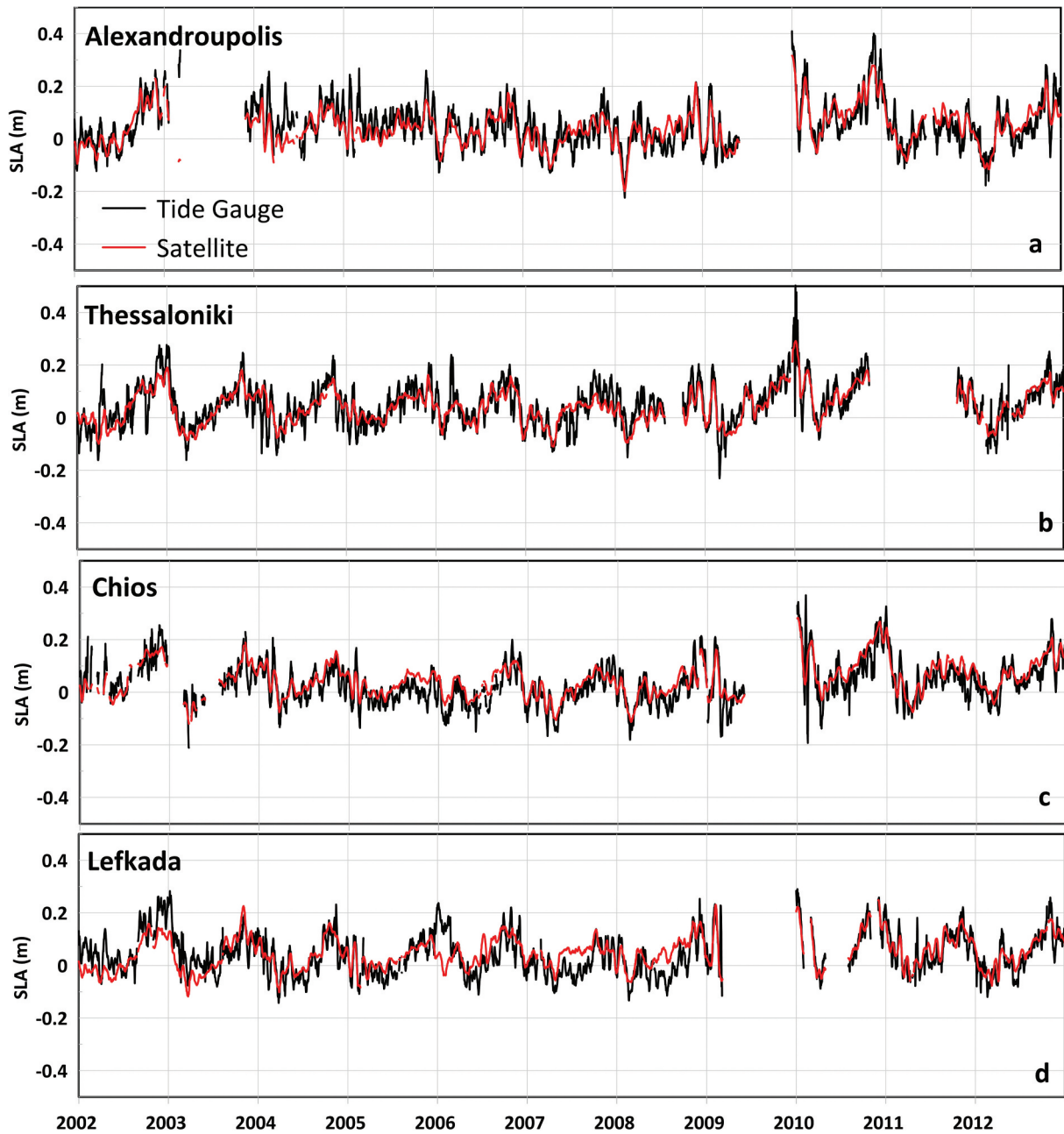


Figure 2. Evolution of daily Sea level Anomaly (SLA; m) derived from the satellite altimetry (red line) and tide gauges (black line) at (a) Alexandroupolis, (b) Thessaloniki, (c) Chios, and (d) Lefkada sites (Figure 1b).

Table 1. Satellite data skill metrics of reproducing the *in situ* observations of SLA (m; Dynamic atmospheric correction (DAC) product removed) in Alexandroupoli, Thessaloniki, Chios, Lefkada derived from mean daily and monthly values from 2002 until 2012; quantitative comparisons are based on the statistical measures: Pearson correlation R_p , root mean square error (RMSE), Willmott skill score (WSS), HRP-index. The asterisk (*) indicates that the hypothesis that the correlation is statistically significant is true (99% MK test of statistically significant trend: $p_{value} < 0.01$).

A/A	Area	R_p	RMSE (m)	RMSE/SLA _{max} (m)	WSS	HRP-index
Daily averaged SLA values						
1	Alexandroupoli	0.813*	0.056	11.25%	0.913	0.99
2	Thessaloniki	0.824*	0.022	9.57%	0.930	0.99
3	Chios	0.846*	0.034	12.10%	0.920	0.99
4	Lefkada	0.713*	0.049	20.30%	0.805	1.00
Monthly averaged SLA values						
1	Alexandroupoli	0.768*	0.044	15.37%	0.881	1.00
2	Thessaloniki	0.902*	0.028	11.16%	0.947	1.00
3	Chios	0.921*	0.028	11.83%	0.947	1.00
4	Lefkada	0.759*	0.042	19.61%	0.869	1.00

decade mean SLR, contributing to the RMSE derived for Lefkada station (~5 cm; Table 1). Near-null movements have been detected in the central and northern Aegean and even a slight uplift in Crete (Anzidei et al. 2014; Fenoglio-Marc, Dietz, and Groten 2004).

The SLA error associated to the transmission from the L3 to L4 product used herein is generally larger near the coast (up to 2.5 cm; supplementary Figure S1b) than offshore, in the open sea of the AICS region (less than 1.5 cm). It is noted that the averaged SLA error over the entire region reduced throughout years during the last three decades from 2.3 cm in 1993 to less than 1.6 cm in 2021 (supplementary Figure S1a) probably due to the several correction improvements and ongoing addition of extra satellite tracks during the 29-year period. Thus, the comparison results support the usage of the remote sensing dataset to assess the sea level interannual variability along the coastal zone of the AICS domain, especially during periods of SLA peaks. These serve as forcing conditions of the coastal flooding simulations (see Section 4).

3.2. Interannual variability

The interannual evolution of the mean annual SLA is characterized by clear positive trends in all AICS sub-regions over the 1993–2021 period (Figure 3a). The general trend over the entire area, based on the computation of the Sen's Slope, was 3.6 mm/year (Table 2; black line in Figure 3a), higher than the overall Mediterranean (2.44 mm/year; Bonaduce et al. 2016) and the eastern Mediterranean (3.1 mm/year; Mohamed and Skliris 2022) trends. All trends are statistically significant ($p_{\text{value}} < 0.01$; Table 2). A clear north-to-south increasing gradient of mean SLA was computed in the Aegean Sea (Figure 4a) with relatively low values south of Chalkidiki and over the north-eastern islands (<4 cm), while higher levels were found in the southern Aegean (>4.5 cm). The spatial distribution of the interannual SLA trends (Figure 4c) shows statistically significant (Figure 4d) strong Sen's Slopes over the Aegean Sea (>3.5 mm/year) and the northern Cretan Sea. The highest Sen's Slopes were derived for the SW Aegean (4.1 mm/year; Table 2 and Figure 3a); specifically, over its northernmost coastal area (south Attika and north-eastern Peloponnesus; Figure 4c), the interannual increase exceeded the value of 4 mm/year. The same area also revealed the highest mean SLA of the entire 29-year period (Figure 4a). Very strong trends were also computed along the eastern Aegean islands and Minor Asia coasts as well as the southern Dodecanese (Figure 4c). Weaker slopes of the annual mean SLA trends were computed offshore in the Ionian and southern Cretan Seas (Figure 4c), with even negative and statistically insignificant values ($p_{\text{values}} > 0.05$;

Figure 4d) in the broader area of the Ierapetra Anticyclone (Menna et al. 2022), which is a semi-permanent ocean eddy in the southeastern Cretan Sea. This agrees with the findings of Mohamed and Skliris (2022) and Bonaduce et al. (2016). The Ierapetra Anticyclone that is usually formed during the summer months (Ioannou et al., 2017), also revealed the highest standard deviation values (>0.1 m; Figure 4f). The characteristics of the Ierapetra Anticyclone (e.g. size, location, intensity, lifetime) are determined by the negative wind stress curl and the blocking of the strong Etesian summer winds by the Cretan orography (Horton et al. 1994; Mkhinini et al. 2014). Generally, the interannual standard deviation showed different behavior between the several sub-regions (Figure 3d), but without revealing any significant trend ($p_{\text{values}} > 0.01$; Table 2).

The highest 99th percentiles in the Aegean Sea were derived for the same regions over the SW Aegean (>0.22 m; Figure 4b), where the strongest increasing trends of the maximum values were also computed (>3.4 mm/year; Table 2; Figure 3b). Although all trends were statistically significant, the smallest p_{values} (<0.0001; Table 2) were found in the SW Aegean and Cretan Seas. High 99th percentiles of SLA were also observed over the Cretan Sea, along the central Anatolia coasts, and around the eastern Aegean islands (e.g. Lesvos and Chios; Figure 4b). The northern Aegean sub-regions revealed the highest 99th percentiles during the "extreme" year of 2010 (>0.25 m; Figure 3b), when the maximum SLA values of the entire study period occurred (Figure 4e). Two additional peaks of annual 99th percentiles were observed in 2019 and 2021 (Figure 3b); large areas of the Ionian Sea and central and southern Aegean sub-regions revealed their highest maximum values during 2021 (Figure 4e). Another area with very high 99th percentiles (Figure 4b), strong positive trends (Figure 4c), and large standard deviation values (Figure 4f) is located south of the Peloponnesus, where the Pelops Gyre is formed (Bonaduce et al. 2016; Menna et al. 2022; Pinardi et al. 2006). On the contrary, the Ionian Sea showed both weaker interannual variations (StDev <7 cm; Figure 4f) and trends (<3 mm/year; Table 2) compared to the Aegean and Cretan seas. Besides the mean and maximum values, very strong increasing trends were also computed for the minimum SLA values (10th percentiles) for all regions (Figure 3c) with steeper Sen's Slopes in the Aegean Sea (>3.5 mm/year; Table 2) and milder ones in the Ionian and Cretan Sea (<3 mm/year; Table 2). This result is associated to the increase of the lowest annual 10th percentiles that are even positive at several years during the last decade (e.g. 2013, 2016, and 2018; Figure 3c).

The heat maps and the respective dendrograms of the mean and the 99th percentile of SLA for each year

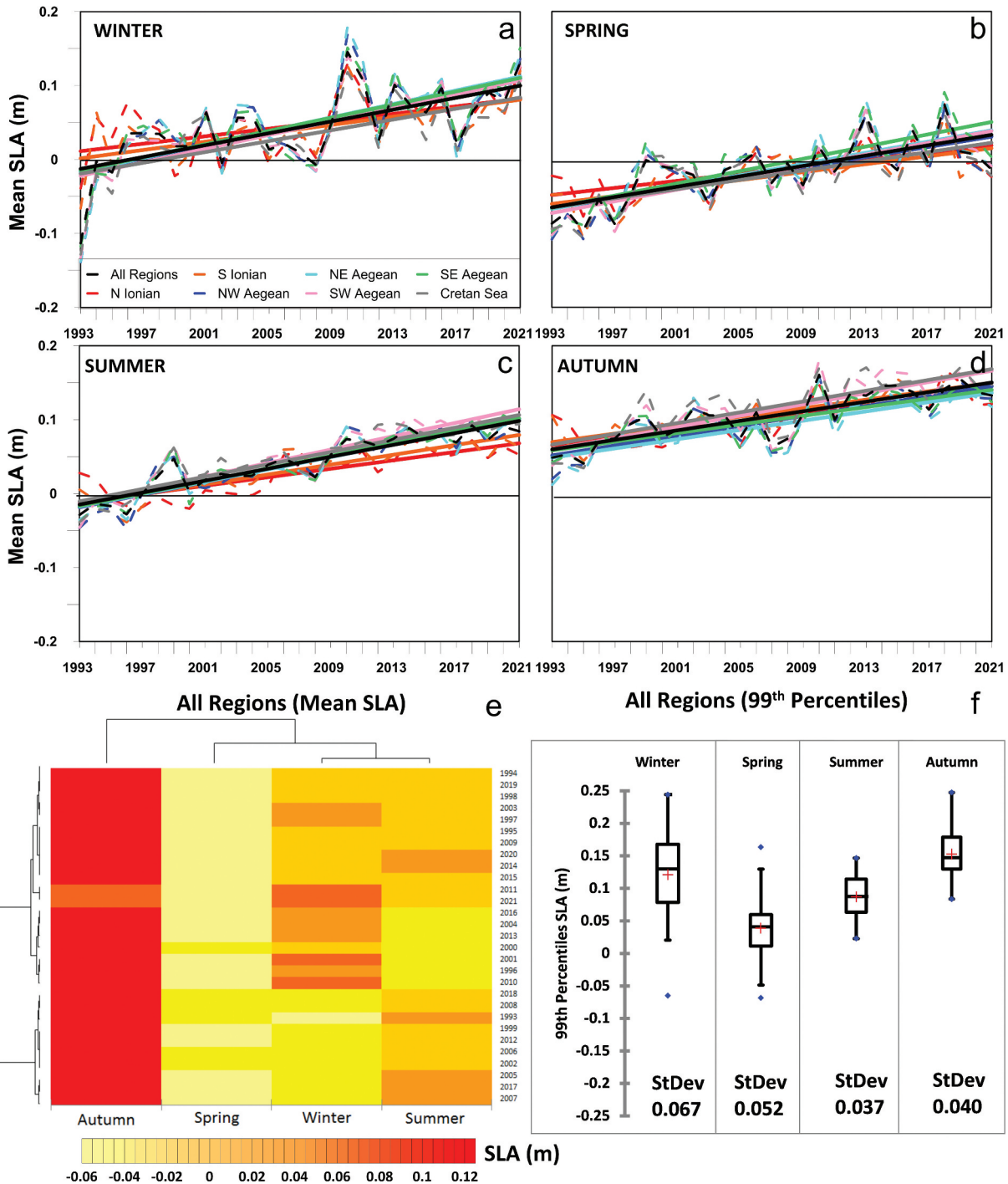


Figure 3. Annual variability (dashed lines) and trends (continuous lines) of: (a) the mean Sea level Anomaly (SLA; m); (b) the 99th percentile; (c) the 10th percentile, and (d) the standard deviation (StDev; m), averaged over 8 regions (all regions: black; N Ionian: red; S Ionian: orange; NW Aegean: dark blue; NE Aegean: light blue; SW Aegean: purple; SE Aegean: light green; Cretan Sea: gray (Figure 1a), for the period 1993–2021. Heat maps with respective dendrograms of the (e) mean and (f) 99th percentile SLA derived from the annual and spatial SLA averages for each year and region.

(row) and each sub-region (columns) are presented in Figure 3e and f, respectively. The 29 annual means are grouped in four categories (Figure 3e). The highest-SLA group (most red in Figure 3e) includes the years of 2010, 2013, 2014, 2016, 2018, 2019, 2020, and 2021, all during the last 12-year period, confirming the strong inter-decadal increase. The other three categories can be grouped into one cluster, including all the years before 2010 (most yellow in Figure 3e). As far as the

highest SLA values (99th percentiles) are concerned, four main categories are also formed. A similar pattern of lower values is observed in two of them for the years before 2010 (most yellow in Figure 3f). The highest 99th percentiles of SLA, similarly to the annual averages, were also detected in 2009, 2010, 2012, 2013, 2014, 2015, 2016, 2018, 2019, 2020, and 2021 (Figure 3f). The areas can also be grouped in two categories with similar patterns of mean annual SLA for the Ionian sub-

Table 2. Sen's slopes (mm/year) and the respective MK statistical significance thresholds (p_{value}) for the mean, the 99th percentiles (99 Perc), the 10th percentiles (10 Perc), and the standard deviation (StDev), derived from annual mean SLA values, averaged over all regions (Figure 1) for the 1993–2021 period.

		All Regions	N Ionian	S Ionian	NW Aegean	NE Aegean	SW Aegean	SE Aegean	Cretan Sea
Mean	Sen's Slope	3.6	2.7	2.9	3.7	3.6	4.1	3.9	3.3
	p_{value}	<0.0001	<0.0001	<0.0001	<0.0001	<0.0001	<0.0001	<0.0001	<0.0001
99 Perc	Sen's Slope	3.0	3.2	3.2	3.2	3.3	3.4	3.2	3.5
	p_{value}	<0.0001	0.0007	0.0006	0.0002	0.0008	<0.0001	0.0003	<0.0001
10 Perc	Sen's Slope	3.6	2.4	2.7	3.8	4.1	3.9	4.6	2.9
	p_{value}	<0.0001	<0.0001	<0.0001	<0.0001	<0.0001	<0.0001	<0.0001	0.0024
StDev	Sen's Slope	-0.1	0.1	0.0	0.0	0.0	0.0	-0.4	0.1
	p_{value}	0.7522	0.6692	0.9852	0.9852	0.9260	0.9852	0.1851	0.6159

regions (1st cluster) and Aegean-Cretan sub-regions (2nd cluster).

3.3. Seasonal variability

The seasonal interannual variability for all AICS sub-regions is characterized by similar increasing trends but reveal remarkable differences among the seasons (Figure 5). The highest SLA levels were detected primarily in autumn (Figure 5d) and secondarily in winter (Figure 5a), while the lowest seasonal means occurred in spring (Figure 5b) in agreement with previous findings, derived from tide-gauges (Tsimplis and Shaw 2010) that showed maximum values in most Mediterranean stations in winter and autumn and smaller levels in spring and summer. The main contribution to the sea level cycle in the Mediterranean Basin is the steric component (Gomis et al. 2008). The maximum seasonal values are represented by the seasonal 99th percentiles that confirm the smaller variance of the autumn values around high mean levels (Mean = 14 cm, StDev = 4 cm and narrow distribution between the 1st and 3rd quartiles; Figure 5f). The autumn mean SLA from all years showed unified variability characteristics (1st group; Figure 5e), while a second group of seasons with similar variability includes winter and summer. Spring also constitutes a separate group that has more similarities with winter and summer. The peak of 2010 is apparent in the winter's timeseries with higher values in the northern Aegean (Figure 5a).

Despite its high mean and maximum values, the interannual Sen's Slopes of autumn were the weakest among all seasons, especially for the Aegean Sea (Table 3). The strongest trends at all regions were detected in the summer, revealing the highest Sen's Slope among all areas and seasons for the SW Aegean (4.7 mm/year) in agreement with the strong annual trends for the same area (Table 2). The Ionian Sea revealed the weakest trends for winter and spring (2.2–2.7 mm/year; Table 3), while both of its northern and southern parts followed the stronger general trend of the AICS domain in the summer and autumn (2.7–3.3 mm/year) due to the high occurrence

frequency of the atmospheric low pressure systems that usually form over the central Mediterranean (between the northern African coast and the Ionian; Cavicchia, von Storch, and Gualdi 2014; Makris et al. 2023) in autumn, contributing on the storm surge formation along the western coasts of Greece (Androulidakis et al. 2015, 2023). The spring SLAs were the lowest among all seasons (Figure 5b) showing also very small maximum values (99th percentiles; Figure 5f). Until 2010, the mean spring SLAs were mainly negative, while the highest spring mean levels occurred in 2018 (7 cm; Figure 5b).

3.4. Atmospheric contribution

The barotropic effects of wind and atmospheric pressure on the SLA variability over the AICS region are separately analyzed and presented in Figure 6. The mean annual wind speed, SLP and SLA were computed and the Pearson correlation coefficient together with the MK statistical test were computed for all domain's cells covering the entire 29-year period. The highest SLP and SLA correlation coefficients, derived from annual means of the 1993–2021 period, were detected for the Aegean Sea (Figure 6a); the Pearson coefficients were higher than 0.5 and statistically significant ($p_{\text{value}} < 0.01$) over the central (Cyclades Archipelago) and eastern Aegean (along the Minor Asia coasts) Sea. On the contrary, the atmospheric pressure has weaker impact on SLA variability over the Ionian Sea ($R_p < 0.3$), where the highest correlation coefficients between wind speed and SLA were derived, especially around the central Ionian coasts ($R_p > 0.5$; Figure 6b). The wind-SLA coefficients were smaller in the Aegean Sea in agreement with previous studies (i.e. Androulidakis et al. 2015; Krestenitis et al. 2011; Marcos and Tsimplis 2007), who showed that high surges are more associated to the inverse barometer effect and favorable winds in the Aegean and Adriatic (including Ionian) Seas, respectively. The northern Aegean coasts were characterized by lower correlation coefficients between SLA

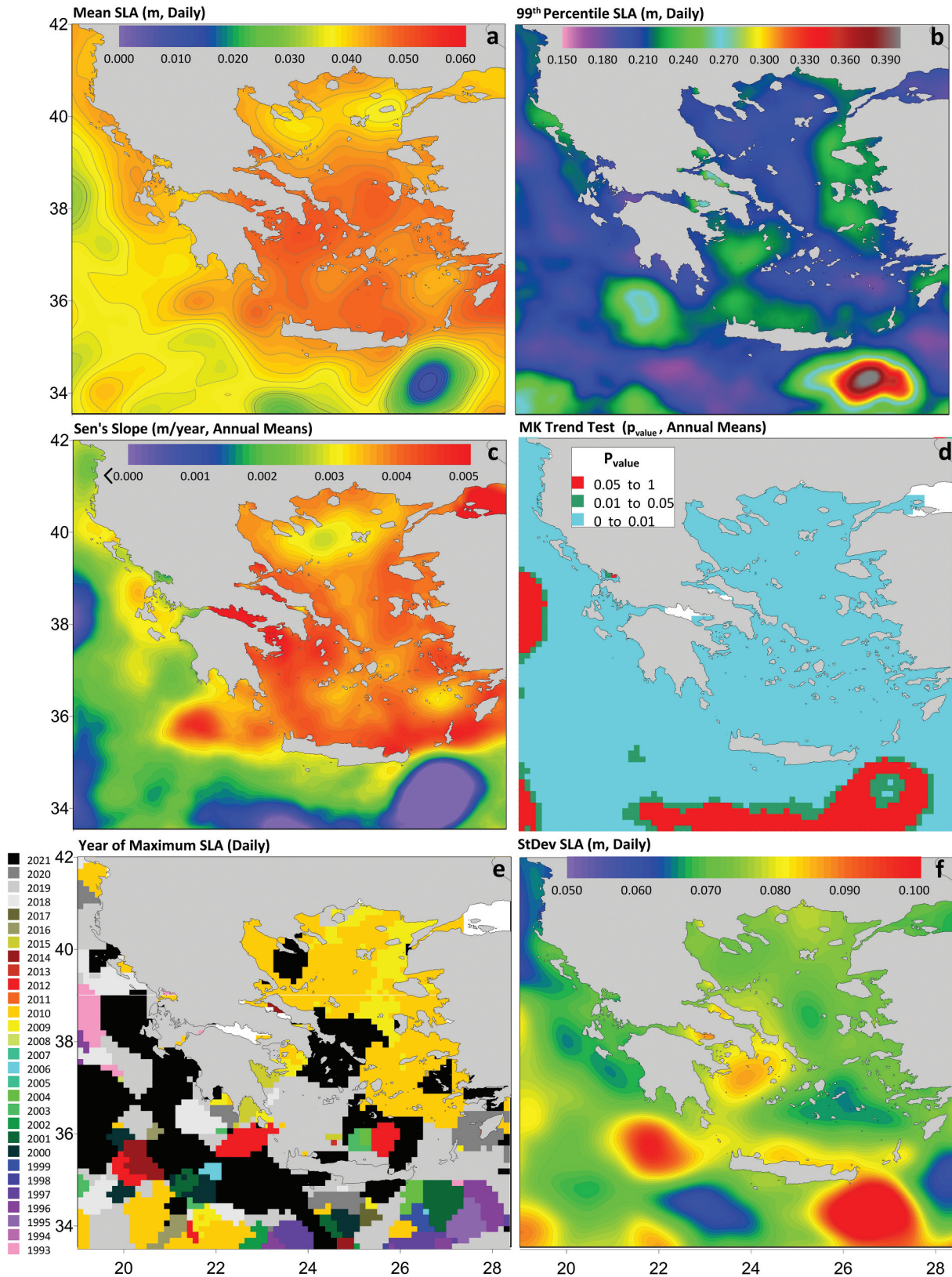


Figure 4. Horizontal distribution of (a) mean Sea level Anomaly (SLA; m), (b) 99th percentile, (c) Sen's Slope (m/year), (d) Mann-Kendall (MK) trend test (p_{value}), (e) year of the maximum SLA, and (f) standard deviation (StDev) derived from the daily and mean annual SLA over the AICS domain during the 1993–2021 period.

and SLP in comparison with the rest of the Aegean Sea (Figure 6a), while the wind effect was relatively stronger (Figure 6b).

The effect of the wind direction (wind component) is examined in Figures 6c (westerlies), 6d

(easterlies), 6e (southerlies) and 6f (northerlies). The positive and statistically significant correlation coefficients (>0.5) between the eastward wind component (positive) and SLA (Figure 6c) represent the increase of SLA under westerlies which are mainly

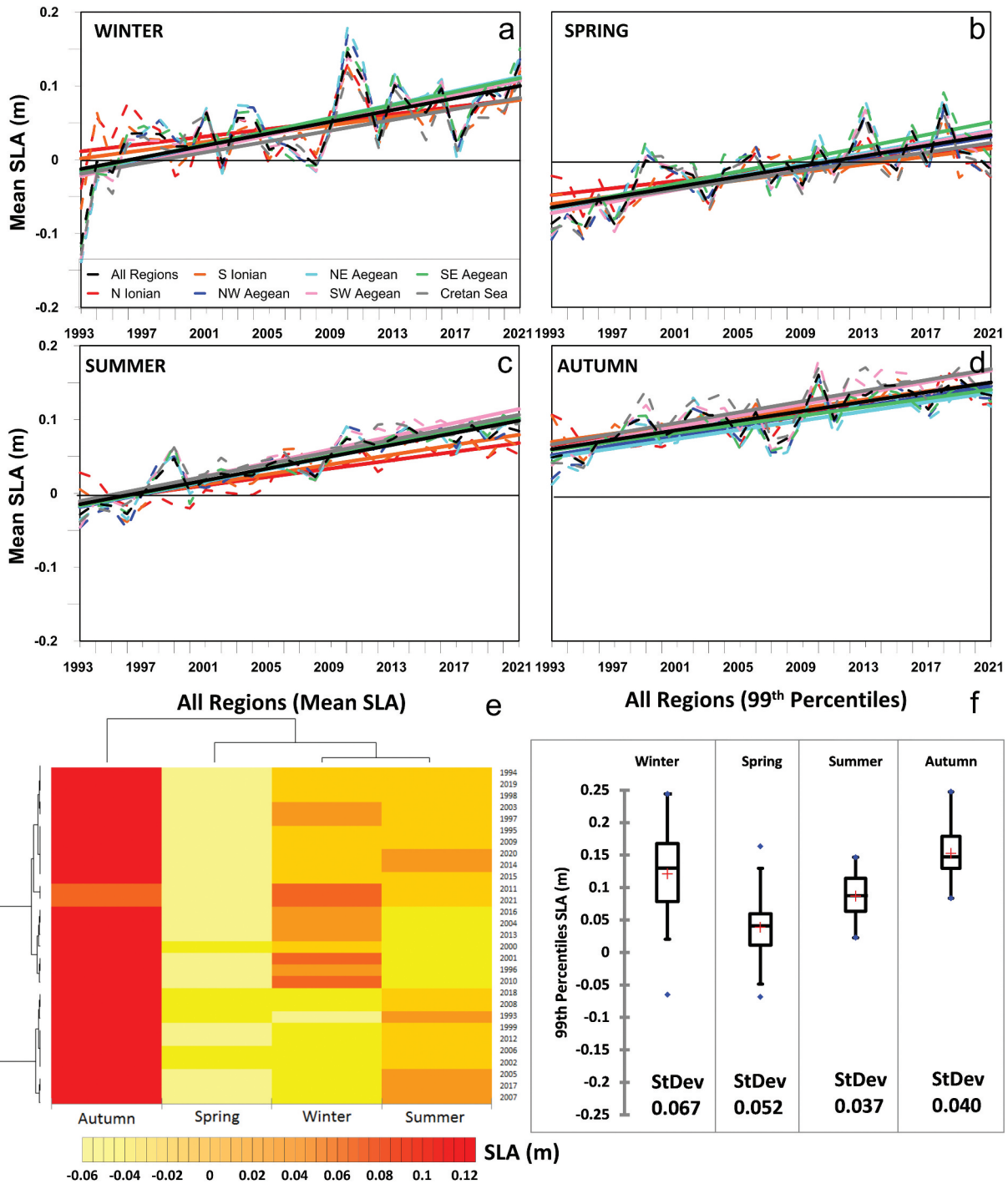


Figure 5. Seasonal variability (dashed lines) and annual trends (continuous lines) of the mean Sea level Anomaly (SLA; m) over (a) winter, (b) spring, (c) summer, and (d) autumn, averaged over 8 regions (all regions: black; N Ionian: red; S Ionian: orange; NW Aegean: dark blue; NE Aegean: light blue; SW Aegean: purple; SE Aegean: light green; Cretan Sea: gray) (Figure 1), for the period 1993–2021. (e) heat map with respective dendrograms derived from the annual and spatial SLA seasonal averages for each year and region. (f) seasonal box plots of the 99th percentiles of SLA of all regions, showing the 1st (lower line) and 3rd (upper line) quartiles, minimum (low dot), maximum (upper dot), mean (cross) and median (middle line), and standard deviation (StDev) value for each season.

detected over areas of the S Ionian, in SE Aegean, along Minor Asia coasts, and in NE Aegean coastal areas. The negative coefficients between the westward wind component (negative sign) and the high SLA (positive sign) highlight the effect of easterly winds on the SLA increases (Figure 6d); the northern Cretan Sea, the SW and SE Aegean and the broader Thermaikos Gulf (NW Aegean) revealed

high negative coefficients (<-0.5). The increased SLA levels of the N Ionian, areas of northern Aegean and SE Aegean were mainly affected by southerly winds (positive correlation coefficients: >0.5; Figure 6e). On the contrary, the northerly winds (negative wind meridional component; Figure 6f) had an opposite effect on the coastal areas of Thermaikos, northern Aegean, and

Table 3. Sen's slopes (mm/year) and the respective MK statistical significance thresholds (p_{value}) for the mean SLA derived from the interannual SLA values for each season, averaged over all regions (Figure 1) for the 1993–2021 period.

		All Regions	N Ionian	S Ionian	NW Aegean	NE Aegean	SW Aegean	SE Aegean	Cretan Sea
Winter	Sen's Slope	3.5	2.5	2.7	4.0	4.1	4.1	4.1	3.2
	P_{value}	0.0004	0.0052	0.0021	0.0003	0.0007	0.0003	0.0003	0.0012
Spring	Sen's Slope	3.4	2.2	2.5	3.4	3.8	4.0	4.0	2.9
	P_{value}	<0.0001	0.0003	0.0006	0.0003	<0.0001	<0.0001	<0.0001	0.0012
Summer	Sen's Slope	4.1	2.9	3.3	4.4	4.4	4.7	4.3	4.2
	P_{value}	<0.0001	<0.0001	<0.0001	<0.0001	<0.0001	<0.0001	<0.0001	<0.0001
Autumn	Sen's Slope	3.2	2.7	3.0	3.3	3.1	3.9	3.0	3.6
	P_{value}	<0.0001	<0.0001	<0.0001	<0.0001	<0.0001	<0.0001	<0.0001	<0.0001

especially along Minor Asia (and eastern Aegean islands) enhancing the reduction of SLA due to the offshore removal of waters (positive correlations: >0.5). The strong Etesian northerly winds (i.e. Meltemia; Poupkou et al. 2011) that prevail over the Aegean Sea during summer months contribute to the coastal upwelling over the eastern Aegean, reducing the sea surface level and temperature (Androulidakis et al. 2017; Mamoutos et al. 2017) and controlling the biochemical processes of the broader area (Chaniotaki et al. 2021).

4. Coastal inundation at selected areas along the AICS coastline

The numerical simulations of coastal flooding were performed with the CoastFLOOD model (Section 2.4 and Appendix; Makris et al. 2023) at the 20 study areas (Figure 1b), covering the long-term period from January 1 1993 to December 31 2021 (29 years). The simulated results were used to provide daily estimations of Flooded Area (FA) based on the SLA derived along the respective shoreline (boundary condition) of each coastal area (realistic simulations). Moreover, apart from the realistic conditions, we have simulated the inundation at all study areas during several reference values of extreme cases for sea level elevation (idealized simulations). These are characteristic threshold values of storm-induced SLA on the Greek coastal zone (Galiatsatou et al. 2019, 2021, 2023), including e.g. the combined influence of storm surges, astronomical tides, mean SLR, and wave setup or conditionally mild estimations of the TWL. To this end, for intercomparison between different scenarios, the idealized numerical experiments involved values of:

- (i) SLA = 0.5 m, equivalent to a rough upper limit of the 98% storm surge quantile level corresponding to a 50-years return period within a stationary Extreme Value Analysis (EVA) context in a yearly time interval under climate change conditions (SRES scenarios) during 1951–2100 (Makris et al. 2016); this also

coincides with the upper threshold of time-dependent (nonstationary EVA) estimates of the most likely event of nearshore storm surge in the Aegean Sea, based on fitted parametric trends of bivariate data analytics (Galiatsatou et al. 2019) or simpler EVA approaches along the entire Mediterranean coastline under more recent (RCP) climate change scenarios (Galiatsatou et al. 2023).

- (ii) SLA = 1.0 m, equivalent to a rough-rounded and common (for Greece) upper limit of the annual return levels of extreme storm surges (0.65–0.75 m), based on the upper 95% confidence bounds under climate change conditions during 1951–2100 (Makris et al. 2016), combined with typical values of the (geographically) mean highest (astronomical) tidal range (≤ 0.35 m; HNHS, 2015).
- (iii) SLA = 1.5 m, corresponding to the above estimate (ii) enhanced by adding a rough upper limit estimate of the wave set-up (0.5 m) based on time-dependent (nonstationary EVA) estimates of the most likely event of extreme nearshore waves incident to the Greek coasts (Galiatsatou et al. 2019).
- (iv) SLA = 2.0 m, corresponding to a conservative lower threshold (to avoid overexaggerated estimations) of the time-dependent estimates of the 100-years return level of extreme TWL (including tides, mean SLR, and wave run-up) for typical Greek mild cross-shore profiles (Galiatsatou et al. 2023).

Please note that the above cases (iii) and (iv) refer to enhanced SLA values by the wave-induced components on the coast (wave set-up and wave run-up, respectively), which are outside the scope of this paper and are presented only for the completeness of coastal inundation simulations. They are not included as upper reference in the coastal inundation hazard assessment calculations below to avoid underestimations of the storm surge-induced hazard.

To allow the comparison between coastal areas with different sizes and to produce a more unbiased

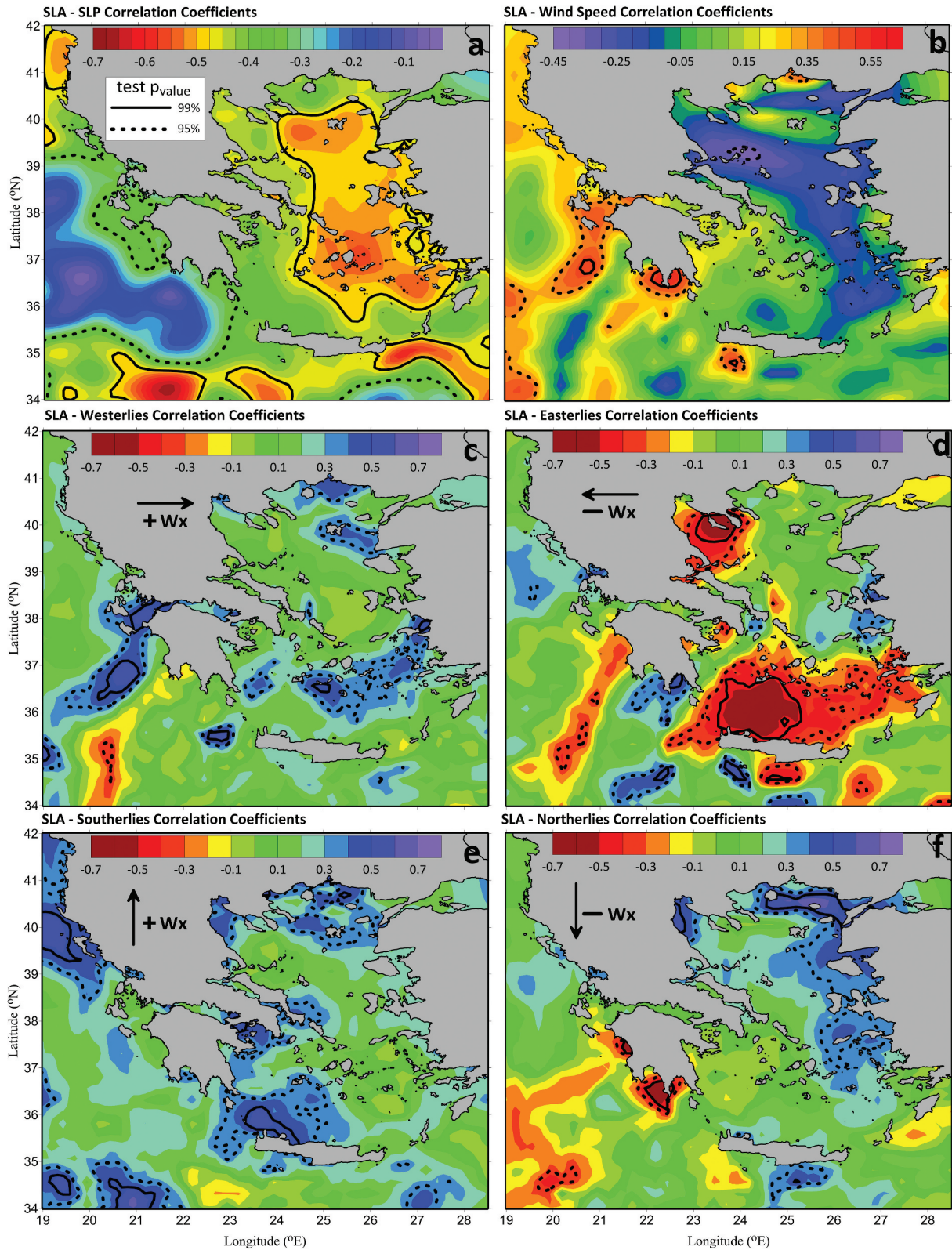


Figure 6. Distribution of Pearson correlation coefficients between Sea level Anomaly (SLA) and (a) Sea level pressure (SLP), (b) wind speed, (c) positive zonal wind component (westerlies), (d) negative zonal wind component (easterlies), (e) positive meridional wind component (southerlies), and (f) negative meridional wind component (northerlies), derived from the mean annual values of the 1993–2021 period. The solid and dashed contours indicate the 99% and 95% p_{values} isolines of the correlation statistical test, respectively.

index for the estimation of the coastal flooding for each area, the daily Flood Coverage Percentages (FCP, %) was computed as:

$$FCP_{i,j} = FA_{i,j}/FA_{ext,j} \quad (2)$$

where $FA_{i,j}$ is the flooded area for each study region j and simulation day, i , based on the respective satellite-derived actual $SLA_{i,j}$; $FA_{ext,j}$ is a considered maximum of the theoretically exposed area to flooding derived for each study region, j , yet based on a common extreme case scenario for the driver of coastal inundation (i.e. SLA). Herein, the $FA_{i,j}$ is derived for all days of the 1993–2021 period (thus producing $ixj = 10,632 \times 20$ values for $FCP_{i,j}$), while the $FA_{ext,j}$ is derived for each area from the CoastFLOOD simulations based on the inundation scenario forced with $SLA = 1$ m (thus producing $j = 20$ values for $FA_{ext,j}$). The upper threshold FA_{ext} , used as a reference, corresponds to a diverse (different for each area) hazard (response) magnitude, i.e. flooded area $FA_{i,j}$, but based on a common value (characteristic to the Greek littoral zone) for the environmental driver of coastal inundation, i.e. SLA_{ext} , in all areas. This was done to secure a common approach for the calculation of unbiased hazard ranking in the 20 areas of study. This way we can compare study areas against each other in terms of flood hazard (please note not risk; this would require a proper quantification of exposure and vulnerability), albeit their sizes differ a lot further adding to quite diverse percentages of lowland parts in the 20 study cases.

4.1. Interannual and spatial variability of coastal inundation

The FCP levels are related to two main factors: the sea level high peaks (e.g. 99th percentile of SLA) and the topographic characteristics of each coastal area (e.g. distribution of low-lying areas). Figure 7 presents the distribution of both factors for each study area, dividing the land elevation percentages (lower than 1 m) at 6 categories with a 20 cm step, derived from the high-resolution DEM dataset (5 m; Section 2.2). The maximum SLA spatial variation (red line in Figure 7) is related to the majority of the study areas' FCP values (similar variation between FCP and SLA); however large differences (e.g. Area 3) occurred due to the different land terrain of the 20 cases. The FCP levels for all study areas, averaged over the 29-year period (black line in Figure 7), show strong spatial variability with very low percentages (<4%) at Areas 3 (Alexandroupolis), 8 (Agiokampos), and 15–20 (central and northern Ionian Sea). Respectively, the 99th percentile of SLA also varies between 0.18 and 0.225 m among the 20 study regions confirming the clear spatial variability of maximum sea levels. It is shown that although relatively high SLA values were recorded for the central and northern Ionian areas (Areas 15–20; >0.21 m 99th percentile), the low FCP levels were mainly associated with the very small percentages of low elevation cells of the respective areas. The majority of the land cells (>40%) are between 0.8–1.0 m, while very high percentages were also computed for categories between 0.4–0.8 m, confining the flooding extension at these coastal areas. Similarly, Area 3 (Alexandroupolis) was also

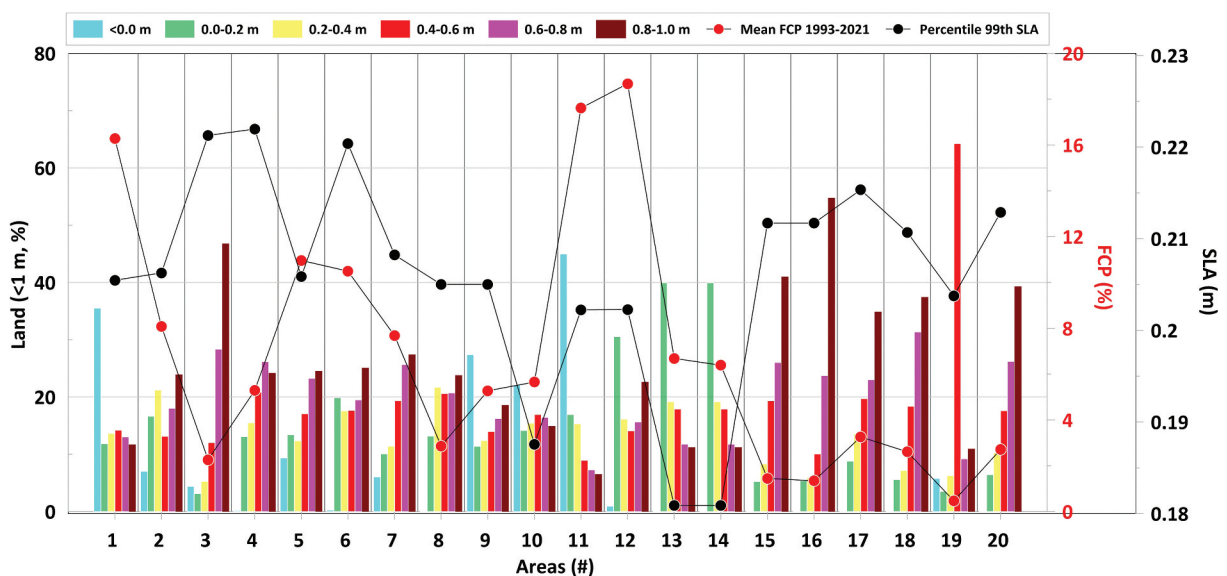


Figure 7. Percentage (%) of land elevation categories (6 categories: <0 m, 0–0.2 m, 0.2–0.4 m, 0.4–0.6 m, 0.6–0.8 m, 0.8–1.0 m) derived from the set of land cells below 1 m of each study area (1–20). The Flood coverage percentages (FCP, %) averaged from daily values (zero values excluded) and the 99th percentile of Sea level Anomaly (SLA, m) over the 1993–2021 period are shown for its study area.

characterized by high SLA levels but with quite few low-lying land cells (only <10% of all cells was less than 20 cm and more than 45% was over 0.8 m), reducing the inundation impact over the inland coastal zone (FCP

<4%). Area 4 (Chios) also revealed very small FCPs (<5%) due to the large area characterized by high land elevations (<30% is lower than 0.4 m). Although, in Area 6 (Rethymno), the maximum SLA ranged at similarly

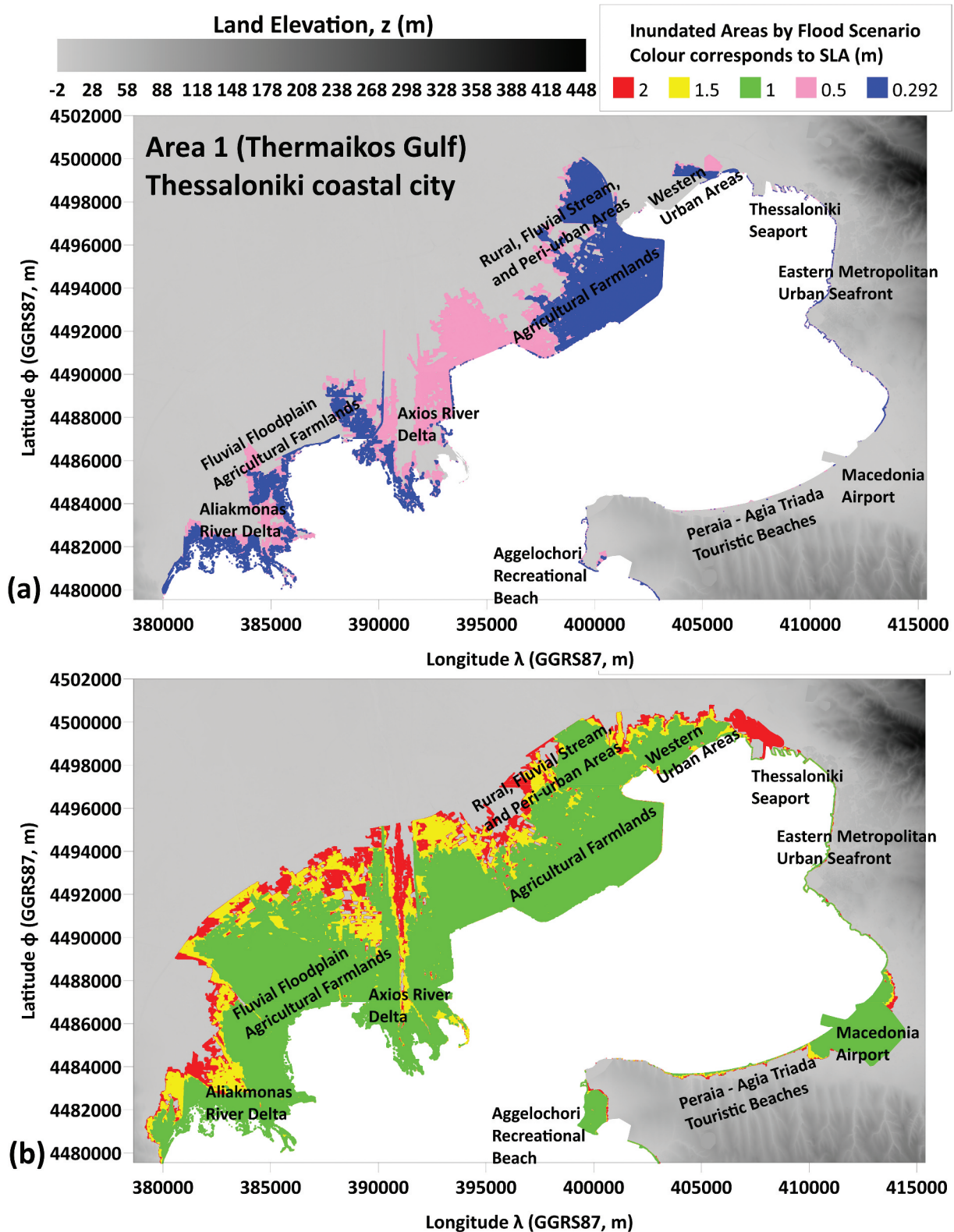


Figure 8. Maps of flood coverage (inundation areas) under the (a) maximum Sea level Anomaly (SLA) derived from the 1993–2021 period ($SLA_{max} = 0.292$ m) and a hypothetical scenario ($SLA = 0.5$ m) over area 1 (Thermaikos Gulf). (b) Flood coverages under more extreme scenarios ($SLA = 1, 1.5$ and 2 m) are also presented. Inundation areas induced by lower SLA are overlaid to the ones driven by higher SLA values. The land terrain showing the area’s elevations is presented with shades of gray. Similar maps for all study areas (2–20) are provided as supplementary material (Figures S2–S20).

high levels as Areas 3 and 4 (99th Percentile SLA >0.22 m), the FCP was three time larger (>10%) due to the more extended lowing-area; the area with elevation over than 0.8 m was less than 23%, while almost 40% was lower than 0.4 m. The very high FCPs computed for the southern Ionian areas (Areas 11 and 12) were related to both relatively high SLA levels (>0.20 m) and the extended low-lying land (e.g. >40% of Area 11 lay even below the mean sea level: <0 m), allowing extended flooding, especially during strong storm surge events (>16% mean FCP).

The inundation extends under four hypothetical sea level elevation scenarios (0.5–2.0 m) and the maximum realistic record, derived during the study period over the Thermaikos Gulf's coastal zone (Area 1), are presented by overlaid discretely colored areas in Figure 8. It is shown that under the maximum realistic sea level conditions for Area 1, derived from the satellite SLA observations (SLA = 0.292 m; Figure 8a), the flooded waters covered large areas located at the western coast of the gulf, especially over the lowland agricultural areas, and around the two, environmentally protected, main river deltas

(Androulidakis et al. 2021). Note that Area 1 is characterized by a large percentage of land elevation below zero (35%; Figure 7), which is mainly located along its western coast (Figure 8). Under higher sea levels (e.g. SLA = 0.5 m; Figure 8a), the simulated flooded area is expanded along the entire western coast (overall FA = 56 km²). The entire western coastal zone up to 4 km inland is even more exposed to extended flooding under extreme conditions of SLA between 1–2 m (FA = 120–180 km²; Figure 8b). Under these extreme conditions, potential inundation may also occur over the urban area of the Thessaloniki port in the north and around the airport of Thessaloniki (Macedonia Airport) at the eastern coast. The daily evolution of the FCP for Area 1 (days with zero FA excluded) during the entire study period is presented in Figure 9a, showing a clear positive trend from approximately 15% in 1993 to 17% at the end of the 29-year period. A peak close to 25%, associated to the SLA = 0.292 m (Figure 8a), is observed at the end of 2009 (Figure 9a). The same year is also the datum of the upward shift (Figure 9b), dividing the 29-period in two separate periods based on the Pettitt's homogeneity test. The FCP averaged over two

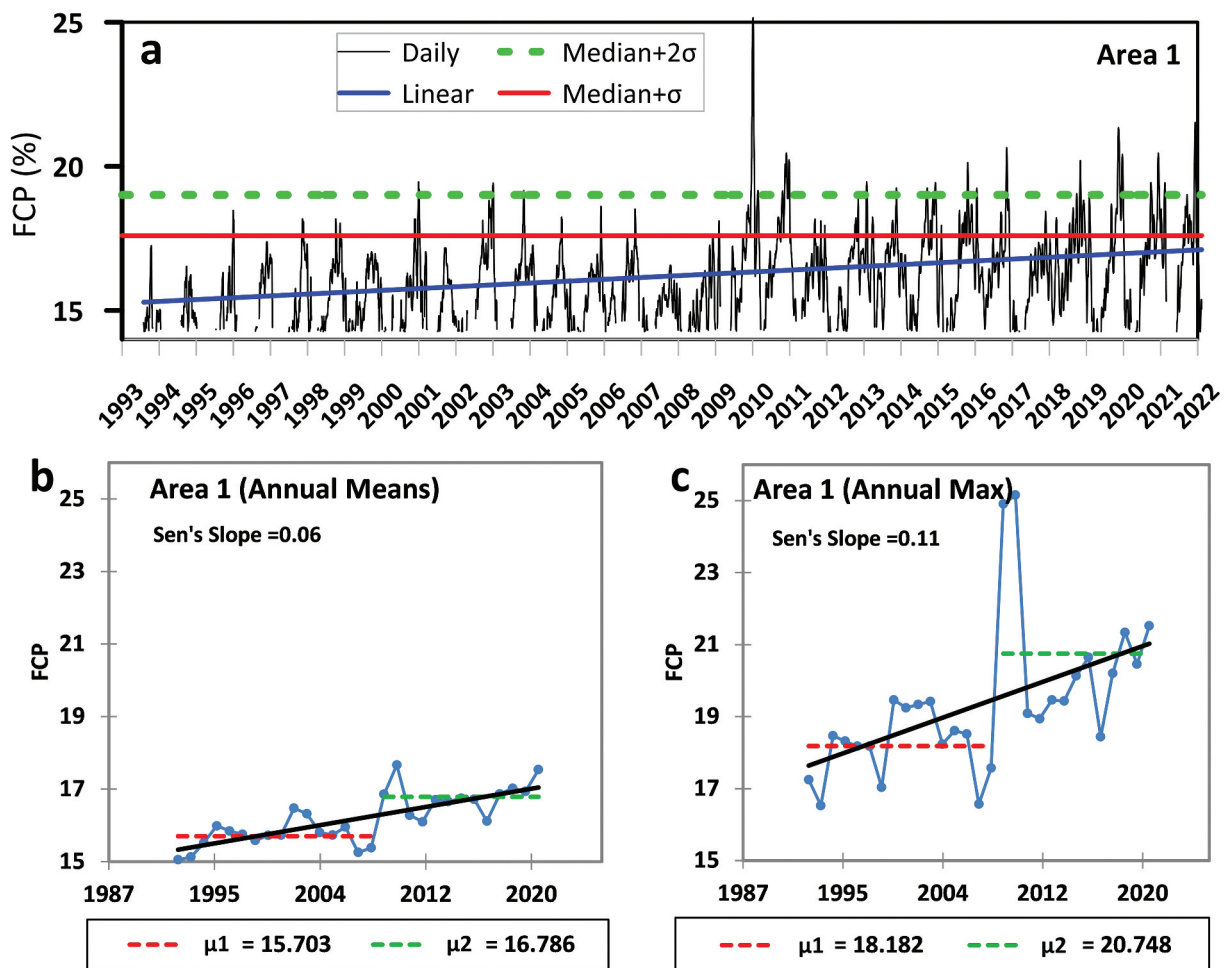


Figure 9. (a) daily evolution of Flood coverage percentage (FCP:0–1) for area 1 (Thermaikos Gulf) during 1993–2021. The green dashed and red lines indicate the median+ σ and median + 2 σ levels. The linear regression is also marked with blue line. The zero FCP values (no flooding) are excluded from computations. Evolution of annual (b) mean and (c) maximum FCP values. The Sen's Slope (%/year) and the linear regression (black line) are also shown. Pettitt's test for homogeneity was also applied to the two annual timeseries showing the shifts in the mean levels (μ_1 , μ_2).

Table 4. Sen’s slopes (%/year) and difference of $\mu_2-\mu_1$ derived from the Pettitt’s homogeneity test of the mean and maximum annual FCP (%/year) for the 20 study areas during the 1993–2021 period. All trends are statistically significant based on the MK trend test ($p_{\text{values}} < 0.01$).

A/A	Mean Annual		Max Annual		A/A	Mean Annual		Max Annual	
	Sen’s Slope	$\mu_2-\mu_1$ (%)	Sen’s Slope	$\mu_2-\mu_1$ (%)		Sen’s Slope	$\mu_2-\mu_1$	Sen’s Slope	$\mu_2-\mu_1$
1	0.06	1.08	0.12	2.60	11	0.07	1.47	0.17	3.30
2	0.11	1.90	0.17	3.90	12	0.19	3.58	0.39	6.70
3	0.02	0.38	0.04	1.38	13	0.04	0.75	0.08	1.65
4	0.11	2.15	0.23	5.20	14	0.06	1.01	0.08	1.70
5	0.15	2.90	0.19	2.68	15	0.02	0.46	0.09	1.58
6	0.25	4.50	0.40	6.20	16	0.07	0.48	0.06	1.10
7	0.03	0.60	0.02	0.50	17	0.02	1.25	0.22	3.75
8	0.11	2.10	0.43	7.50	18	0.04	0.67	0.09	1.50
9	0.07	1.24	0.10	2.02	19	0.01	0.14	0.02	0.30
10	0.01	0.24	0.02	0.34	20	0.05	0.95	0.14	3.20
ALL	0.07	1.39	0.15	2.86					

periods, before (μ_1) and after (μ_2) the datum of the upward shift was also computed and shown in Figure 9. The difference between the two FCP means (before and after 2009; $\mu_2-\mu_1$) for Area 1 is around 1.1% for the mean annual levels (Figure 9b). The Sen’s Slope is almost double for the maximum annual FCP levels (Sen’s Slope = 0.11%/year; Figure 9c) showing that the increasing trend is stronger for the more severe flooding conditions than the mean annual levels, confirming the increase of the maximum inundation extension throughout the years, especially after 2009. The $\mu_2-\mu_1$ for the two periods (before and after 2009) is also double (2.4%) for the maximum values compared to the mean levels. The

results of Area 1 agree with the general Sen’s Slope (Table 4), derived from all 20 study areas’ slopes (0.07%/year for the mean levels and 0.15%/year for the maximum levels). In all study cases, the trends are positive and statistically significant ($p_{\text{value}} < 1\%$) with stronger slopes for Area 6 (Rethymno) considering both mean (0.25%/year) and maximum (0.40%/year) annual FCP levels. These follow the respective SLA trends, which showed that the Cretan Sea revealed the strongest inter-annual trend of the SLA 99th percentiles (3.5 mm/year; Table 2). In all cases, the upward shift took place after 2009, ranging around 1.39% for the mean and 2.86% for the maximum levels (Table 4). The empirical significance

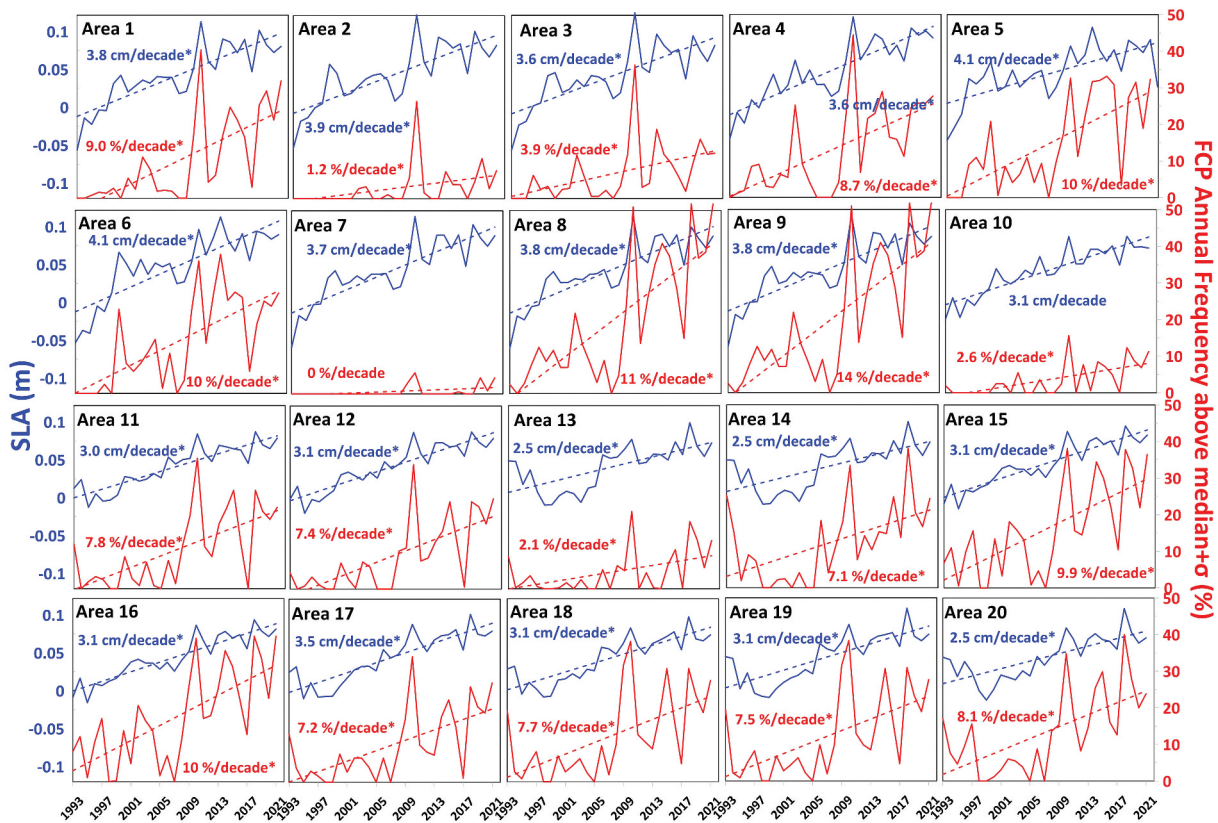


Figure 10. Annual evolution of mean Sea level Anomaly (SLA; blue lines) and annual frequency of flooding indices above median + σ level (red lines) for 20 coastal areas during 1993–2021. The linear regressions and the respective Sen’s slopes for each case are also shown.

level (p_{value} ; significance level of 1%) was performed for all study areas confirming that the hypothesis of a shift in the mean in the dataset is valid. As a matter of fact, inundation maps for all study areas, similar to Area 1 (Figure 8) are provided as supplementary material (Figures S2-S21).

Before 2009, the daily FCP values were usually lower than the thresholds derived from the summation of the median with once ($\text{median}+\sigma$) or twice ($\text{median}+2\sigma$) the standard deviation (σ) representing two kinds of extreme levels for the overall FCP values during the 1993–2021 period (Figure 9a). These two FCP thresholds were used to detect occurrence frequency of the severe flooding events during all years of the study period. In particular, the occurrence frequency of the FCP over the $\text{median}+\sigma$ for all study areas is presented in Figure 10. The FCP exceeds the extreme threshold at several dates during the most recent 13 years (2009–2021), when the highest SLA occurred. The interannual variability of both mean SLA and percentages of FCP for each case ranges at different levels between the 20 study areas, confirming the strong spatial variability of both sea level and flooding levels shown in Figure 7. In most of the areas (except Area 7), the interannual trend of the frequency is positive and statistically significant showing very high frequencies during several years after 2009, in agreement with the trends of the mean annual SLA; the variability between the two variables (SLA and FCP) is very similar in all cases. As shown in the regional SLA fields (Section 3), the stronger SLA trends were detected for the southern regions of the AICS (Figure 3) and especially in the Cretan Sea (Table 2). Thus, high coastal Sen's Slopes for Area 5 (Ierapetra; 4.1 cm/decade) and Area 6 (Rethymno; 4.1 cm/decade) resulted to stronger and more frequent flooding events ($>\text{median}+\sigma$) throughout the years (10%/decade; Figure 10). Very strong trends of severe flooding were also computed for several areas of the Ionian Sea (e.g. Areas 15 and 16, ~10%/decade) that are more exposed to storm surge events associated to the impacts of deep atmospheric depression systems (Makris et al. 2023), e.g. Medicanes (Nastos, Papadimou, and Matsangouras 2018) that form over the central Mediterranean and propagate toward the Ionian Sea (Androulidakis et al. 2023; Lagouvardos et al. 2022). Although the mean FCP levels were relatively low for these two areas mainly due to their topographic characteristics (Figure 7), the extreme flooding events ($>\text{median}+\sigma$) were more frequent in the last decade resulting to strong interannual trends from 1993 until 2021. Very strong flooding trends were also computed along the northern Aegean coastal zone, particularly in Thermaikos Gulf (Area 1; 9%/decade) and especially along the north-

western coastal zone (Areas 8 and 9; >11%/decade), which are exposed to major coastal erosion processes (Kombiadou and Krestenitis 2012; Tsoukala et al. 2015) that may downgrade the natural protection of the coastal zone against sea-originated inundation.

4.2. Seasonal variability of coastal inundation

The FCP daily variability presented in Figure 9a for Area 1 is characterized by a clear seasonal signal with higher values in autumn (September–November) and winter (December–February) and lower levels during spring (March–May) and summer (June–August). The seasonal distribution of FCP for all study areas is presented in Figure 11a. In all cases, the higher FCP percentages were computed for autumn, reaching very high levels ($>20\%$) for Areas 11 (Katakolo) and 12 (Laganas) located in the south-central Ionian Sea. The higher autumn FCP values are related to the occurrence of storm surges, related to low-pressure systems (e.g. Medicanes) which are mainly formed in the autumn and early winter months (September to January; Nastos, Papadimou, and Matsangouras 2018). The autumn mean SLA from all years showed unified variability characteristics (1st group; Figure 5e) determining the high FCP autumn levels. There are a few cases during the spring months, and even fewer during summer, which implies that the “warm” season of the year is not a period of Medicanes-induced storm surges (Zhang et al. 2021). In agreement with the Medicanes' seasonality, high FCP levels were also detected in winter with increased values in Katakolo and Laganas (~17%; Figure 11a). Higher FCP values, comparatively to winter levels, were also computed in the summer period for the northern Aegean areas (e.g. Thermaikos, Nestos, Alexandroupolis). The mean seasonal cycle of sea level peaks between October and November everywhere in the Mediterranean Sea, except in the Aegean Sea where it peaks in August.

The interannual variability of the seasonal FCP values, spatially averaged over the selected 20 study areas, confirms the higher flooding level during autumn, which is characterized by the highest Sen's Slope (1.3%/decade) among all seasons. Although the lowest FCP levels were detected for spring in relation with the lowest spring SLA values (Figure 5f), the respective trend slope was also high (1.3%/decade). Winter and summer trend slopes were also positive, but weaker, ranging around 1%/decade and 1.1%/decade, respectively. Almost zero spring values were only detected during the first decade (1993–2003) indicating the total absence of flooding events (e.g. 1993, 1995, 1997, and 2003). This result agrees with the low mean spring SLA levels observed during the same years (between -0.05 to -0.1 m; Figure 5b). The SLA

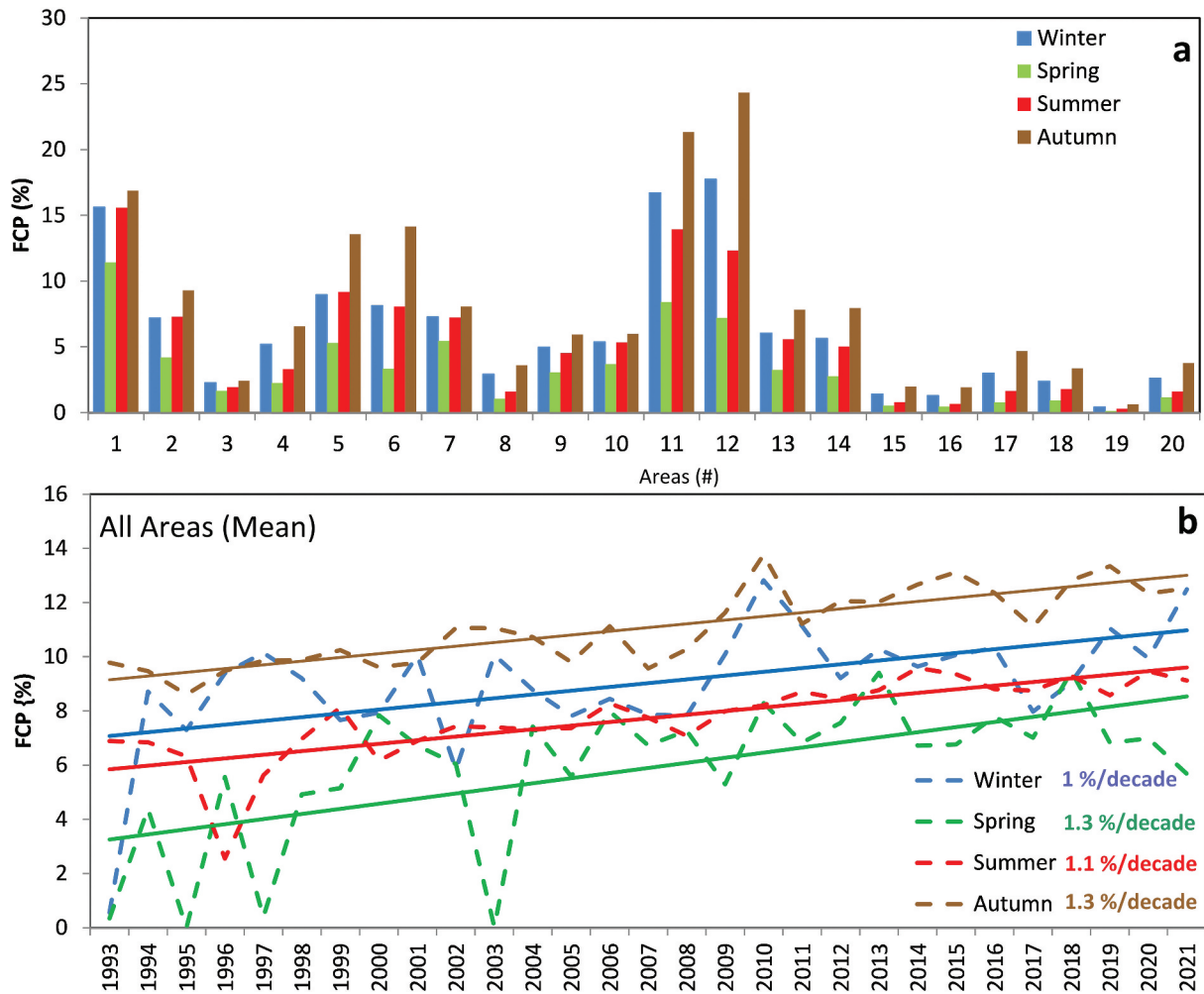


Figure 11. (a) seasonal Flood coverage percentage (FCP, %) for all study areas during 1993–2021 and (b) evolution of mean FCP averaged over all areas and seasons. The linear regressions and the respective Sen's slopes (%/decade) for each season are shown. All trends are statistically significant based on the MK trend test ($p_{\text{values}} < 0.01$).

increase during spring after 2003 also enhanced the spring flooding conditions in agreement with Cavicchia et al. (2014) who showed that beside autumn and winter a low number of Medicanes may also form in the spring months. The interannual variability of the seasonal SLP 10th percentiles over the entire AICS domain shows that the lowest atmospheric pressure levels for all seasons occurred after 2003 (Figure 12), and especially after 2010 for spring (Figure 12b). These low SLPs are associated with the formation of low-pressure systems that control the storm surge variability over the region. De la Vara et al. (2021) found the highest Mediane activity in the winter months, with an intermediate activity also in spring and autumn. Although De la Vara et al. (2021) also argued that there is no Mediane activity in the summer months, the interannual variability of the summer minimum SLPs during the 1993–2021 period was characterized by a clear ($p_{\text{value}} < 5\%$) change after 2003, with generally low-pressure levels during the following period based on the Pettitt's homogeneity test (Figure 12c). This increase is probably related to

frequency increases (or intensification) of more ordinary low-pressure systems than to Medicanes which are mainly formed during autumn and winter. Androulidakis et al. (2015), based on climatic predictions, showed that there is a possible 10% increase of the future (21st century) storm surges during the summer months. Although cyclogenesis in the Mediterranean is more intense from November to March, there are types of cyclones, like Sahara cyclones, whose frequency is larger in summer (Lionello et al. 2006). The FCP peak of 2010 (Figure 11b) occurred during autumn and winter (>12%), when the highest SLA levels occurred (>0.15 m; Figure 5).

4.3. Coastal inundation hazard index

To identify a generic categorization of coastal impacts from the flood inundation modeling output, a case-specific and heuristic Coastal Inundation Hazard Index (CIHI) was defined as the product of the Frequency of Occurrence (FO, %) of the days with extreme $FCP_{i,j}$ multiplied with the temporal mean of the $FCP_{i,\text{ext}}$

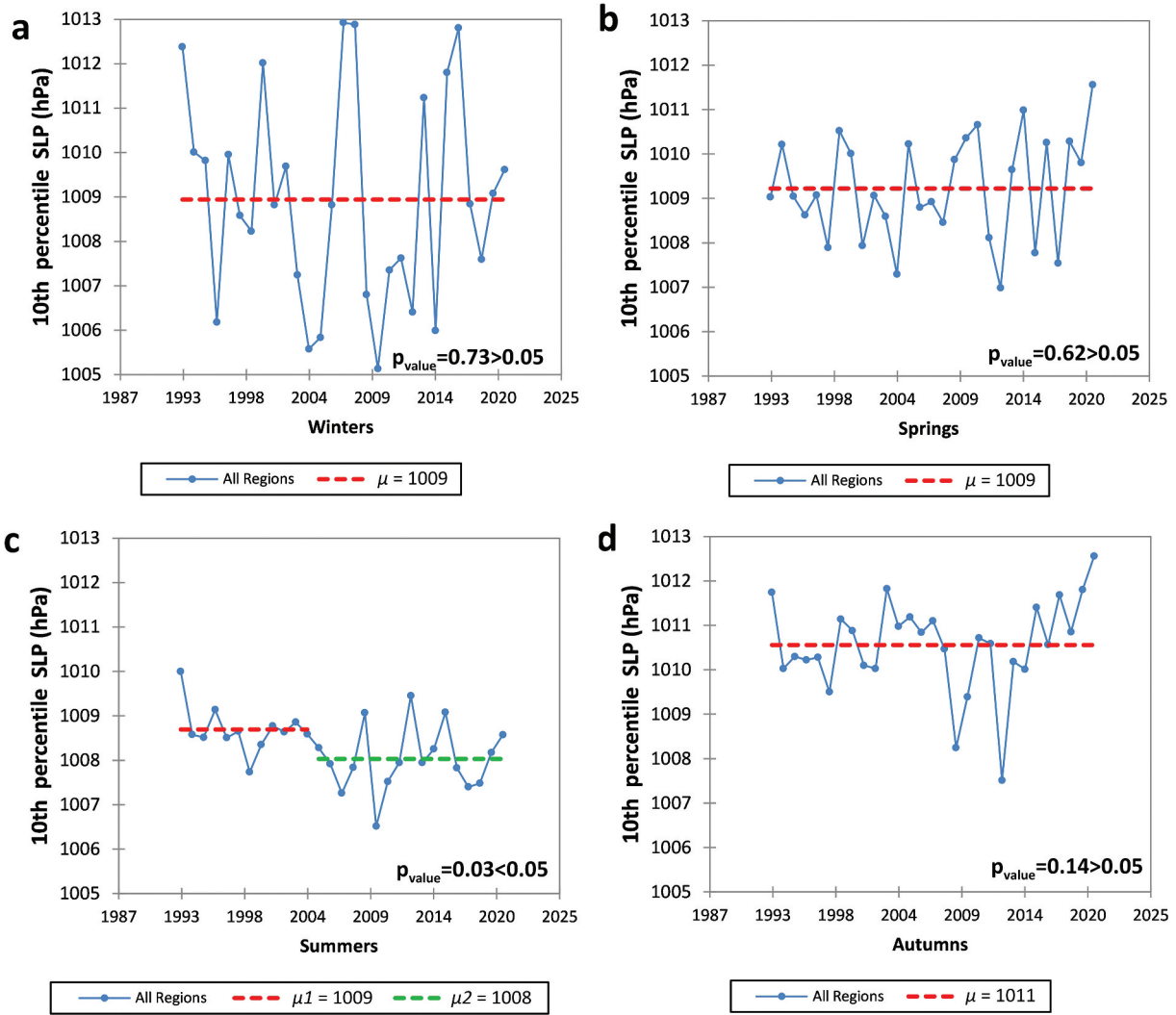


Figure 12. Pettitt's tests for homogeneity for all (a) winters, (b) springs, (c) summers, (d) autumns based on the 10th percentiles of Sea level pressure (SLP) over the AICS domain (all regions), showing the potential shifts in the mean levels (μ , μ_1 , μ_2). The p_{value} (alpha = 5%) of the homogeneity test (if there is a date at which there is a change in data) for each season is also shown.

(from the daily values, i , of the 1993–2021 period), and calculated for each study area (j) as shown in Equation 3. The average ($FCP_{i,ext}$) _{j} is expressed by the mean of the $FCP_{i,j}$ values above the sum of the median and standard deviation ($>median + \sigma$, %) derived from the entire study period for each study area.

$$CIHI_j = FO_j \times \overline{FCP_{i,extj}} \quad (3)$$

The CIHI values were normalized over their min – max range for the 20 studied areas in Greece, to produce individual hazard index results for each of them directly comparable to each other (i.e. ranked values are case-specific), by following a Likert scale classification ranging from very low to very high corresponding to a 1–5 ranking system. The lower and higher CIHI values were chosen as the lower and upper limit of the Likert scale, equally dividing the intermediate ranks of the scale. The ranking of the 20 study areas along the AICS coastal zone, based on the CIHI index, is presented in Table 5. Although this is a case-specified

index derived from the 20 study areas, it can be considered representative for the entire Greek coastal zone, since the flooding conditions, the topography characteristics and the sea level of the 20 study regions are characteristic of the entire Greek coastline. The lowest CIHI (1) was derived for several study areas that both FO and mean $FCP_{i,ext}$ were low (e.g. FO = 0.6% and mean FCP = 9.2% for Pineios). Five areas (Areas 1, 5, 6, 11, 12) with CIHI larger than 3 were detected, characterized by a higher hazard of coastal inundation, as derived for the 1993–2021 period. Thermaikos Gulf (Area 1) and especially its western coastal area (Figure 8) revealed high FO (10.4%) of extended flooding ($FCP_{i,ext}$), while the mean $FCP_{i,ext}$ was around 19% resulting to CIHI = 4. More hazardous flooding conditions (CIHI = 5) were detected for the two areas in Cretan Sea (Ierapetra and Rethymno) showing FO > 14% and mean $FCP_{i,ext}$ > 16%. The highest 99th percentiles of SLA (Figure 4b) and the strongest interannual trend of the 99th percentiles (3.5 cm/decade; Table 2) among all AICS sub-regions were

Table 5. Means and ranking (1–5) of frequency of occurrence (FO, %), mean Flood coverage percentage (mean- FCP_{i,ext_j}) (%) and coastal inundation hazard index (CIHI*) derived for the 20 coastal areas and the 1993–2021 period. The FO and FCP_{ext} levels were derived from the daily values with $FCP > \text{median} + \sigma$. Ranking: 1 (very low), 2 (low), 3 (medium), 4 (high), 5 (very high). CIHI over 3 (high and very high) are highlighted with red color.

j	Area	FO (%)	(mean- FCP_{i,ext_j}) (%)	CIHI (product)	CIHI (Ranked)
1	Thermaikos	10.4	18.8	0.019	4
2	Nestos	2.8	14.4	0.004	1
3	Alexandroupoli	2.8	5.0	0.001	1
4	Chios	13.0	1.3	0.013	3
5	Ierapetra	14.6	16.8	0.025	5
6	Rethymno	14.0	19.6	0.027	5
7	Pineios	0.6	9.2	0.001	1
8	Agiokampos	14.2	8.3	0.012	2
9	Katerini	19.7	7.4	0.015	3
10	Kalamata	3.5	6.5	0.002	1
11	Katakolo	10.6	26.4	0.028	5
12	Laganas	9.0	32.1	0.029	5
13	Manolada	4.4	9.8	0.004	1
14	Patra	6.8	9.7	0.007	2
15	Argostoli	16.0	2.9	0.005	1
16	Livadi	17.4	2.9	0.005	1
17	Vassiliki	10.0	7.5	0.008	2
18	Palairos	12.3	4.5	0.006	1
19	Preveza	12.2	0.9	0.001	1
20	Igoumenitsa	13.2	5.9	0.008	2

*Note that the CIHI ranked output is case-specific to the 20-area analysis along the Greek coastal zone and not valid for “global” comparisons application.

computed for the Cretan Sea. Similarly, high CIHI values were computed for two areas of the South Ionian (Katakolo and Laganas), mainly associated with the extended flooding area (mean $FCP_{i,ext} > 26\%$) and less with the temporal occurrence frequency of extreme floods (FO was around 10%); the larger FCP values among all study areas were computed for Laganas (mean $FCP_{i,ext} = 32\%$). Very low CIHI levels were derived for almost half of the study areas (9), located at all sub-regions of the AICS domain. Nestos and Alexandroupolis (Areas 2 and 3) in the northern coast of the Aegean were ranked with $CIHI = 1$ mainly due to the low occurrence frequency of extreme floods (2.8%); very weak interannual trends were also computed for these two areas (1.2%/decade and 3.9%/decade; [Figure 10](#)). Low ($CIHI = 2$) and very low ($CIHI = 1$) hazardousness was also estimated for several areas of the central northern Ionian Sea (Manolada, Patra, Argostoli, Livadi, Vassiliki, Palairos, Preveza, Igoumenitsa) although the occurrence frequency for most of them was relatively high ($>10\%$); the low values of CIHI in these cases are mainly related to the modeled flood extents, i.e. smaller inundated areas ($<10\%$). Although low CIHI values indicate a weak hazard level of the overall selected ensemble of coastal areas, flooding impacts at specific low-lying parts of the study’s coastal zones can be quite high due to a large occurrence frequency of extreme events. Although very low overall CIHIs were derived for Argostoli and Livadi ($CIHI = 1$), the flooding hazard for the low-lying areas of these cases remains relatively high due to the high frequency occurrence levels ($>16\%$). Moreover, there are areas with very high FCPs (e.g. Nestos) that resulted to low CIHI indices due to the very low frequency of occurrence ($<3\%$).

Although it is not very common, this type of areas may experience extended flooding as derived by the computed $FCP_{i,j}$. Therefore, although the CIHI index may provide very useful information about the hazard threat of a coastal area, it is necessary to evaluate separately the levels of both flooding coverage (spatial component) and frequency (temporal component).

5. Discussion

The variability of the SLA over the AICS has been evaluated with the use of satellite-derived observations during a 29-year period (1993 to 2021). The SLAs along the coastal zone of the AICS domain were used to force numerical simulations of coastal inundation at 20 selected low-lying areas to estimate their hazard levels due to increase in sea level elevation. Targeted comparisons of the satellite-derived SLA estimations against coastal tide-gauges showed that especially the high sea level peaks were well captured by the satellites, efficiently describing the extreme conditions, responsible for the formation of littoral inundation events over the coastal zone of the AICS domain. Nevertheless, the gridded coastal values of SLA over the entire Mediterranean basin and its nearshore marine areas, derived from interpolations of satellite altimetry over certain tracks, are known to have contained discrepancies and underestimations of actual sea levels in the past induced by the smoothing effects of gridding. However, several researchers have recently pointed out the ongoing quality enhancement of such products (e.g. Cipollini et al. 2017).

It is furthermore noted that the sea level dataset does not include the influence of the high-frequency sea-surface dynamics controlled by wave-induced

processes that also contribute to coastal flooding (e.g. by wave runup and overtopping). The SLA observations contain though the most important components that control the sea level variability related to long- and mid-term coastal inundation, such as the sea level rise (due to climatic changes, e.g. global warming effect) and especially the contribution of storminess. The latter controls the formation of storm surges and the respective coastal flooding during severe low-pressure meteorological systems. Storm surge is the main controlling factor of inundation variability over the coastal zone, especially for floods that extend further inland than the proximal area to the coastline. Waves can contribute to the total water level by means of wave setup through the radiation stress in the surf zone (Wolf 2009), and mainly affect the coastal area by onshore wave runup and overtopping of protection structures. These can cause damages on the built and natural environment along the coast, but mainly in a zone rather close to the shoreline, at least for the Greek coastal zone that is not affected by high and long swells.

The numerical simulations of coastal inundation were performed with CoastFLOOD model (Makris et al. 2023) at 20 study areas of the AICS domain, covering the same 29-year period. The simulated results were used to provide daily estimations of flooded area based on the satellite-derived SLA along the respective shoreline (boundary condition) of its coastal area. CoastFLOOD is a reduced complexity hydraulic flood model, based on the Manning-type mass balance approach for coastal inundation by a wet/dry storage cell concept on fine-resolution raster grids. Therefore, it is susceptible to inconsistencies of the implemented DEM that may induce inaccuracies to flooded area derivation (Karamouz and Fereshtehpour 2019; West, Horswell, and Quinn 2018). We consider that the use of a quite high resolution raster grid ($dx = 5$ m) may include the most prominent topographic features in the coastal zone, such as the man-made infrastructure, urban settings, ports, coastal structures, roads, and the natural land formations in the floodplain, such as farmlands, beach slopes, dunes, barriers, geodetic anomalies, and other rural land elevation peculiarities (Kahl et al. 2022; Murdukhayeva et al. 2013). Their terrain roughness is also considered, thus including detailed representations of flood flow bottom friction, by taking advantage of freely available official EU-scale land cover data (see Appendix). Nonetheless, CoastFLOOD does not account for the effects of porous bed percolation or floodwater mass flow in sewage and drainage systems, land level conduits, bridge culverts, wells, shafts, etc. in the urban environment. The coastal inundation levels are related to three main factors: a) the sea level high peaks, and b) the topographic characteristics of each coastal area, and c) the flood-prone land's terrain roughness.

We have categorized the study areas based on the computation of a heuristic Coastal Inundation Hazard Index (CIHI) that is determined by the occurrence frequency of extreme floods (temporal component) and their coverage area (spatial component). The CIHI ranking of the coastal areas range from 1 to 5 showcasing the hazard level (very low to very high) for each area, and it is case-specific (i.e. implementing study-related min-max thresholds). High flooding levels occurred at coastal regions of either extended low-lying areas and/or high sea level rise. Although, high storm surges may occur in the Ionian Sea, the topography characteristics of several coastal areas in the central and northern parts (e.g. Argostoli, Livadi, Vassiliki, Palairos, Preveza, Igoumenitsa) controlled the flooding extents, resulting to relatively low CIHI (<3). Two areas of the southern Ionian (Katakolo and Laganas) were characterized by extended inundation incidents during the 1993–2021 period due to both high sea levels and extended low-lying areas in the coastal zone (CIHI = 5). The Sen's Slopes of the inundation levels computed for all 20 study areas were positive (increasing trends) and statistically significant (0.07%/year for the mean levels and 0.15%/year for the maximum levels). In all cases, a clear upward shift took place after 2009, ranging around 1.39% for the mean and 2.86% for the maximum levels. The highest SLA for all areas occurred in the years of 2010, 2013, 2014, 2016, 2018, 2019, 2020, and 2021, all during the last 12-year period, confirming the strong inter-decadal increase that enhanced the flooding levels after 2009. Moreover, in most of the areas, the interannual trend of the frequency of extreme floods ($>$ median+standard deviation) is positive and statistically significant, revealing high frequencies during several yearly cycles after 2009 in agreement with the trend of the mean annual SLA. Very strong trends of extreme flooding were computed for the Cretan Sea, where the strongest trends of maximum SLA occurred. More hazardous flooding conditions (CIHI = 5) were detected for the two areas of the Cretan Sea (Ierapetra and Rethymno) showing both high frequency ($>14\%$) and large inundation areas ($>16\%$), agreeing with findings in relevant literature (Martzikos et al. 2018; Makropoulos et al., 2015). Strong trends of extreme flooding were also derived for several areas of the Ionian Sea (e.g. Argostoli and Livadi, $\sim 10\%$ /decade) that are more exposed to storm surge events associated to the impacts of severe low-pressure systems (e.g. Medicanes; Nastos, Papadimou, and Matsangouras 2018). Romera et al. (2017) investigated the future formation of Medicanes up to 2100, and estimated a future reduction in their number but an increase in the intensity of the strongest cyclones that may lead to more severe storm surges and respective coastal floods during the 21st century. The area between Sicily and Greece extending southward to the coast of Libya is the second preferred area where

Medicanes usually form (Cavicchia, von Storch, and Gualdi 2014). These extreme meteorological phenomena are triggered by the simultaneous formation of cold air aloft and the presence of very warm surface waters. The increased sea surface temperature (SST) trends during the last decades over the Mediterranean Sea (Androulidakis and Krestenitis 2022; Darmaraki et al. 2019) formed more favorable conditions (warmer water pools), strengthening their intensity and the accompanying storm surges.

To extend the findings of our research, the next step is to develop climatic projections of coastal inundation under different climate-change scenarios (Makris et al. 2023) and to further test if the current increasing trends in the AICS domain are also probable in the 21st century (Krestenitis et al. 2021). Moreover, for the complete assessment of integrated seawater flood probability at coastal sites of the AICS domain that are at risk due to littoral inundation (Masina, Lamberti, and Archetti 2015), the next step is to include satellite observations of waves. This will allow for a better estimation of the combined effect of waves and water levels on coastal flooding, especially in shoreline proximal zones along low-lying littoral areas.

6. Conclusions

In the current study, the Sea Level Anomaly (SLA) variability over the Aegean, Ionian, and Cretan Seas (AICS) and the associated coastal inundation along the coastline were investigated based on long-term sea level observations, high-resolution land elevation data, and numerical simulations of coastal flooding.

The general SLA trend over the entire AICS domain was 3.6 mm/year, which is higher than the overall Mediterranean (2.44 mm/year; Bonaduce et al. 2016) and the eastern Mediterranean (3.1 mm/year; Mohamed and Skliris 2022) trends. The highest Sen's Slopes were derived for the Aegean Sea with strongest trends for the SW Aegean (4.1 mm/year). Moreover, the Cretan Sea revealed the strongest interannual trend of the maximum SLA values (99th percentiles; 3.5 mm/year). The highest SLA levels were detected primarily in autumn and secondarily in winter, while the lowest seasonal means occurred in spring in agreement with Tsimplis and Shaw (2010). The inundation levels and the respective positive trends were higher in autumn associated with the low-pressure systems (storm surge formation) that mainly develop in the autumn and early winter months (September to January). Although the lowest inundation levels were detected during spring season related to the lowest spring SLA values (caused by the coincidence of neap tides with extended calm weather periods of high barometric systems), the respective trend slope of spring floods was also high.

This is in agreement with Cavicchia et al. (2014), who showed that besides autumn and winter a significant number of severe storms may also form during spring. The Ionian Sea revealed weak SLA trends for winter and spring, while both of its northern and southern parts followed the stronger general trend of the AICS domain in the summer and autumn seasons. This is due to the high occurrence frequency of the atmospheric low-pressure systems that usually form over the central Mediterranean (between the northern African coast and the Ionian; Cavicchia, von Storch, and Gualdi 2014) during early- to mid-autumn, contributing to the storm surge formation along the western coasts of Greece (Androulidakis et al. 2015, 2023).

The meteorological residual of the sea level, controlled by Sea Level Pressure (SLP) and winds, shows a strong spatial variability over the AICS domain, with a stronger SLP impact over the Aegean Sea and more significant wind effects in the Ionian Sea. Moreover, the sea level variability is also controlled by the direction of the prevailing wind, whose effect varied along the topographically complicated AICS coastal zone. The occurrence of storm surges in the Ionian Sea is strongly related to the wind-induced accumulation of waters along the Ionian coasts, especially during severe low-pressure systems that usually form over the central Mediterranean. Androulidakis et al. (2023) showed that the accompanying winds of an extreme meteorological system in September 2020 (Ianos Mediane) increased the water level even before the landfall of the cyclone's core to the central and southern Ionian coastal zone. Similar conditions have mainly affected the large low-lying areas of the southern Ionian Sea, such as Katakolo and Laganas, characterized by both large inundation extents and high occurrence frequency of floods. On the contrary, the inverse barometer effect was more profound in the Aegean Sea due to the morphological complexity of the archipelago that reduced the wind impact on storm surge formation in comparison to the direct impact by the SLP (Krestenitis et al. 2011; Makris et al. 2023). Strong flooding trends were also computed along the northern Aegean coastal zone, particularly in Thermaikos Gulf (9%/decade) and especially along the north-western coastal zone (>11%/decade). These are exposed to coastal erosion processes (Kombiadou and Krestenitis 2012; Tsoukala et al. 2015) that might have downgraded the natural protection of the coastal zone against seawater inundation.

The 20 study areas represent different parts of the AICS coastal zone that are characterized by different morphological features and sea level conditions. The study areas were categorized based on the Coastal Inundation Hazard Index (CIHI), based on the occurrence frequency and flood coverage of

inundation events. The interannual trends and the seasonality of the flooding also showed intense variation between the study areas. Our approach and study findings provide useful information about the hazard level of sea level-induced coastal flooding in the AICS domain that can hopefully support more robust coastal zone management. We set the full assessment of coastal flood risk as a future goal, by further quantifying the exposure, vulnerability, and resilience of the study areas.

Acknowledgments

This study has been conducted using E.U. Copernicus Marine Service Information: SEALEVEL_EUR_PHY_L4_MY_008_068 (<https://doi.org/10.48670/moi-00141>) and EU-DEM v1.1 (<https://land.copernicus.eu/imagery-in-situ/eu-dem/eu-dem-v1.1>). The high resolution (5 m) land elevation dataset was provided by the official Greek service Hellenic Cadastre (<https://www.ktimatologio.gr/en>). Tide-gauge measurements were provided by the Hellenic Navy Hydrographic Service (HNHS; <https://www.hnhs.gr/en/>).

Disclosure statement

No potential conflict of interest was reported by the author(s).

References

- Adloff, F., G. Jordà, S. Somot, F. Sevault, T. Arsouze, B. Meyssignac, L. Li, and S. Planton. 2018. "Improving Sea Level Simulation in Mediterranean Regional Climate Models." *Climate Dynamics* 51 (3): 1167–1178. <https://doi.org/10.1007/s00382-017-3842-3>.
- Adloff, F., S. Somot, F. Sevault, G. Jordà, R. Aznar, M. Déqué, M. Herrmann, et al. 2015. "Mediterranean Sea Response to Climate Change in an Ensemble of Twenty First Century Scenarios." *Climate Dynamics* 45 (9): 2775–2802. <https://doi.org/10.1007/s00382-015-2507-3>.
- Afshari, S., A. A. Tavakoly, M. A. Rajib, X. Zheng, M. L. Follum, E. Omranian, and B. M. Fekete. 2018. "Comparison of New Generation Low-Complexity Flood Inundation Mapping Tools with a Hydrodynamic Model." *Journal of Hydrology* 556:539–556. <https://doi.org/10.1016/j.jhydrol.2017.11.036>.
- Alvarado-Aguilar, D., J. A. Jiménez, and R. J. Nicholls. 2012. "Flood Hazard and Damage Assessment in the Ebro Delta (NW Mediterranean) to Relative Sea Level Rise." *Natural Hazards* 62 (3): 1301–1321. <https://doi.org/10.1007/s11069-012-0149-x>.
- Androulidakis, Y., V. Kolovoyiannis, C. Makris, Y. Krestenitis, V. Baltikas, N. Stefanidou, A. Chatziantoniou, K. Topouzelis, and M. Moustaka-Gouni. 2021. "Effects of Ocean Circulation on the Eutrophication of a Mediterranean Gulf with River Inlets: The Northern Thermaikos Gulf." *Continental Shelf Research* 221:104416. <https://doi.org/10.1016/j.csr.2021.104416>.
- Androulidakis, Y., K. Kombiadou, C. Makris, V. Baltikas, and Y. Krestenitis. 2015. "Storm Surges in the Mediterranean Sea: Variability and Trends Under Future Climatic Conditions." *Dynamics of Atmospheres and Oceans* 71:56–82. <https://doi.org/10.1016/j.dynatmoce.2015.06.001>.
- Androulidakis, Y. S., and Y. N. Krestenitis. 2022. "Sea Surface Temperature Variability and Marine Heat Waves Over the Aegean, Ionian, and Cretan Seas from 2008–2021." *Journal of Marine Science and Engineering* 10 (1): 42. <https://doi.org/10.3390/jmse10010042>.
- Androulidakis, Y. S., Y. N. Krestenitis, and S. Psarra. 2017. "Coastal Upwelling Over the North Aegean Sea: Observations and Simulations." *Continental Shelf Research* 149:32–51. <https://doi.org/10.1016/j.csr.2016.12.002>.
- Androulidakis, Y., C. Makris, Z. Mallios, I. Pytharoulis, V. Baltikas, and Y. Krestenitis. 2023. "Storm Surges and Coastal Inundation During Extreme Events in the Mediterranean Sea: The IANOS Medicane." *Natural Hazards, Springer* 117 (1): 939–978. <https://doi.org/10.1007/s11069-023-05890-6>.
- Anzidei, M., K. Lambeck, F. Antonioli, S. Furlani, G. Mastronuzzi, E. Serpelloni, and G. Vannucci. 2014. "Coastal Structure, Sea-Level Changes and Vertical Motion of the Land in the Mediterranean." *Geological Society, London, Special Publications* 388 (1): 453–479. <https://doi.org/10.1144/SP388.20>.
- Arcement, G. J., and V. R. Schneider. 1989. "Guide for Selecting Manning's Roughness Coefficients for Natural Channels and Flood Plains." *US Geological survey, Water supply paper* 2339.
- Aucelli, P. P. C., G. Di Paola, P. Incontri, A. Rizzo, G. Vilardo, G. Benassai, B. Buonocore, and G. Pappone. 2017. "Coastal Inundation Risk Assessment Due to Subsidence and Sea Level Rise in a Mediterranean Alluvial Plain (Volturno Coastal Plain–Southern Italy)." *Estuarine, Coastal and Shelf Science* 198:597–609. <https://doi.org/10.1016/j.ecss.2016.06.017>.
- Bates, P. D., R. J. Dawson, J. W. Hall, M. S. Horritt, R. J. Nicholls, J. Wicks, and M. Hassan. 2005. "Simplified Two-Dimensional Numerical Modelling of Coastal Flooding and Example Applications." *Coastal Engineering* 52 (9): 793–810. <https://doi.org/10.1016/j.coastaleng.2005.06.001>.
- Bates, P. D., and A. P. J. De Roo. 2000. "A Simple Raster-Based Model for Flood Inundation Simulation." *Journal of Hydrology* 236 (1–2): 54–77. [https://doi.org/10.1016/S0022-1694\(00\)00278-X](https://doi.org/10.1016/S0022-1694(00)00278-X).
- Bates, P. D., M. S. Horritt, and T. J. Fewtrell. 2010. "A Simple Inertial Formulation of the Shallow Water Equations for Efficient Two-Dimensional Flood Inundation Modelling." *Canadian Journal of Fisheries and Aquatic Sciences* 387 (1–2): 33–45. <https://doi.org/10.1016/j.jhydrol.2010.03.027>.
- Bevacqua, E., D. Maraun, M. I. Voudoukas, E. Voukouvalas, M. Vrac, L. Mentaschi, and M. Widmann. 2019. "Higher Probability of Compound Flooding from Precipitation and Storm Surge in Europe Under Anthropogenic Climate Change." *Science Advances* 5 (9): eaaw5531. <https://doi.org/10.1126/sciadv.aaw5531>.
- Bickici Arikan, B., and E. Kahya. 2019. "Homogeneity Revisited: Analysis of Updated Precipitation Series in Turkey." *Theoretical and Applied Climatology* 135 (1–2): 211–220. <https://doi.org/10.1007/s00704-018-2368-x>.
- Bijlsma, L., C. N. Ehler, R. J. T. Klein, S. M. Kulshrestha, R. F. McLean, N. Mimura, R. J. Nicholls, et al. 1996. "Coastal zones and small islands. In: Climate Change 1995: Impacts, Adaptations and Mitigation of Climate Change." *Intergovernmental Panel on Climate Change*. 289–324. Cambridge, UK: Cambridge University Press.
- Bonaduce, A., N. Pinaridi, P. Oddo, G. Spada, and G. Larnicol. 2016. "Sea-Level Variability in the Mediterranean Sea from Altimetry and Tide Gauges." *Climate Dynamics* 47 (9–10): 2851–2866. <https://doi.org/10.1007/s00382-016-3001-2>.

- Bosom, E., and J. A. Jiménez. 2010. "Storm-Induced Coastal Hazard Assessment at Regional Scale: Application to Catalonia (NW Mediterranean)." *Advances in Geosciences* 26:83–87. <https://doi.org/10.5194/adgeo-26-83-2010>.
- Bradbrook, K. F., S. N. Lane, S. G. Waller, and P. D. Bates. 2004. "Two-Dimensional Diffusion Wave Modelling of Flood Inundation Using a Simplified Channel Representation." *International Journal of River Basin Management* 2 (3): 211–223. <https://doi.org/10.1080/15715124.2004.9635233>.
- Burkey, J., 2023. "Mann-Kendall Tau-B with Sen's Method (Enhanced)." MATLAB Central File Exchange. Accessed March 1, 2023 <https://www.mathworks.com/matlabcentral/fileexchange/11190-mann-kendall-tau-b-with-sen-s-method-enhanced>.
- Calafat, F. M., D. P. Chambers, and M. N. Tsimplis. 2012. "Mechanisms of Decadal Sea Level Variability in the Eastern North Atlantic and the Mediterranean Sea." *Journal of Geophysical Research: Oceans* 117 (C9). <https://doi.org/10.1029/2012JC008285>.
- Calafat, F. M., T. Wahl, M. G. Tadesse, and S. N. Sparrow. 2022. "Trends in Europe Storm Surge Extremes Match the Rate of Sea-Level Rise." *Nature* 603:841–845. <https://doi.org/10.1038/s41586-022-04426-5>.
- Carillo, A., G. Sannino, V. Artale, P. M. Ruti, S. Calmanti, and A. Dell'aquila. 2012. "Steric Sea Level Rise Over the Mediterranean Sea: Present Climate and Scenario Simulations." *Climate Dynamics* 39 (9–10): 2167–2184. <https://doi.org/10.1007/s00382-012-1369-1>.
- Cavicchia, L., H. von Storch, and S. Gualdi. 2014. "A Long-Term Climatology of Medicanes." *Climate Dynamics* 43 (5–6): 1183–1195. <https://doi.org/10.1007/s00382-013-1893-7>.
- Cazenave, A., H. B. Dieng, B. Meyssignac, K. Von Schuckmann, B. Decharme, and E. Berthier. 2014. "The Rate of Sea-Level Rise." *Nature Climate Change* 4 (5): 358–361. <https://doi.org/10.1038/nclimate2159>.
- Chaniotaki, M., V. Kolovoyiannis, E. Tragou, L. A. Herold, I. E. Batjakas, and V. Zervakis. 2021. "Investigation of the Response of the Aegean Sea to the Etesian Wind Forcing." *Continental Shelf Research* 225:104485. <https://doi.org/10.1016/j.csr.2021.104485>.
- Chow, V. T. 1959. *Open-Channel Hydraulics*. New York: McGraw-Hill.
- Chrisafinos, D., and I. Kavvadas. 2016. "Quality Assessment of the New Backgrounds LSO25." *Proceedings of the 14th National Conference on Cartography of the Greek Scientific Association of Cartography "The cartography in a changing world"*, Thessaloniki, Greece (in Greek).
- Church, J. A., D. Monselesan, J. M. Gregory, and B. Marzeion. 2013. "Evaluating the Ability of Process Based Models to Project Sea-Level Change." *Environmental Research Letters* 8 (1): 014051. <https://doi.org/10.1088/1748-9326/8/1/014051>.
- Cid, A., M. Menéndez, S. Castanedo, A. J. Abascal, F. J. Méndez, and R. Medina. 2016. "Long-Term Changes in the Frequency, Intensity and Duration of Extreme Storm Surge Events in Southern Europe." *Climate Dynamics* 46 (5–6): 1503–1516. <https://doi.org/10.1007/s00382-015-2659-1>.
- Cipollini, P., F. M. Calafat, S. Jevrejeva, A. Melet, and P. Prandi. 2017. "Monitoring Sea Level in the Coastal Zone with Satellite Altimetry and Tide Gauges." *Integrative Study of the Mean Sea Level and Its Components* 35–59. <https://doi.org/10.1007/s10712-016-9392-0>.
- Clemente, M. F., V. D'Ambrosio, and M. Focareta. 2022. "The Proposal of the Coast-RiskBysea: COASTal Zones RISK Assessment for Built Environment by extreme SEA Level, Based on the New Copernicus Coastal Zones Data." *International Journal of Disaster Risk Reduction* 75:102947. <https://doi.org/10.1016/j.ijdrr.2022.102947>.
- Darmaraki, S., S. Somot, F. Sevault, and P. Nabat. 2019. "Past Variability of Mediterranean Sea Marine Heatwaves." *Geophysical Research Letters* 46 (16): 9813–9823. <https://doi.org/10.1029/2019GL082933>.
- Dasallas, L., and S. Lee. 2019. "Topographical Analysis of the 2013 Typhoon Haiyan Storm Surge Flooding by Combining the JMA 1313 Storm Surge Model and the FLO-2D Flood Inundation Model." *Water* 11 (1): 144. <https://doi.org/10.3390/w11010144>.
- de la Vara, A., J. Gutiérrez-Fernández, J. Jesús González-Alemán, and M. Ángel Gaertner. 2021, April. A Proposal for Medicane Detection in Long High-Resolution Climate Model Simulations with a Minimal Amount of Data. In *EGU General Assembly Conference Abstracts*, Vienna, Austria, EGU21–2948.
- Denamiel, C., I. Tojčić, and I. Vilibić. 2021. "Balancing Accuracy and Efficiency of Atmospheric Models in the Northern Adriatic During Severe Bora Events." *Journal of Geophysical Research: Atmospheres* 126 (5): e2020JD033516. <https://doi.org/10.1029/2020JD033516>.
- Denamiel, C., and I. Vilibić. 2022. "Next-Generation (Sub-) Kilometre-Scale Climate Modelling for Extreme Storm-Surge Hazard Projections." *Nature Communications*. <https://doi.org/10.21203/rs.3.rs-1532623/v1>.
- Desmet, K., R. E. Kopp, S. A. Kulp, D. K. Nagy, M. Oppenheimer, E. Rossi-Hansberg, and B. H. Strauss. 2021. "Evaluating the Economic Cost of Coastal Flooding." *American Economic Journal: Macroeconomics, American Economic Association* 13 (2): 444–486. <https://doi.org/10.1257/mac.20180366>.
- Diakakis, M., G. Deligiannakis, and S. Mavroulis. 2011. "Flooding in Peloponnese, Greece: A Contribution to Flood Hazard Assessment." *Advances in the Research of Aquatic Environment* 1:199–206.
- Dieng, H. B., A. Cazenave, Y. Gouzenes, and B. A. Sow. 2021. "Trends and Inter-Annual Variability of Altimetry-Based Coastal Sea Level in the Mediterranean Sea: Comparison with Tide Gauges and Models." *Advances in Space Research* 68 (8): 3279–3290. <https://doi.org/10.1016/j.asr.2021.06.022>.
- Diffenbaugh, N. S., and F. Giorgi. 2012. "Climate Change Hotspots in the CMIP5 Global Climate Model Ensemble." *Climatic Change* 114 (3): 813–822. <https://doi.org/10.1007/s10584-012-0570-x>.
- Enríquez, A. R., M. Marcos, A. Falqués, and D. Roelvink. 2019. "Assessing Beach and Dune Erosion and Vulnerability Under Sea Level Rise: A Case Study in the Mediterranean Sea." *Frontiers in Marine Science* 6:4. <https://doi.org/10.3389/fmars.2019.00004>.
- Favaretto, C., L. Martinelli, and P. Ruol. 2019. "A Model of Coastal Flooding Using Linearized Bottom Friction and Its Application to a 1365 Case Study in Caorle, Venice, Italy." *International Journal of Offshore and Polar Engineering* 29 (2): 182–190. <https://doi.org/10.17736/ijope.2019.ak32>.
- Favaretto, C., L. Martinelli, and P. Ruol. 2021. "A Spatial Structure Variable Approach to Characterize Storm Events for Coastal Flood Hazard Assessment." *Water* 13 (18): 2556. <https://doi.org/10.3390/w13182556>.
- Fenoglio-Marc, L. 2002. "Long-Term Sea Level Change in the Mediterranean Sea from Multi-Satellite Altimetry and Tide Gauges." *Physics and Chemistry of the Earth, Parts A/B/C* 27 (32–34): 1419–1431. [https://doi.org/10.1016/S1474-7065\(02\)00084-0](https://doi.org/10.1016/S1474-7065(02)00084-0).

- Fenoglio-Marc, L., C. Dietz, and E. Groten. 2004. "Vertical Land Motion in the Mediterranean Sea from Altimetry and Tide Gauge Stations." *Marine Geodesy* 27 (3–4): 683–701. <https://doi.org/10.1080/01490410490883441>.
- Ferrarin, C., M. Bajo, A. Benetazzo, L. Cavaleri, J. Chiggiato, S. Davison, S. Davolio, P. Lionello, M. Orlić, and G. Umgiesser. 2021. "Local and Large-Scale Controls of the Exceptional Venice Floods of November 2019." *Progress in Oceanography* 197:102628. <https://doi.org/10.1016/j.pocean.2021.102628>.
- Ferrarin, C., F. Pantillon, S. Davolio, M. Bajo, M. M. Miglietta, E. Avolio, D. S. Carrió, et al. 2023. "Assessing the Coastal Hazard of Mediane Ianos Through Ensemble Modelling." *Natural Hazards and Earth System Sciences* 23 (6): 2273–2287.
- Fewtrell, T., P. Bates, A. de Wit, N. Asselman, and P. Sayers. 2008. Comparison of Varying Complexity Numerical Models for the Prediction of Flood Inundation in Greenwich, UK. Proceedings of FLOODrisk 2008, Keble College, Oxford, UK, 30/9-2/10/2008.
- Fewtrell, T. J., J. C. Neal, P. D. Bates, and P. J. Harrison. 2011. "Geometric and Structural River Channel Complexity and the Prediction of Urban Inundation." *Hydrological Processes* 25 (20): 3173–3186. <https://doi.org/10.1002/hyp.8035>.
- Flaounas, E., S. Davolio, S. Raveh-Rubin, F. Pantillon, M. M. Miglietta, M. A. Gaertner, M. Hatzaki, et al. 2022. "Mediterranean Cyclones: Current Knowledge and Open Questions on Dynamics, Prediction, Climatology and Impacts." *Weather and Climate Dynamics* 3 (1): 173–208. <https://doi.org/10.5194/wcd-3-173-2022>.
- Galassi, G., and G. Spada. 2014. "Sea-Level Rise in the Mediterranean Sea by 2050: Roles of Terrestrial Ice Melt, Steric Effects and Glacial Isostatic Adjustment." *Global and Planetary Change* 123:55–66. <https://doi.org/10.1016/j.gloplacha.2014.10.007>.
- Galiatsatou, P., C. Makris, V. Baltikas, Y. Krestenitis, and P. Prinos. 2023. Analysis of Extreme Storm Surges at the Mediterranean Coastline Under Climate Change. *Proceedings of the 2nd International Conference DMPCO*, Thessaloniki, Greece:1:36–40.
- Galiatsatou, P., C. Makris, Y. Krestenitis, and P. Prinos. 2021. "Nonstationary Extreme Value Analysis of Nearshore Sea-State Parameters Under the Effects of Climate Change: Application to the Greek Coastal Zone and Port Structures." *Journal of Marine Science and Engineering* 9 (8): 817. <https://doi.org/10.3390/jmse9080817>.
- Galiatsatou, P., C. Makris, P. Prinos, and D. Kokkinos. 2019. "Nonstationary Joint Probability Analysis of Extreme Marine Variables to Assess Design Water Levels at the Shoreline in a Changing Climate." *Natural Hazards* 98 (3): 1051–1089. <https://doi.org/10.1007/s11069-019-03645-w>.
- Ghionis, G., S. E. Poulos, E. Verykiou, A. Karditsa, G. Alexandrakis, and P. Andris. 2015. "The Impact of an Extreme Storm Event on the Barrier Beach of the Lefkada Lagoon, NE Ionian Sea (Greece)." *Mediterranean Marine Science* 16 (3): 562–572. <https://doi.org/10.12681/mms.948>.
- Gomis, D., S. Ruiz, M. G. Sotillo, E. Álvarez-Fanjul, and J. Terradas. 2008. "Low Frequency Mediterranean Sea Level Variability: The Contribution of Atmospheric Pressure and Wind." *Global and Planetary Change* 63 (2–3): 215–229. <https://doi.org/10.1016/j.gloplacha.2008.06.005>.
- Gualdi, S., S. Somot, L. Li, V. Artale, M. Adani, A. Bellucci, A. Braun, et al. 2013. "The CIRCE Simulations: Regional Climate Change Projections with Realistic Representation of the Mediterranean Sea." *Bulletin of the American Meteorological Society* 94 (1): 65–81. <https://doi.org/10.1175/BAMS-D-11-00136.1>.
- Haddad, M., H. Hassani, and H. Taibi. 2013. "Sea Level in the Mediterranean Sea: Seasonal Adjustment and Trend Extraction within the Framework of SSA." *Earth Science Informatics* 6 (2): 99–111. <https://doi.org/10.1007/s12145-013-0114-6>.
- Hallegate, S., C. Green, R. J. Nicholls, and J. Corfee-Morlot. 2013. "Future Flood Losses in Major Coastal Cities." *Nature Climate Change* 3 (9): 802–806. <https://doi.org/10.1038/nclimate1979>.
- Hauer, M. E., D. Hardy, S. A. Kulp, V. Mueller, D. J. Wrathall, and P. U. Clark. 2021. "Assessing Population Exposure to Coastal Flooding Due to Sea Level Rise." *Nature Communications* 12 (1): 1–9. <https://doi.org/10.1038/s41467-021-27260-1>.
- HNHS (Hellenic Navy Hydrographic Service). 2015. *Statistical Data of Sea Level in Hellenic Ports, B Ed.*. HNHS: Athens, Greece. (In Greek).
- Horritt, M. S., and P. D. Bates. 2001. "Predicting Floodplain Inundation: Raster-Based Modelling versus the Finite-Element Approach." *Hydrological Processes* 15 (5): 825–842. <https://doi.org/10.1002/hyp.188>.
- Horritt, M. S., and P. D. Bates. 2002. "Evaluation of 1D and 2D Numerical Models for Predicting River Flood Inundation." *Journal of Hydrology* 268 (1–4): 87–99. [https://doi.org/10.1016/S0022-1694\(02\)00121-X](https://doi.org/10.1016/S0022-1694(02)00121-X).
- Horton, C., J. Kerling, G. Athey, J. Schmitz, and M. Clifford. 1994. "Airborne Expendable Bathythermograph Surveys of the Eastern Mediterranean." *Journal of Geophysical Research* 99 (C5): 9891–9905. <https://doi.org/10.1029/94JC00058>.
- Hunter, N. M., P. D. Bates, M. S. Horritt, and M. D. Wilson. 2006. "Improved Simulation of Flood Flows Using Storage Cell Models." *Proceedings of the Institution of Civil Engineers-Water Management*, 159, 9–18. <https://www.icevirtuallibrary.com/doi/epdf/10.1680/wama.2006.159.1.9>.
- Hunter, N. M., P. D. Bates, M. S. Horritt, and M. D. Wilson. 2007. "Simple Spatially-Distributed Models for Predicting Flood Inundation: A Review." *Geomorphology* 90 (3–4): 208–225. <https://doi.org/10.1016/j.geomorph.2006.10.021>.
- Hunter, N. M., M. S. Horritt, P. D. Bates, M. D. Wilson, and M. G. Werner. 2005. "An Adaptive Time Step Solution for Raster-Based Storage Cell Modelling of Floodplain Inundation." *Advances in Water Resources* 28 (9): 975–991. <https://doi.org/10.1016/j.advwatres.2005.03.007>.
- Hurrell, J. W. 1995. "Decadal Trends in the North Atlantic Oscillation: Regional Temperatures and Precipitation." *Science* 269 (5224): 676–679. <https://doi.org/10.1126/science.269.5224.676>.
- Ioannou, A., A. Stegner, B. Le Vu, I. Taupier-Letage, and S. Speich. 2017. "Dynamical evolution of intense Ierapetra eddies on a 22 year long period." *Journal of Geophysical Research: Oceans* 122 (11): 9276–9298.
- Jeon, T., K. W. Seo, B. H. Kim, J. S. Kim, J. Chen, and C. R. Wilson. 2021. "Sea Level Fingerprints and Regional Sea Level Change." *Earth and Planetary Science Letters* 567:116985. <https://doi.org/10.1016/j.epsl.2021.116985>.
- Jibhakate, S. M., P. V. Timbadiya, and P. L. Patel. 2022. "Flood Hazard Assessment for the Coastal Urban Floodplain Using 1D/2D Cou-1303 Pled Hydrodynamic Model." *Natural Hazards* 1–34. <https://doi.org/10.1007/s11069-022-05728-7>.
- Jiménez, J. A., H. I. Valdemoro, E. Bosom, A. Sánchez-Arcilla, and R. J. Nicholls. 2017. "Impacts of Sea-Level Rise-Induced Erosion on the Catalan Coast." *Regional Environmental*

- Change* 17 (2): 593–603. <https://doi.org/10.1007/s10113-016-1052-x>.
- Jordà, G., and D. Gomis. 2013. "On the Interpretation of the Steric and Mass Components of Sea Level Variability: The Case of the Mediterranean Basin." *The Journal* 118 (2): 953–963. <https://doi.org/10.1002/jgrc.20060>.
- Jordà, G., D. Gomis, E. Álvarez-Fanjul, and S. Somot. 2012. "Atmospheric Contribution to Mediterranean and Nearby Atlantic Sea Level Variability Under Different Climate Change Scenarios." *Global and Planetary Change* 80–81:198–214. <https://doi.org/10.1016/j.gloplacha.2011.10.013>.
- Kahl, D. T., J. E. Schubert, A. Jong-Levinger, and B. F. Sanders. 2022. "Grid Edge Classification Method to Enhance Levee Resolution in Dual-Grid Flood Inundation Models." *Advances in Water Resources* 168:104287. <https://doi.org/10.1016/j.advwatres.2022.104287>.
- Karamouz, M., and M. Fereshtehpour. 2019. "Modeling DEM Errors in Coastal Flood Inundation and Damages: A Spatial Nonstationary Approach." *Water Resources Research* 55 (8): 6606–6624. <https://doi.org/10.1029/2018WR024562>.
- Kendall, M. 1975. *Rank Correlation Measures*. London: Charles Griffin.
- Kombiadou, K., and Y. N. Krestenitis. 2012. "Fine Sediment Transport Model for River Influenced Microtidal Shelf Seas with Application to the Thermaikos Gulf (NW Aegean Sea)." *Continental Shelf Research* 36:41–62. <https://doi.org/10.1016/j.csr.2012.01.009>.
- Kombiadou, K., Y. N. Krestenitis, V. Baltikas, and G. Kalantzi. 2012. "Coastal Erosion Problems in Katerini: Methods and Measures." *Protection and Restoration of the Environment XI, July*, Thessaloniki, Greece, 3–6.
- Kontogianni, A., C. Tourkolias, M. Skourtos, and M. Papanikolaou. 2012. "Linking sea level rise damage and vulnerability assessment: the case of Greece." In *International Perspectives on Global Environmental Change*, edited by Young, S. S., and Silvern, S. E., 375–398. IntechOpen London. <https://doi.org/10.5772/27807>.
- Kouroutzoglou, J., H. A. Flocas, K. Keay, I. Simmonds, and M. Hatzaki. 2011. "Climatological Aspects of Explosive Cyclones in the Mediterranean." *International Journal of Climatology* 31 (12): 1785–1802. <https://doi.org/10.1002/joc.2203>.
- Krestenitis, Y. N., Y. S. Androulidakis, Y. N. Kontos, and G. Georgakopoulos. 2011. "Coastal Inundation in the North-Eastern Mediterranean Coastal Zone Due to Storm Surge Events." *Journal of Coastal Conservation* 15 (3): 353–368. <https://doi.org/10.1007/s11852-010-0090-7>.
- Krestenitis, Y., Y. Androulidakis, C. Makris, V. Baltikas, Y. Pytharoulis, and K. Tolika. 2021. Sea Level Variations and Coastal Floods: Short-Term Forecasts and Climatic Changes. *Proceedings of the 4th Scientific Forum for Disaster Risk Reduction in Greece*. Athens, Greece, 18-19 March 2021.
- Krvavica, N., and I. Ružić. 2020. "Assessment of Sea-Level Rise Impacts on Salt-Wedge Intrusion in Idealized and Neretva River Estuary." *Estuarine, Coastal and Shelf Science* 234:106638. <https://doi.org/10.1016/j.ecss.2020.106638>.
- Kulp, S. A., and B. H. Strauss. 2019. "New Elevation Data Triple Estimates of Global Vulnerability to Sea-Level Rise and Coastal Flooding." *Nature Communications* 10 (1): 1–12. <https://doi.org/10.1038/s41467-019-12808-z>.
- Kulp, S., and B. H. Strauss. 2016. "Global DEM Errors Underpredict Coastal Vulnerability to Sea Level Rise and Flooding." *Frontiers in Earth Science* 4:36. <https://doi.org/10.3389/feart.2016.00036>.
- Kulp, S., and B. H. Strauss. 2017. "Rapid Escalation of Coastal Flood Exposure in US Municipalities from Sea Level Rise." *Climatic Change* 142 (3): 477–489. <https://doi.org/10.1007/s10584-017-1963-7>.
- Lagouvardos, K., A. Karagiannidis, S. Dafis, A. Kalimeris, and V. Kotroni. 2022. "Ianos—A Hurricane in the Mediterranean." *Bulletin of the American Meteorological Society* 103 (6): E1621–E1636. <https://doi.org/10.1175/BAMS-D-20-0274.1>.
- Landerer, F. W., and D. L. Volkov. 2013. "The Anatomy of Recent Large Sea Level Fluctuations in the Mediterranean Sea." *Geophysical Research Letters* 40 (3): 553–557. <https://doi.org/10.1002/grl.50140>.
- Levitus, S., J. I. Antonov, T. P. Boyer, O. K. Baranova, H. E. Garcia, R. A. Locarnini, A. V. Mishonov, et al. 2012. "World Ocean Heat Content and Thermosteric Sea Level Change (0–2000 M), 1955–2010." *Geophysical Research Letters* 39 (10). <https://doi.org/10.1029/2012GL051106>.
- Lionello, P., F. Abrantes, L. Congedi, F. Dulac, M. Gacic, D. Gomis, C. Goodess et al, 2012. "Introduction: Mediterranean climate: background information in." In *The Climate of the Mediterranean Region. From the Past to the Future*, edited by Lionello, P., XXXV–IXXX. Amsterdam: Elsevier (NETHERLANDS).
- Lionello, P., D. Barriopedro, C. Ferrarin, R. J. Nicholls, M. Orlić, F. Raicich, M. Reale, G. Umgiesser, M. Vousdoukas, and D. Zanchettin. 2021. "Extreme Floods of Venice: Characteristics, Dynamics, Past and Future Evolution." *Natural Hazards and Earth System Sciences* 21 (8): 2705–2731. <https://doi.org/10.5194/nhess-21-2705-2021>.
- Lionello, P., J. Bhend, A. Buzzi, P. M. Della-Marta, S. O. Krichak, A. Jansa, P. Maheras, A. Sanna, I. F. Trigo, and R. Trigo. 2006. "Cyclones in the Mediterranean Region: Climatology and Effects on the Environment." In *Developments in Earth and Environmental Sciences*, 325–372. Vol. 4. Elsevier. [https://doi.org/10.1016/S1571-9197\(06\)80009-1](https://doi.org/10.1016/S1571-9197(06)80009-1).
- Makris, C., Y. Androulidakis, Z. Mallios, V. Baltikas, and Y. Krestenitis (2022). Towards an Operational Forecast Model for Coastal Inundation Due to Storm Surges: Application During Ianos Medicane. *Proceedings of the 9th International Conference on Civil Protection & New Technologies, SafeThessaloniki 2022, 29 September - 1 October*, Thessaloniki, Greece, 69–72. Part of ISSN 2654-1823.
- Makris, C., P. Galiatsatou, K. Tolika, C. Anagnostopoulou, K. Kombiadou, P. Prinos, K. Velikou, et al. 2016. "Climate Change Effects on the Marine Characteristics of the Aegean and the Ionian Seas." *Ocean Dynamics* 66 (12): 1603–1635. <https://doi.org/10.1007/s10236-016-1008-1>.
- Makris, C., Z. Mallios, Y. Androulidakis, and Y. Krestenitis. 2023. "CoastFlood: A High-Resolution Model for the Simulation of Coastal Inundation Due to Storm Surges." *Hydrology* 10 (5): 103. <https://doi.org/10.3390/hydrology10050103>.
- Makris, C., K. Tolika, V. Baltikas, K. Velikou, and Y. Krestenitis. 2023. "The Impact of Climate Change on the Storm Surges of the Mediterranean Sea: Coastal Sea Level Responses to Deep Depression Atmospheric Systems." *Ocean Modelling* 102149. <https://doi.org/10.1016/j.ocemod.2022.102149>.
- Makropoulos, C., V. Tsoukala, K. Belibbasakis, A. Lykou, M. Chondros, P. Gourgoura, and D. Nikolopoulos. 2015. "Managing flood risk in coastal cities through an integrated modelling framework supporting stakeholders' involvement: The case of Rethymno, Crete, 2015." In *Proceedings of the 36th IAHR World Congress*, The Hague. The Netherlands, 28 June - 3 July.

- Mamoutos, I., V. Zervakis, E. Tragou, M. Karydis, C. Frangoulis, V. Kolovoyiannis, D. Georgopoulos, and S. Psarra. 2017. "The Role of Wind-Forced Coastal Upwelling on the Thermohaline Functioning of the North Aegean Sea." *Continental Shelf Research* 149:52–68. <https://doi.org/10.1016/j.csr.2017.05.009>.
- Mann, H. B. 1945. "Nonparametric Tests Against Trend." *Economy Journal Economy Society* 13 (3): 245–259. <https://doi.org/10.2307/1907187>.
- Marcos, M., and M. N. Tsimplis. 2007. "Variations of the Seasonal Sea Level Cycle in Southern Europe." *Journal of Geophysical Research: Oceans* 112 (C12). <https://doi.org/10.1029/2006JC004049>.
- Marcos, M., and M. N. Tsimplis. 2008. "Coastal Sea Level Trends in Southern Europe." *Geophysical Journal International* 175 (1): 70–82. <https://doi.org/10.1111/j.1365-246X.2008.03892.x>.
- Marcos, M., M. N. Tsimplis, and A. G. Shaw. 2009. "Sea Level Extremes in Southern Europe." *Journal of Geophysical Research Oceans (1978–2012)* 114 (C1): 114 (C1). <https://doi.org/10.1029/2008JC004912>.
- Martinelli, L., B. Zanuttigh, and C. Corbau. 2010. "Assessment of Coastal Flooding Hazard Along the Emilia Romagna Littoral, IT." *Coastal Engineering* 57 (11–12): 1042–1058. <https://doi.org/10.1016/j.coastaleng.2010.06.007>.
- Martzikos, N., V. Afentoulis, V. Tsoukala, N. Martzikos, V. Afentoulis, and V. Tsoukala. 2018. "Storm Clustering and Classification for the Port of Rethymno in Greece." *Water Utilities Journal* 20:67–79.
- Martzikos, N. T., P. E. Prinos, C. D. Memos, and V. K. Tsoukala. 2021. "Statistical Analysis of Mediterranean Coastal Storms." *Oceanologia* 63 (1): 133–148. <https://doi.org/10.1016/j.oceano.2020.11.001>.
- Masina, M., A. Lamberti, and R. Archetti. 2015. "Coastal Flooding: A Copula Based Approach for Estimating the Joint Probability of Water Levels and Waves." *Coastal Engineering* 97:37–52. <https://doi.org/10.1016/j.coastaleng.2014.12.010>.
- Međugorac, I., M. Orlic, I. Janekovic, Z. Pasaric, and M. Pasaric. 2018. "Adriatic Storm Surges and Related Cross-Basin Sea-Level Slope." *Journal of Marine Systems: Journal of the European Association of Marine Sciences and Techniques* 181:79–90. <https://doi.org/10.1016/j.jmarsys.2018.02.005>.
- Menna, M., M. Gačić, R. Martellucci, G. Notarstefano, G. Fedele, E. Mauri, R. Gerin, and P. M. Poulain. 2022. "Climatic, Decadal, and Interannual Variability in the Upper Layer of the Mediterranean Sea Using Remotely Sensed and in-Situ Data." *Remote Sensing* 14 (6): 1322. <https://doi.org/10.3390/rs14061322>.
- Messmer, M., J. J. Gómez-Navarro, and C. C. Raible. 2015. "Climatology of Vb Cyclones, Physical Mechanisms and Their Impact on Extreme Precipitation Over Central Europe." *Earth System Dynamics* 6 (2): 541–553. <https://doi.org/10.5194/esd-6-541-2015>.
- Mkhinini, N., A. L. S. Coimbra, A. Stegner, T. Arsouze, I. Taupier-Letage, and K. Béranger. 2014. "Long-Lived Mesoscale Eddies in the Eastern Mediterranean Sea: Analysis of 20 Years of AVISO Geostrophic Velocities." *Journal of Geophysical Research: Oceans* 119 (12): 8603–8626. <https://doi.org/10.1002/2014JC010176>.
- Mohamed, B., A. M. Abdallah, K. Alam El-Din, H. Nagy, and M. Shaltout. 2019. "Inter-Annual Variability and Trends of Sea Level and Sea Surface Temperature in the Mediterranean Sea Over the Last 25 Years." *Pure and Applied Geophysics* 176 (8): 3787–3810. <https://doi.org/10.1007/s00024-019-02156-w>.
- Mohamed, B., and N. Skliris. 2022. "Steric and Atmospheric Contributions to Interannual Sea Level Variability in the Eastern Mediterranean Sea Over 1993–2019." *Oceanologia* 64 (1): 50–62. <https://doi.org/10.1016/j.oceano.2021.09.001>.
- Monioudi, I. N., A. Karditsa, A. Chatzipavlis, G. Alexandrakis, O. P. Andreadis, A. F. Velegrakis, S. E. Poulos, et al. 2016. "Assessment of Vulnerability of the Eastern Cretan Beaches (Greece) to Sea Level Rise." *Regional Environmental Change* 16 (7): 1951–1962. <https://doi.org/10.1007/s10113-014-0730-9>.
- Monioudi, I. N., A. F. Velegrakis, A. E. Chatzipavlis, A. Rigos, T. Karambas, M. I. Voudoukas, T. Hasiotis, et al. 2017. "Assessment of Island Beach Erosion Due to Sea Level Rise: The Case of the Aegean Archipelago (Eastern Mediterranean)." *Natural Hazards and Earth System Sciences* 17 (3): 449–466. <https://doi.org/10.5194/nhess-17-449-2017>.
- Morsy, M. M., N. R. Lerma, Y. Shen, J. L. Goodall, C. Huxley, J. M. Sadler, D. Voce, G. L. O'Neil, I. Maghami, and F. T. Zahura. 2021. "Impact of Geospatial Data Enhancements for Regional-Scale 2D Hydrodynamic Flood Modeling: Case Study for the Coastal Plain of Virginia." *Journal of Hydrologic Engineering* 26 (4): 05021002. [https://doi.org/10.1061/\(ASCE\)HE.1943-5584.0002065](https://doi.org/10.1061/(ASCE)HE.1943-5584.0002065).
- Murdukhayeva, A., P. August, M. Bradley, C. LaBash, and N. Shaw. 2013. "Assessment of Inundation Risk from Sea Level Rise and Storm Surge in Northeastern Coastal National Parks." *Journal of Coastal Research* 29 (6A): 1–16. Coconut Creek (Florida), ISSN 0749-0208. <https://doi.org/10.2112/JCOASTRES-D-12-00196.1>.
- Nastos, P. T., K. K. Papadimou, and I. T. Matsangouras. 2018. "Mediterranean Tropical-Like Cyclones: Impacts and Composite Daily Means and Anomalies of Synoptic Patterns." *Atmospheric Research* 208:156–166. <https://doi.org/10.1016/j.atmosres.2017.10.023>.
- Neal, J., G. Schumann, T. Fewtrell, M. Budimir, P. Bates, and D. Mason. 2011. "Evaluating a New LISFLOOD-FP Formulation with Data from the Summer 2007 Floods in Tewkesbury, UK." *Journal of Flood Risk Management* 4 (2): 88–95. <https://doi.org/10.1111/j.1753-318X.2011.01093.x>.
- Neal, J., I. Villanueva, N. Wright, T. Willis, T. Fewtrell, and P. Bates. 2012. "How Much Physical Complexity is Needed to Model Flood Inundation?" *Hydrological Processes* 26 (15): 2264–2282. <https://doi.org/10.1002/hyp.8339>.
- Neu, U., M. G. Akperov, N. Bellenbaum, R. Benestad, R. Blender, R. Caballero, A. Coccozza, et al. 2013. "A Community Effort to Intercompare Extratropical Cyclone Detection and Tracking Algorithms: Assessing Method-Related Uncertainties." *Bulletin of the American Meteorological Society* 94 (4): 529–547. <https://doi.org/10.1175/BAMS-D-11-00154.1>.
- Neumann, B., A. T. Vafeidis, J. Zimmermann, R. J. Nicholls, and L. Kumar. 2015. "Future Coastal Population Growth and Exposure to Sea-Level Rise and Coastal Flooding-A Global Assessment." *PloS One* 10 (3): e0118571. <https://doi.org/10.1371/journal.pone.0118571>.
- Nicholls, R. J. 2002. "Rising sea level: potential impacts and responses." In *Issues in Environmental Science and Technology*, edited by Hester R. E. and R. M. Harrison, Vol. 17, 83–107.
- Nicholls, R. J., and F. M. J. Hoozemans. 1996. "The Mediterranean: Vulnerability to Coastal Implications of Climate Change." *Ocean & Coastal Management* 31 (2–3): 105–132. [https://doi.org/10.1016/S0964-5691\(96\)00037-3](https://doi.org/10.1016/S0964-5691(96)00037-3).
- Pariartha, G., A. Goonetilleke, P. Egodawatta, and H. Mirfenderesk. 2020. "The Prediction of Flood Damage

- in Coastal Urban 1301 Areas." *IOP Conference Series: Earth and Environmental Science* 419 (1): 012136. 1302. <https://doi.org/10.1088/1755-1315/419/1/012136>.
- Pearson, K. 1903. "I. Mathematical contributions to the theory of evolution.—XI. On the influence of natural selection on the variability and correlation of organs." *Philosophical Transactions of the Royal Society of London. Series A, Containing Papers of a Mathematical or Physical Character* 200 (321–330): 1–66.
- Pettitt, A. N. 1979. "A Non-Parametric Approach to the Change-Point Problem." *Journal of the Royal Statistical Society: Series C (Applied Statistics)* 28 (2): 126–135. <https://doi.org/10.2307/2346729>.
- Pinardi, N., E. Arneri, A. Crise, M. Ravaioli, and M. Zavatarelli. 2006. "The Physical, Sedimentary and Ecological Structure and Variability of Shelf Areas in the Mediterranean Sea (27)." In *The Sea*, edited by Robinson, A. R., and Brink, K. A., 1243–1330. Harvard University Press.
- Poulos, S., A. Karditsa, M. Hatzaki, A. Tsapanou, C. Papapostolou, and K. Chouvardas. 2022. "An Insight into the Factors Controlling Delta Flood Events: The Case of the Evros River Deltaic Plain (NE Aegean Sea)." *Water* 14 (3): 497. <https://doi.org/10.3390/w14030497>.
- Poupkou, A., P. Zanis, P. Nastos, D. Papanastasiou, D. Melas, K. Tourpali, and C. Zerefos. 2011. "Present Climate Trend Analysis of the Etesian Winds in the Aegean Sea." *Theoretical and Applied Climatology* 106 (3–4): 459–472. <https://doi.org/10.1007/s00704-011-0443-7>.
- Prime, T., J. M. Brown, and A. J. Plater. 2016. "Flood Inundation Uncertainty: The Case of a 0.5% Annual Probability Flood Event." *Environ Sci Pol* 59:1–9. <https://doi.org/10.1016/j.envsci.2016.01.018>.
- Pujol, M. I., S. Dupuy, O. Vergara, A. Sánchez Román, Y. Faugère, P. Prandi, M. L. Dabat, et al. 2023. "Refining the Resolution of DUACS Along-Track Level-3 Sea Level Altimetry Products." *Remote Sensing* 15 (3): 793. <https://doi.org/10.3390/rs15030793>.
- Pujol, M. I., and G. Larnicol. 2005. "Mediterranean Sea Eddy Kinetic Energy Variability from 11 Years of Altimetric Data." *Journal of Marine Systems* 58 (3–4): 121–142. <https://doi.org/10.1016/j.jmarsys.2005.07.005>.
- Ray, S., S. S. Das, P. Mishra, and A. M. G. Al Khatib. 2021. "Time Series SARIMA Modelling and Forecasting of Monthly Rainfall and Temperature in the South Asian Countries." *Earth Systems and Environment* 5 (3): 531–546. <https://doi.org/10.1007/s41748-021-00205-w>.
- Refaat, M. M., and Y. Eldeberky. 2016. "Assessment of Coastal Inundation Due to Sea-Level Rise Along the Mediterranean Coast of Egypt." *Marine Geodesy* 39 (3–4): 290–304. <https://doi.org/10.1080/01490419.2016.1189471>.
- Reimann, L., A. T. Vafeidis, S. Brown, J. Hinkel, and R. S. Tol. 2018. "Mediterranean UNESCO World Heritage at Risk from Coastal Flooding and Erosion Due to Sea-Level Rise." *Nature Communications* 9 (1): 1–11. <https://doi.org/10.1038/s41467-018-06645-9>.
- Rizzo, A., V. Vandelli, C. Gauci, G. Buhagiar, A. S. Micallef, and M. Soldati. 2022. "Potential Sea Level Rise Inundation in the Mediterranean: From Susceptibility Assessment to Risk Scenarios for Policy Action." *Water* 14 (3): 416. <https://doi.org/10.3390/w14030416>.
- Romera, R., M.Á. Gaertner, E. Sánchez, M. Domínguez, J. J. González-Alemán, and M. M. Miglietta. 2017. "Climate Change Projections of Medicanes with a Large Multi-Model Ensemble of Regional Climate Models." *Global and Planetary Change* 151:134–143. <https://doi.org/10.1016/j.gloplacha.2016.10.008>.
- Satta, A., M. Puddu, S. Venturini, and C. Giupponi. 2017. "Assessment of Coastal Risks to Climate Change Related Impacts at the Regional Scale: The Case of the Mediterranean Region." *International Journal of Disaster Risk Reduction* 24:284–296. <https://doi.org/10.1016/j.ijdrr.2017.06.018>.
- Schoetter, R., P. Hoffmman, D. Rechid, and K. H. Schlunzen. 2012. "Evaluation and Bias Correction of Regional Climate Model Results Using Model Evaluation Measures." *Journal of Applied Meteorology and Climatology* 51 (9): 1670–1684. <https://doi.org/10.1175/JAMC-D-11-0161.1>.
- Seenath, A. 2015. "Modelling Coastal Flood Vulnerability: Does Spatially-Distributed Friction Improve the Prediction of Flood Ex-1424 Tent?" *Applied Geography* 64:97–107. <https://doi.org/10.1016/j.apgeog.2015.09.010>.
- Seenath, A., M. Wilson, and K. Miller. 2016. "Hydrodynamic versus GIS Modelling for Coastal Flood Vulnerability Assessment: Which is Better for Guiding Coastal Management?" *Ocean & Coastal Management* 120:99–109. <https://doi.org/10.1016/j.ocecoaman.2015.11.019>.
- Sen, P. K. 1968. "Estimates of the Regression Coefficient Based on Kendall's Tau." *Journal of the American Statistical Association* 63 (324): 1379–1389. <https://doi.org/10.1080/01621459.1968.10480934>.
- Šepić, J., I. Vilibić, G. Jordà, and M. Marcos. 2012. "Mediterranean Sea Level Forced by Atmospheric Pressure and Wind: Variability of the Present Climate and Future Projections for Several Period Bands." *Global and Planetary Change* 86:20–30. <https://doi.org/10.1016/j.gloplacha.2012.01.008>.
- Šepić, J., I. Vilibic, A. Lafon, L. Macheboeuf, and Z. Ivanovic. 2015. "High-Frequency Sea Level Oscillations in the Mediterranean and Their Connection to Synoptic Patterns." *Progress in Oceanography* 137:284–298. <https://doi.org/10.1016/j.pocean.2015.07.005>.
- Shalem, Y., Y. Weinstein, E. Levi, B. Herut, M. Goldman, and Y. Yechieli. 2015. "The Extent of Aquifer Salinization Next to an Estuarine River: An Example from the Eastern Mediterranean." *Hydrogeology Journal* 23 (1): 69–79. <https://doi.org/10.1007/s10040-014-1192-3>.
- Shaltout, M., K. Tonbol, and A. Omstedt. 2015. "Sea-Level Change and Projected Future Flooding Along the Egyptian Mediterranean Coast." *Oceanologia* 57 (4): 293–307. <https://doi.org/10.1016/j.oceano.2015.06.004>.
- Sharaan, M., and K. Udo. 2020. "Projections of Future Beach Loss Along the Mediterranean Coastline of Egypt Due to Sea-Level Rise." *Applied Ocean Research* 94:101972. <https://doi.org/10.1016/j.apor.2019.101972>.
- Shen, Y., M. M. Morsy, C. Huxley, N. Tahvildari, and J. L. Goodall. 2019. "Flood Risk Assessment and Increased Resilience for Coastal Urban Watersheds Under the Combined Impact of Storm Tide and Heavy Rainfall." *Canadian Journal of Fisheries and Aquatic Sciences* 579:124159. <https://doi.org/10.1016/j.jhydrol.2019.124159>.
- Shustikova, I., A. Domeneghetti, J. C. Neal, P. Bates, and A. Castellarin. 2019. "Comparing 2D Capabilities of HEC-RAS and LISFLOOD-FP on Complex Topography." *Hydrological Sciences Journal* 64 (14): 1769–1782. <https://doi.org/10.1080/02626667.2019.1671982>.
- Skoulikaris, Ch., Ch. Makris, M. Katirtzidou, V. Baltikas, and Y. Krestenitis. 2021. "Assessing the Vulnerability of a Deltaic Environment Due to Climate Change Impact on Surface and Coastal Waters: The Case of Nestos River (Greece)." *Environmental Modeling & Assessment* 26 (4): 459–486. <https://doi.org/10.1007/s10666-020-09746-2>.

- Smith, R. A., P. D. Bates, and C. Hayes. 2012. "Evaluation of a Coastal Flood Inundation Model Using Hard and Soft Data." *Environ Model Soft* 30:35–46. <https://doi.org/10.1016/j.envsoft.2011.11.008>.
- Snoussi, M., T. Ouchani, and S. Niazi. 2008. "Vulnerability Assessment of the Impact of Sea-Level Rise and Flooding on the Moroccan Coast: The Case of the Mediterranean Eastern Zone." *Estuarine, Coastal and Shelf Science* 77 (2): 206–213. <https://doi.org/10.1016/j.ecss.2007.09.024>.
- Spencer, T., M. Schuerch, R. J. Nicholls, J. Hinkel, D. Lincke, A. T. Vafeidis, R. Reef, L. McFadden, and S. Brown. 2016. "Global Coastal Wetland Change Under Sea-Level Rise and Related Stresses: The DIVA Wetland Change Model." *Global and Planetary Change* 139:15–30. <https://doi.org/10.1016/j.gloplacha.2015.12.018>.
- Stavropoulos, S., G. N. Zaimes, E. Filippidis, D. C. Diaconu, and D. Emmanouloudis. 2020. "Mitigating Flash Floods with the Use of New Technologies: A Multi-Criteria Decision Analysis to Map Flood Susceptibility for Zakynthos Island, Greece." *Journal of Urban and Regional Analysis* 12 (2): 233–248. <https://doi.org/10.37043/JURA.2020.12.2.7>.
- Tragaki, A., C. Gallousi, and E. Karymbalis. 2018. "Coastal Hazard Vulnerability Assessment Based on Geomorphic, Oceanographic and Demographic Parameters: The Case of the Peloponnese (Southern Greece)." *Land* 7 (2): 56. <https://doi.org/10.3390/land7020056>.
- Tsimplis, M. N., F. M. Calafat, M. Marcos, G. Jordá, D. Gomis, L. Fenoglio-Marc, M. V. Struglia, S. A. Josey, and D. P. Chambers. 2013. "The Effect of the NAO on Sea Level and on Mass Changes in the Mediterranean Sea." *Journal of Geophysical Research: Oceans* 118 (2): 944–952. <https://doi.org/10.1002/jgrc.20078>.
- Tsimplis, M. N., and A. G. P. Shaw. 2010. "Seasonal Sea Level Extremes in the Mediterranean Sea and at the Atlantic European Coasts." *Natural Hazards and Earth System Sciences* 10 (7): 1457–1475. <https://doi.org/10.5194/nhess-10-1457-2010>.
- Tsoukala, V. K., M. Chondros, Z. G. Kapelonis, N. Martzikos, A. Lykou, K. Belibassakis, and C. Makropoulos. 2016. "An Integrated Wave Modelling Framework for Extreme and Rare Events for Climate Change in Coastal Areas—The Case of Rethymno, Crete." *Oceanologia* 58 (2): 71–89. <https://doi.org/10.1016/j.oceano.2016.01.002>.
- Tsoukala, V. K., V. Katsardi, K. Hadjibiros, and C. I. Moutzouris. 2015. "Beach Erosion and Consequential Impacts Due to the Presence of Harbours in Sandy Beaches in Greece and Cyprus." *Environmental Processes* 2 (1): 55–71. <https://doi.org/10.1007/s40710-015-0096-0>.
- USACE (US Army Corps of Engineers). 2022 December. *Hydrologic Engineering Center River Analysis System (HEC-RAS) 2D User's Manual, Version 6.3*.
- Vandelli, V., N. Sarkar, A. S. Micallef, M. Soldati, and A. Rizzo. 2022. "Coastal Inundation Scenarios in the North-Eastern Sector of the Island of Gozo (Malta, Mediterranean Sea) as a Response to Sea Level Rise." *Journal of Maps* 19 (1): 1–10. <https://doi.org/10.1080/17445647.2022.2145918>.
- Vigo, I., D. Garcia, and B. F. Chao. 2005. "Change of Sea Level Trend in the Mediterranean and Black Seas." *Journal of Marine Research* 63 (6): 1085–1100. <https://doi.org/10.1357/002224005775247607>.
- Vitousek, S., P. L. Barnard, C. H. Fletcher, N. Frazer, L. Erikson, and C. D. Storlazzi. 2017. "Doubling of Coastal Flooding Frequency within Decades Due to Sea-Level Rise." *Scientific Reports* 7 (1): 1–9. <https://doi.org/10.1038/s41598-017-01362-7>.
- Vousdoukas, M. I., L. Mentaschi, E. Voukouvalas, M. Verlaan, and L. Feyen. 2017. "Extreme Sea Levels on the Rise Along Europe's Coasts." *Earth's Future* 5 (3): 304–323. <https://doi.org/10.1002/2016EF000505>.
- Vousdoukas, M. I., E. Voukouvalas, L. Mentaschi, F. Dottori, A. Giardino, D. Bouziotas, A. Bianchi, P. Salamon, and L. Feyen. 2016. "Developments in Large-Scale Coastal Flood Hazard Mapping." *Natural Hazards and Earth System Sciences* 16 (8): 1841–1853. <https://doi.org/10.5194/nhess-16-1841-2016>.
- Werner, M. G. F., N. M. Hunter, and P. D. Bates. 2005. "Identifiability of Distributed Floodplain Roughness Values in Flood Extent Estimation." *Journal of Hydrology* 314 (1–4): 139–157. <https://doi.org/10.1016/j.jhydrol.2005.03.012>.
- West, H., M. Horswell, and N. Quinn. 2018. "Exploring the Sensitivity of Coastal Inundation Modelling to DEM Vertical Error." *International Journal of Geographical Information Science* 32 (6): 1172–1193. <https://doi.org/10.1080/13658816.2018.1444165>.
- Willmott, C. J., S. M. Robeson, and K. Matsuura. 2012. "A Refined Index of Model Performance." *International Journal of Climatology* 32 (13): 2088–2094. <https://doi.org/10.1002/joc.2419>.
- Wolf, J. 2009. "Coastal Flooding: Impacts of Coupled Wave–Surge–Tide Models." *Natural Hazards* 49 (2): 241–260. <https://doi.org/10.1007/s11069-008-9316-5>.
- Wolff, C., A. T. Vafeidis, S. Muis, D. Lincke, A. Satta, P. Lionello, J. A. Jimenez, D. Conte, and J. Hinkel. 2018. "A Mediterranean Coastal Database for Assessing the Impacts of Sea-Level Rise and Associated Hazards." *Scientific Data* 5 (1): 1–11. <https://doi.org/10.1038/sdata.2018.44>.
- Xafoulis, N., Y. Kontos, E. Farsirotou, S. Kotsopoulos, K. Perifanos, N. Alamanis, D. Dedousis, and K. Katsifarakis. 2023. "Evaluation of Various Resolution DEMs in Flood Risk Assessment and Practical Rules for Flood Mapping in Data-Scarce Geospatial Areas: A Case Study in Thessaly, Greece." *Hydrology* 10 (4): 91. <https://doi.org/10.3390/hydrology10040091>.
- Zanchettin, D., S. Bruni, F. Raicich, P. Lionello, F. Adloff, A. Androsov, F. Antonioli, et al. 2021. "Sea-Level Rise in Venice: Historic and Future Trends (Review Article)." *Natural Hazards and Earth System Sciences* 21 (8): 2643–2678. <https://doi.org/10.5194/nhess-21-2643-2021>.
- Zellou, B., and H. Rahali. 2017. "Assessment of Reduced-Complexity Landscape Evolution Model Suitability to Adequately Simulate Flood Events in Complex Flow Conditions." *Natural Hazards* 86 (1): 1–29. <https://doi.org/10.1007/s11069-016-2671-8>.
- Zhang, C., K. Yin, X. Shi, and X. Yan. 2021. "Risk Assessment for Typhoon Storm Surges Using Geospatial Techniques for the Coastal Areas of Guangdong, China." *Ocean & Coastal Management* 213:105880. <https://doi.org/10.1016/j.ocecoaman.2021.105880>.
- Ziv, B., T. Harpaz, H. Saaroni, and R. Blender. 2015. "A New Methodology for Identifying Daughter Cyclogenesis: Application for the Mediterranean Basin." *International Journal of Climatology* 35 (13): 3847–3861. <https://doi.org/10.1002/joc.4250>.

Appendix: CoastFLOOD Model

For the special cases of simulating the long-term coastal inundation due to SLR or mid-term coastal flooding due to episodic events of storm surge and high tides, excluding the influence of high-frequency short-term events, such as the wave-induced run-up, numerous 2-D horizontal models exist. These refer to established model suites, such as FLO-2D (Dasallas and Lee 2019), MIKE FLOOD 2D (e.g., Jibhakate, Timbadiya, and Patel 2022; Pariartha et al. 2020), and LISFLOOD-FP (Bates and De Roo 2000; Bates et al. 2005; Bates, Horritt, and Fewtrell 2010), among others. Many researchers discuss the need for reduced physical complexity approaches to adequately simulate 2-D flood or inundation compared to full scale 3-D hydrodynamic or 2-D Shallow Water Equation (SWE) modelling of complex flood flow routing (e.g., Afshari et al. 2018, mainly for 2-D river floodplains; Fewtrell et al. 2008, 2011; Neal et al. 2012; Zellou and Rahali 2017). CoastFLOOD is a depth-averaged, 2-D horizontal, mass balance, flood flow model, especially indicated for coastal areas. It follows the concept of the 2-D floodplain version of the LISFLOOD-FP model (Bates et al. 2005; Bates, Horritt, and Fewtrell 2010; Hunter et al. 2005). The robustness of such model approaches has been thoroughly validated and broadly applied in 2-D floodplain areas (Horritt and Bates 2002; Hunter et al. 2007; Neal et al. 2011; Seenath, Wilson, and Miller 2016; Smith, Bates, and Hayes 2012). CoastFLOOD also has a simplistic finite difference module for inundation hydraulic flows, based on fine-resolution raster grids, able to reproduce the 2-D floodwater expansion due to the storm surge on the coastline (Horritt and Bates 2001; Hunter et al. 2007; Bates, Horritt, and Fewtrell 2010; Skoulikaris et al. 2021, Makris et al., 2022; Makris et al. 2023). The flood propagation is decomposed in meridional and zonal direction components, allowing for 1-D flow equations in x- and y-directions to represent the seawater overland routing (Bates et al. 2005; Bradbrook et al. 2004; Hunter et al. 2005). In each typical 2-D raster grid cell, the simplified versions of the continuity and momentum equations are solved separately on the cell center and each of the two cell fronts, respectively. This approach provides an easy 2-D solution representation by a staggered grid scheme and final integration of the flow (Bates, Horritt, and Fewtrell 2010; Hunter et al. 2007). The continuity equation corresponds to the mass conservation principle for the calculation of localized water volume, leading to the estimation of the floodwater depth in each grid cell (Bates et al. 2005). The simplified momentum equations describe the flow rate in each cell and direction, derived from a Manning's law approach using the spatiotemporal differences of water surface elevation above land level while incorporating local bottom friction (Neal et al. 2011; Seenath 2015; Skoulikaris et al. 2021). CoastFLOOD considers the floodwater friction on the land bed by defining an effective grid-scale Manning's bottom roughness on each cell of the model's raster domain or by estimating a characteristic "global" effective grid-scale Manning coefficient value either on the entire domain or large parts of it (Favaretto, Martinelli, and Ruol 2019; Makris et al. 2023; Seenath 2015). Based on a collective ensemble of proposed Manning roughness coefficients in relevant literature (e.g., Arcement and Schneider 1989; Chow 1959; Martinelli, Zanuttigh, and Corbau 2010; Morsy et al. 2021; Prime, Brown, and Plater 2016; Seenath, Wilson, and Miller 2016; Shen et al. 2019; Shustikova et al. 2019; USACE, US 2022; Werner, Hunter, and Bates 2005) we have integrated a detailed list of Manning's n values specifically fitted to 36 discrete cases of terrain material for 2-D coastal floodplains and urban areas (Makris et al. 2023). These values are set on the fine-resolution model's raster grid based on the terrain material derived from the 44 classes' inventory of the EU's CORINE Land Cover (CLC-2018) database (Copernicus Land Monitoring Service; available online: <https://land.copernicus.eu/pan-european/corine-land-cover>; accessed in March 2023). The main advantage of such a method for flood routing is the easy use of very fine spatial resolution ($dx = 2\text{-}5\text{ m}$ derived from Hellenic Cadastre's official DEM; see Section 2.2) computational domains based on raster grids (Horritt and Bates 2001; Hunter et al. 2007). The flood flow route is then estimated, based on the difference of hydraulic head between neighbouring cells, by a simplistic quad-tree search algorithm for downstream cells and saved in an updated matrix every timestep by a wet/dry cell storage module (Hunter et al. 2006; Makris et al. 2023). The time limit of computations is set when the farthest flooded area is reached, i.e., the simulations do not include the retreat of seawater from the inundated areas back to the marine environment.

Table S1 List of characteristic coastal inundation events due to storm surge (and/or compound flooding) in Greek littoral regions that were reported in journalistic mass and social media (in English or Greek) and assisted us to pinpoint the study areas (and aquatic basins) of Figure 1 (accessed on 21/06/2023). A characteristic storm for each area and the respective conditions (minimum pressure, winds, date) are also given. The weather conditions were derived from the automatic weather stations network of the National Observatory of Athens (Lagouvardos et al., 2017). A relevant literature list for each area is shown.

A/A	Study Area	Sub-region	Storm characteristics (date, min pressure, winds)	Relevant literature	Media Link reporting storm/flood events
1	Thermaikos	NW Aegean	06-10/09/2016 (1008 hPa, 12.5 m/sec)	Kapsimalis et al. (2005)	https://www.ecmwf.int/en/newsletter/150/news/flash-floods-over-greece-early-september-2016
2	Nestos	NE Aegean	26/01/2019 (995 hPa, 23.7 m/sec)	Skoulikaris et al. (2021)	https://www.pronews.gr/perivallon/746479_makedonia-thraki-megala-provlimata-apo-tis-plimmyres-yperheilise-o-nestos/
3	Alexandroupolis	NE Aegean	05/07/2019 (1004 hPa, 30.4 m/sec)	Poulos et al. (2022)	https://evrosonline.gr/zimies-apo-tin-kataigida-chthes-stin-ale/
4	Chios	SE Aegean	18-19/10/2010 (1003 hPa, 27.7 m/sec)	Krestenitis et al. (2011)	https://www.youtube.com/watch?v=UYGO3x0y20A&ab_channel=TheodorosKolydas
5	Ierapetra	E Cretan	15/10/2022 (1002 hPa, 31.7 m/sec)	Monioudi et al. (2014)	https://www.efas.eu/en/news/floods-greece-october-2022
6	Rethymno	N Cretan	10/11/2020 (1013 hPa, 32.2 m/sec)	Tsoukala et al. (2016)	https://www.youtube.com/watch?v=tnUOTQaE-1s
7	Pineios	NW Aegean	N/A	N/A	N/A
8	Agiokampos	NW Aegean	11/01/2022 (996 hPa, 15.6 m/sec)	N/A	https://www.mixanitouxronou.com.cy/epikerotita/o-keros-trelathike-plimmirise-o-agiokampos-sti-larisa/
9	Katerini	NW Aegean	01/12/2022 (1008 hPa, 10.3 m/sec)	Kombiadou et al. (2012)	https://www.youtube.com/watch?v=G_cESXRa5Q0&ab_channel=%CE%95%CE%A1%CE%A4%CE%91%CE%95
10	Kalamata	S Ionian	06-10/09/2016 (1007 hPa, 18.3 m/sec)	Martzikos et al. (2021)	https://www.dailymail.co.uk/news/article-3778130/It-total-destruction-Four-people-killed-Greek-floods-heavy-rain-batters-country-washes-cars-streets-Thermaikos-Kalamata-Sparta.html
11	Katakolo	S Ionian	18/09/2020 (1003 hPa, 13.9 m/sec)	Ferrarin et al. (2023)	https://edcm.edu.gr/images/docs/newsletters/Newsletter_20_2020_lanos.pdf

12	Laganas (Zakynthos)	S Ionian	25/01/2023 (N/A)	Stavropoulos et al. (2020)	https://www.youtube.com/watch?v=M_0cNZ2tEY
13	Manolada	S Ionian	15/10/2021 (998 hPa, 13.3 m/sec)	Diakakis et al. (2011)	https://europost.gr/kakokairia-mpallos-plimmyres-provlimata-se-oli-ti-chora-prognosi-kairoy/
14	Patra	S Ionian	29/09/2018 (987 hPa, 33.3 m/sec)	Tragaki et al. (2018)	https://www.keeptalkinggreece.com/2018/09/29/floods-medicane-zorbas-greece/
15	Argostoli (Kefalonia)	S Ionian	18/09/2020 (992 hPa, 25.3 m/sec)	Makris et al. (2023)	https://www.protothema.gr/greece/article/1049137/kefalonia-plimmurise-i-paraliaki-tou-argostoliou/
16	Livadi (Kefalonia)	S Ionian	18/09/2020 (992 hPa, 25.3 m/sec)	Ghionis et al. (2015)	https://www.enikos.gr/society/ianos-kefalonia-eikones-katastrofis-ston-karavomylo-kai-tin-agia/1467506/
17	Vassiliki (Lefkada)	N Ionian	18/09/2020 (1001 hPa, 23.3 m/sec)	Androulidakis et al. (2023)	https://www.youtube.com/watch?v=bUeFHvBdaOY&ab_channel=MyLefkada
18	Palairos	N Ionian	18/09/2020 (1001 hPa, 23.3 m/sec)	Androulidakis et al. (2023)	https://www.agrinionews.gr/kakokairia-ianos-krisimo-to-epomeno-9oro-poy-tha-chtypisei-okyklonas/
19	Preveza	N Ionian	30/11/2021 (999 hPa, 18.3 m/sec)	Makris et al. (2023)	https://www.newsit.gr/topikes-eidhseis/kakokairia-preveza-metraei-pliges-apo-plimmyres-kai-anemostrovilous/3419041/
20	Igoumenitsa	N Ionian	12/11/2017 (1002 hPa, 14.7 m/sec)	Kontogianni et al. (2012)	https://www.youtube.com/watch?v=IMyI5C05u1w&ab_channel=NIKOSFATSIOS

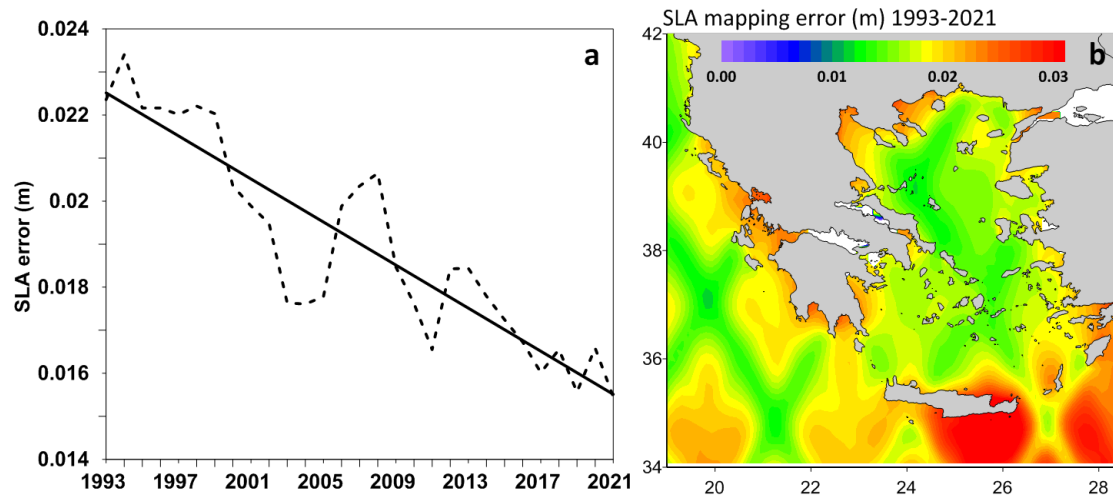


Figure S1 (a) Evolution of the mean annual SLA error, averaged over the AICS region over the 1993-2021 period. (b) Horizontal distribution of the SLA error, averaged over the 1993-2021 period.

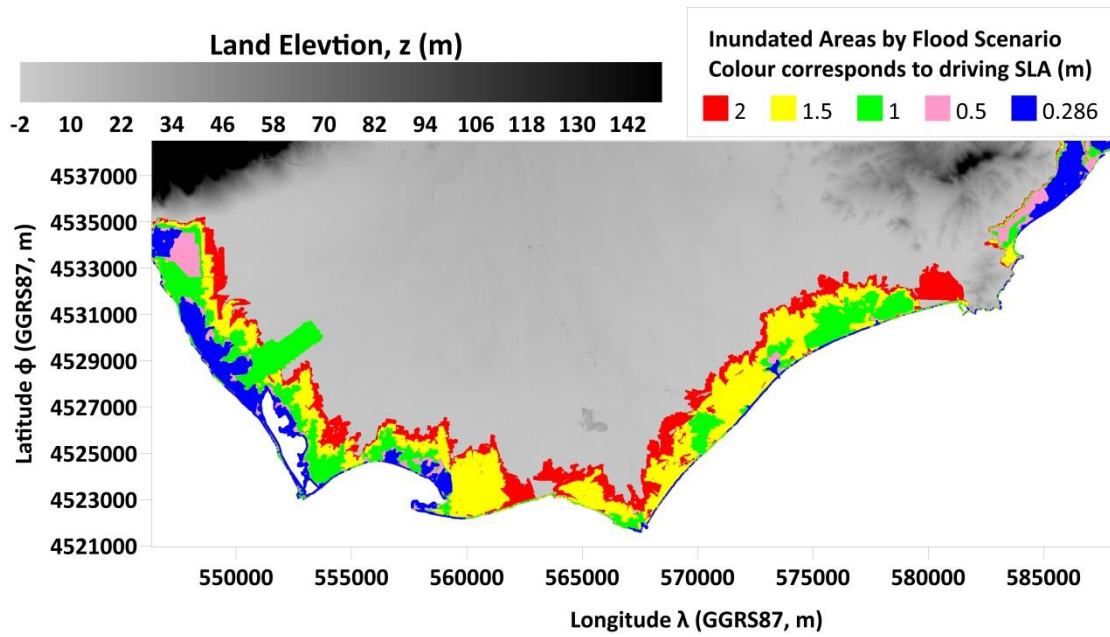


Figure S2 (a) Map of flooding coverage under the maximum Sea Level Anomaly (SLA) derived from the 1993-2021 period ($SLA_{max}=0.286$ m) and different SLA scenarios (0.5, 1, 1.5, 2 m) over Area 2 (Nestos).

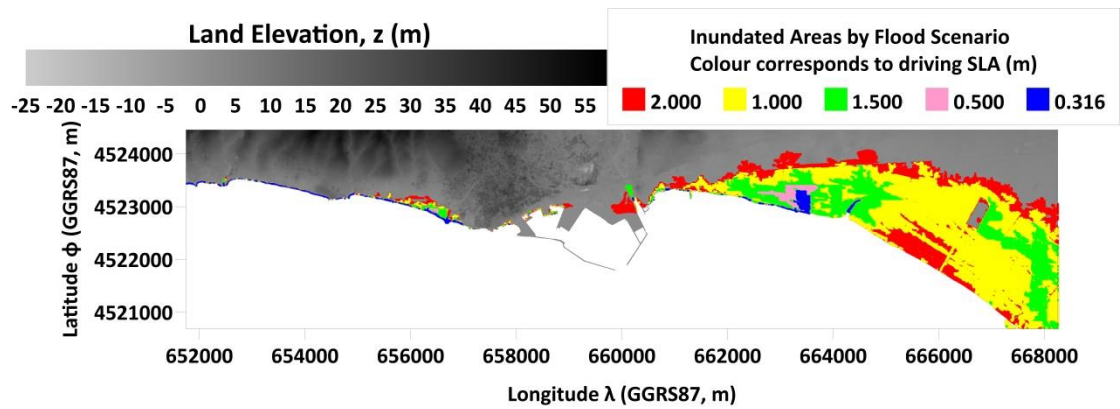


Figure S3 (a) Map of flooding coverage under the maximum Sea Level Anomaly (SLA) derived from the 1993-2021 period ($SLA_{max}=0.286$ m) and different SLA scenarios (0.5, 1, 1.5, 2 m) over Area 3 (Alexandroupolis).

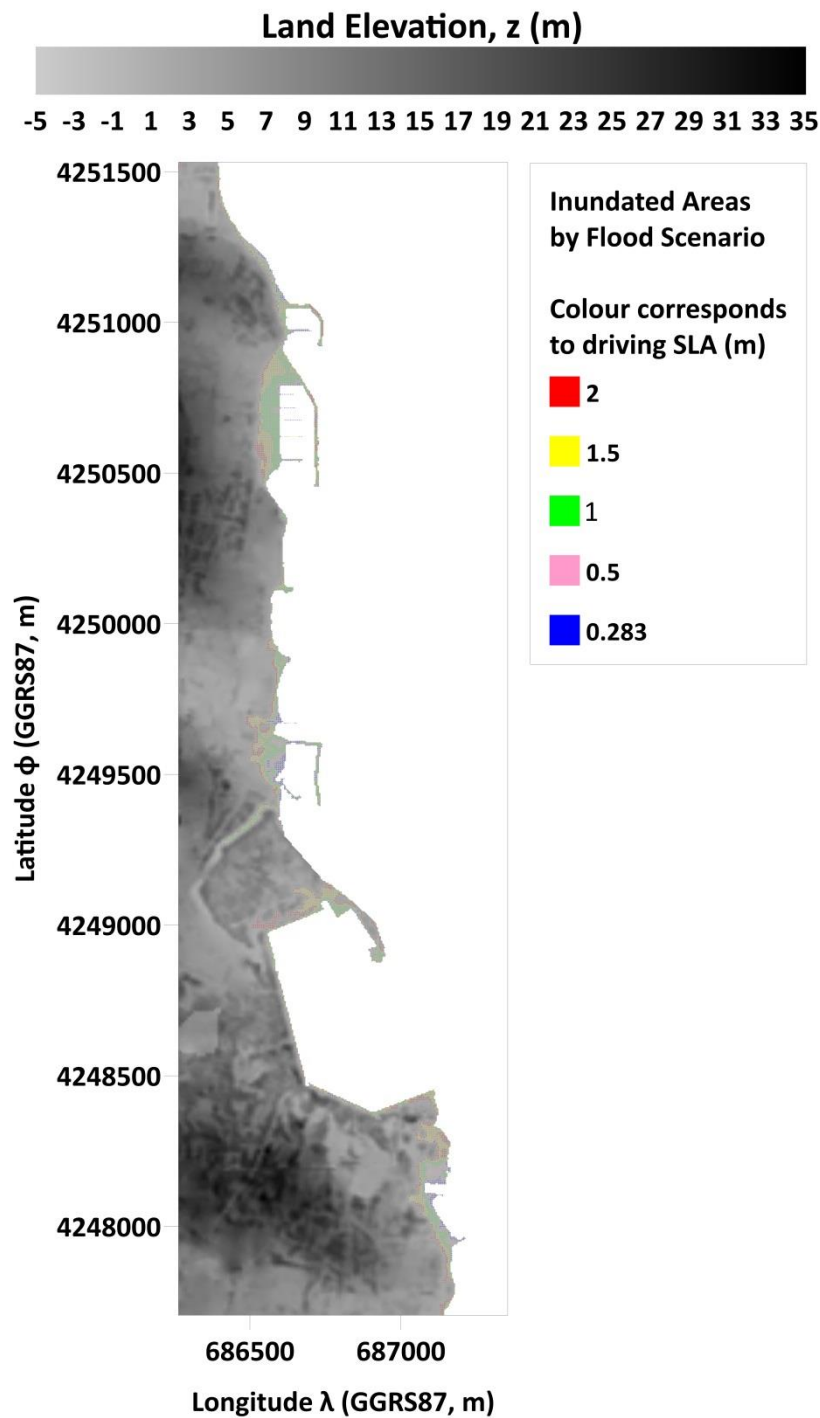


Figure S4 (a) Map of flooding coverage under the maximum Sea Level Anomaly (SLA) derived from the 1993-2021 period ($SLA_{max}=0.286$ m) and different SLA scenarios (0.5, 1, 1.5, 2 m) over Area 4 (Chios).

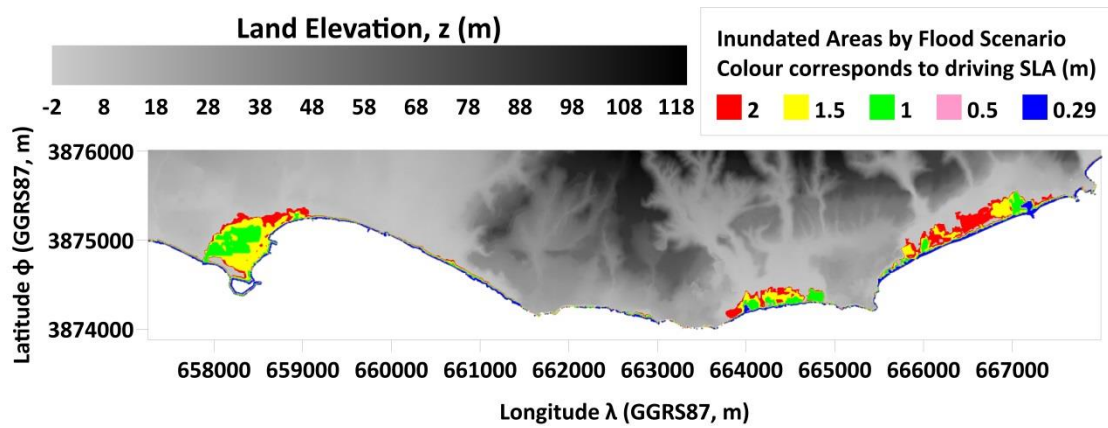


Figure S5 (a) Map of flooding coverage under the maximum Sea Level Anomaly (SLA) derived from the 1993-2021 period ($SLA_{max}=0.286$ m) and different SLA scenarios (0.5, 1, 1.5, 2 m) over Area 5 (Ierapetra).

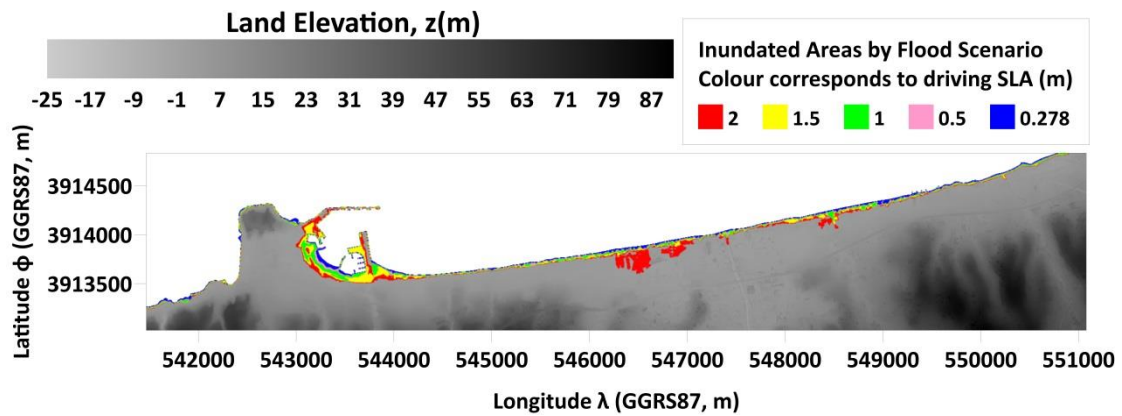


Figure S6 (a) Map of flooding coverage under the maximum Sea Level Anomaly (SLA) derived from the 1993-2021 period ($SLA_{max}=0.278$ m) and different SLA scenarios (0.5, 1, 1.5, 2 m) over Area 6 (Rethymno).

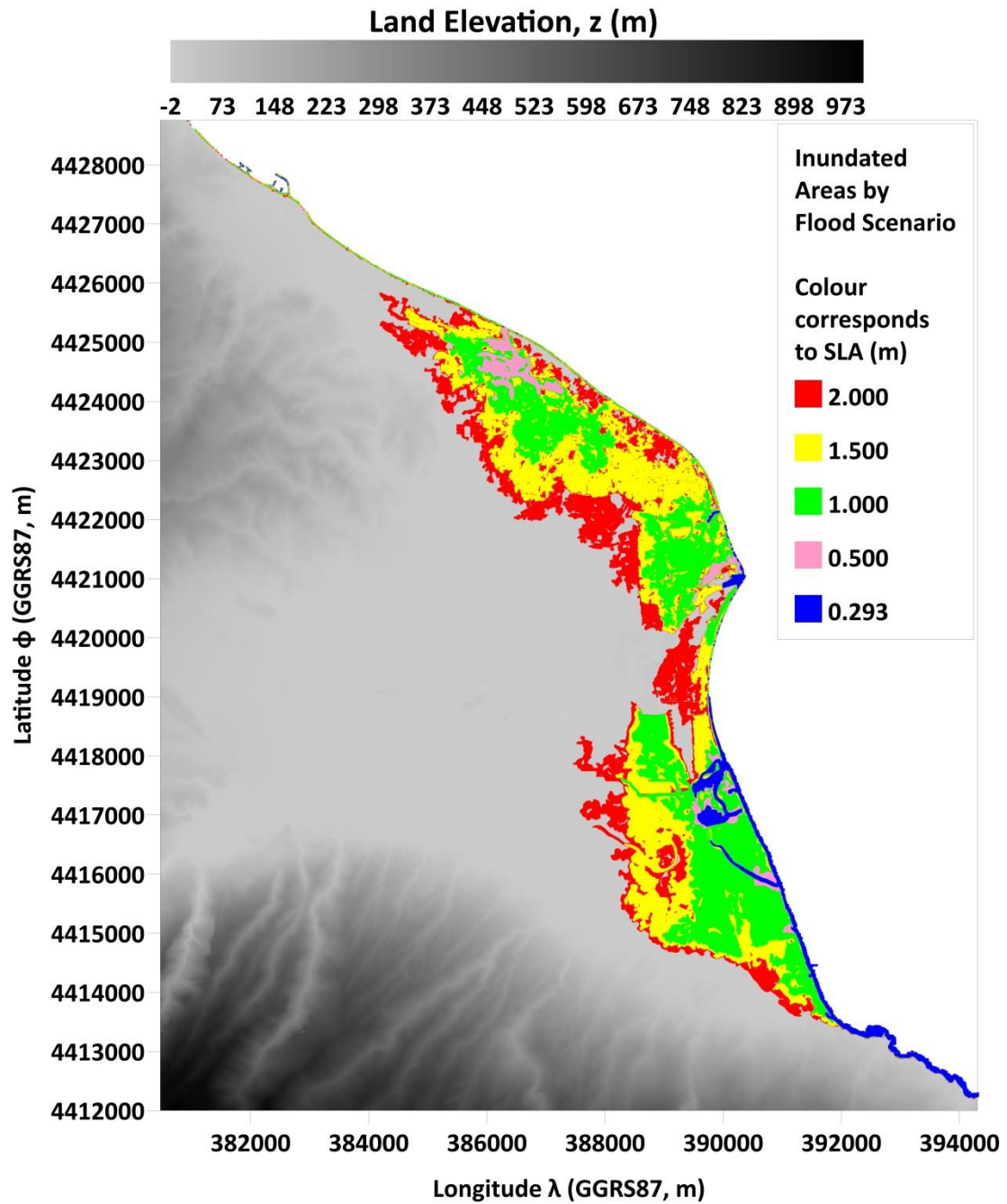


Figure S7 (a) Map of flooding coverage under the maximum Sea Level Anomaly (SLA) derived from the 1993-2021 period ($SLA_{max}=0.293$ m) and different SLA scenarios (0.5, 1, 1.5, 2 m) over Area 7 (Pineios).

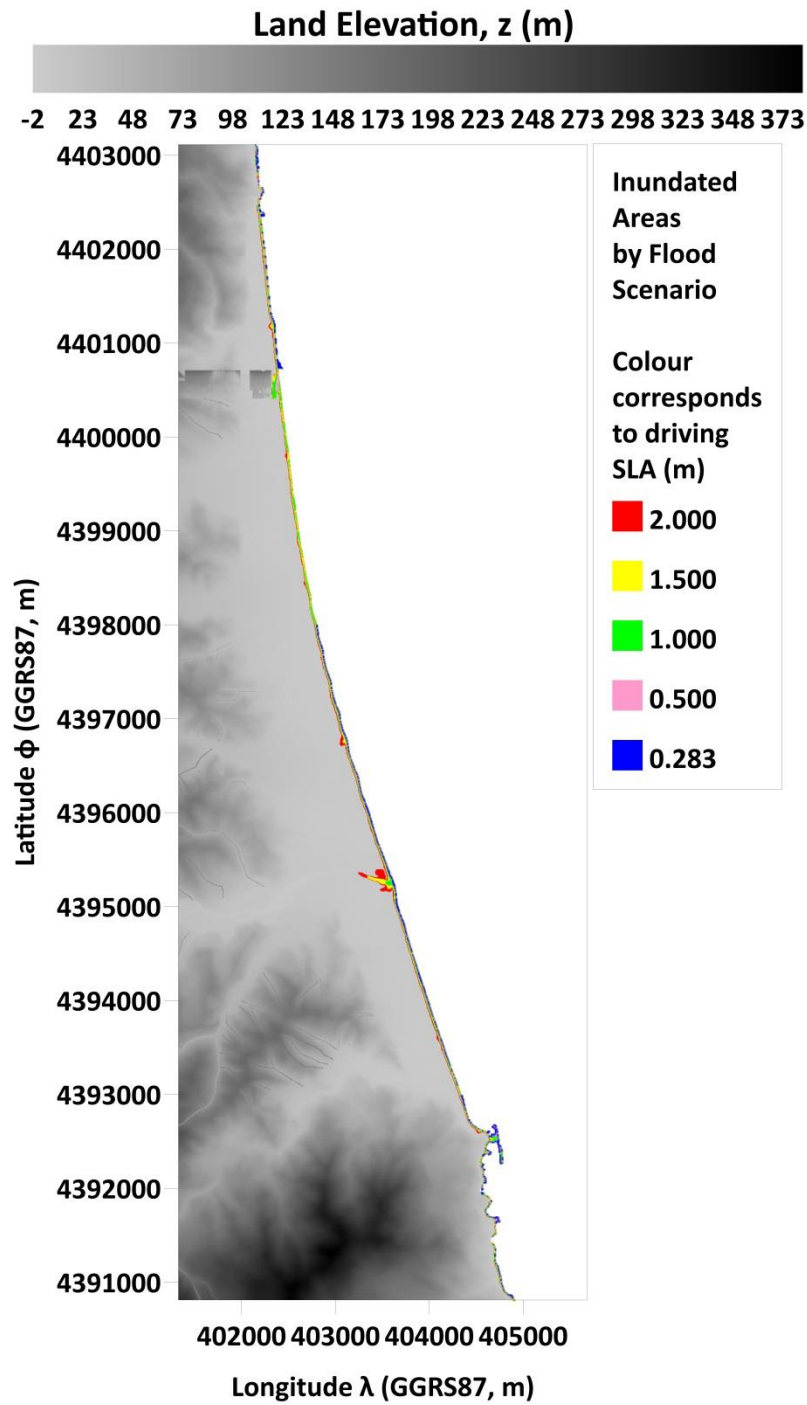


Figure S8 (a) Map of flooding coverage under the maximum Sea Level Anomaly (SLA) derived from the 1993-2021 period ($SLA_{max}=0.283$ m) and different SLA scenarios (0.5, 1, 1.5, 2 m) over Area 8 (Agiokampos).

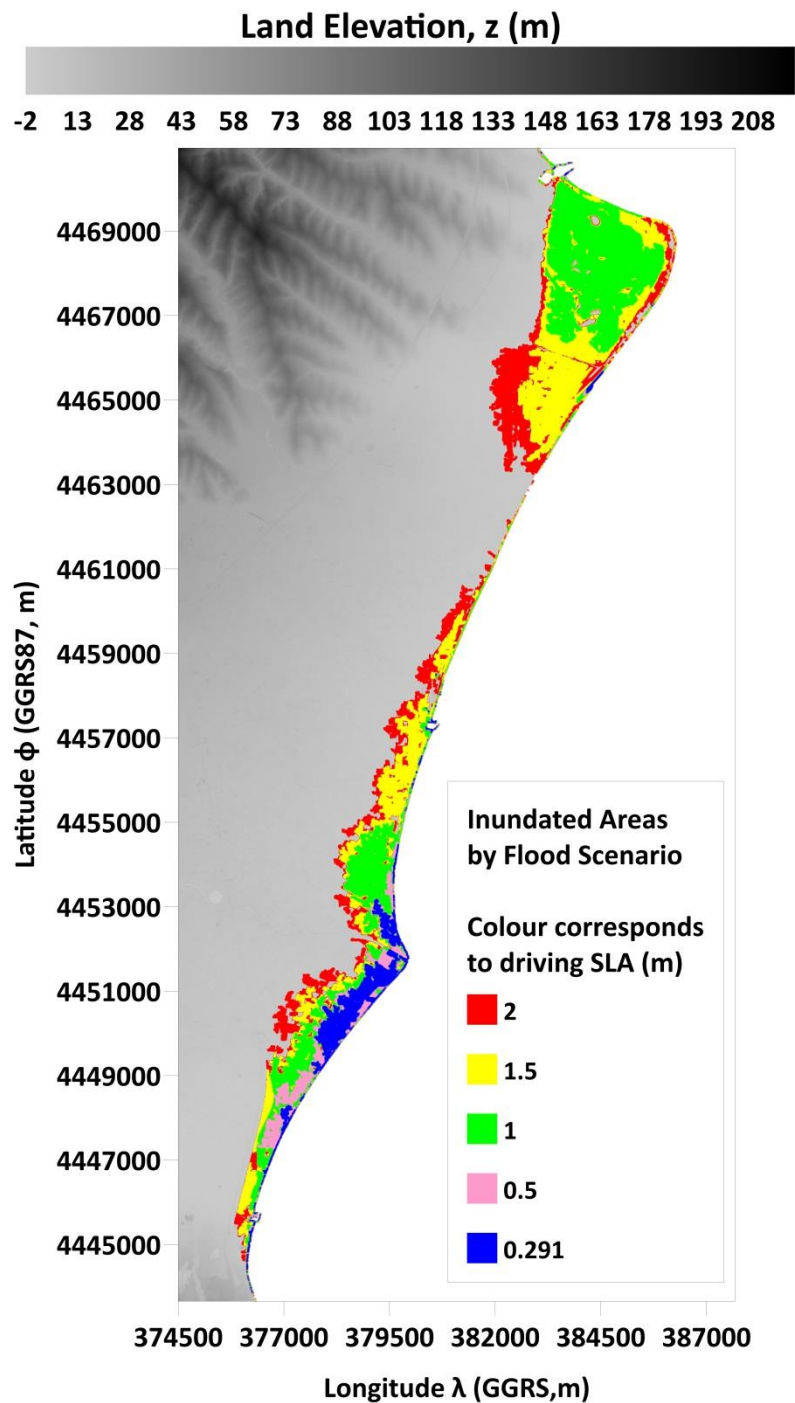


Figure S9 (a) Map of flooding coverage under the maximum Sea Level Anomaly (SLA) derived from the 1993-2021 period ($SLA_{max}=0.291$ m) and different SLA scenarios (0.5, 1, 1.5, 2 m) over Area 9 (Katerini).

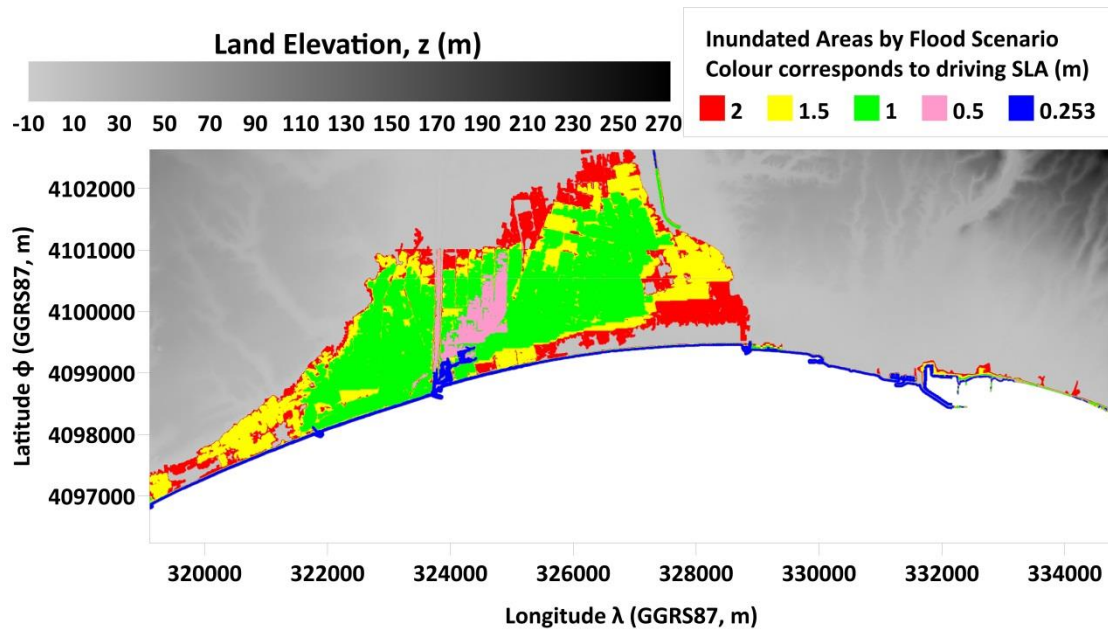


Figure S10 (a) Map of flooding coverage under the maximum Sea Level Anomaly (SLA) derived from the 1993-2021 period ($SLA_{max}=0.253$ m) and different SLA scenarios (0.5, 1, 1.5, 2 m) over Area 10 (Kalamata).

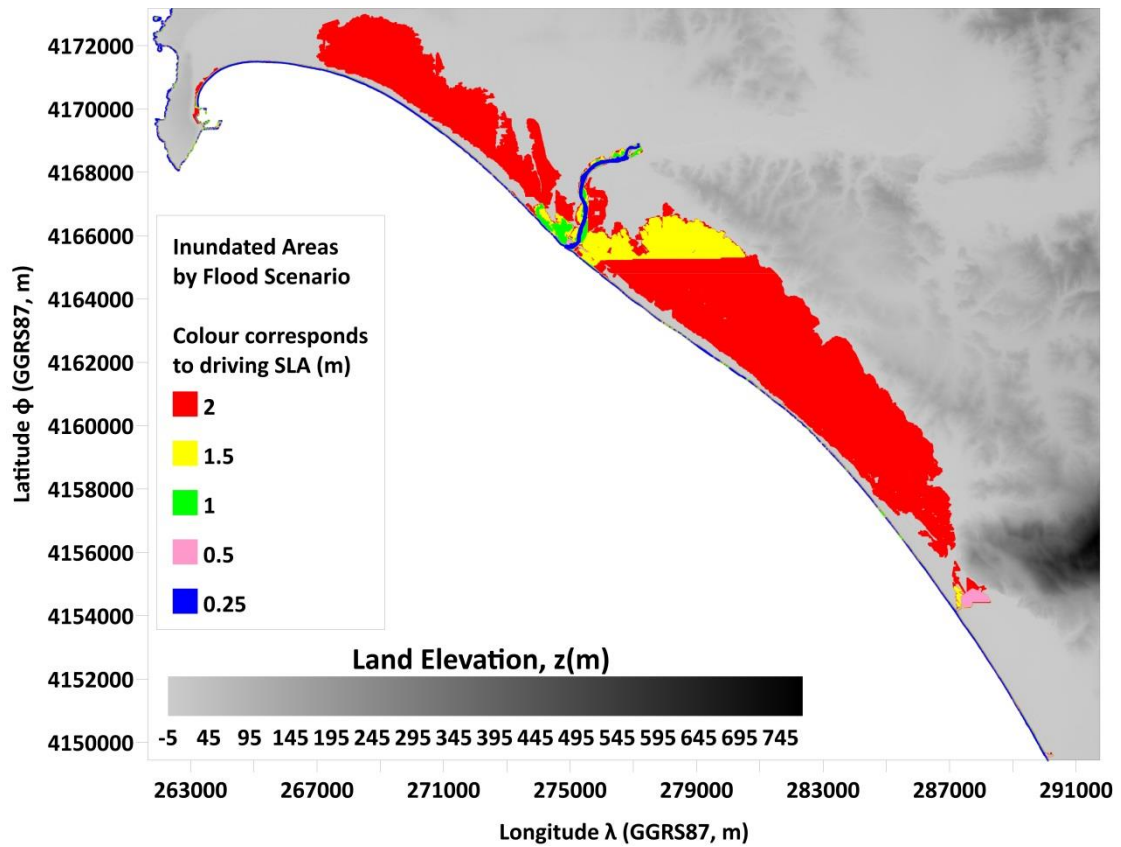


Figure S11 (a) Map of flooding coverage under the maximum Sea Level Anomaly (SLA) derived from the 1993-2021 period ($SLA_{max}=0.25$ m) and different SLA scenarios (0.5, 1, 1.5, 2 m) over Area 11 (Katakolo).

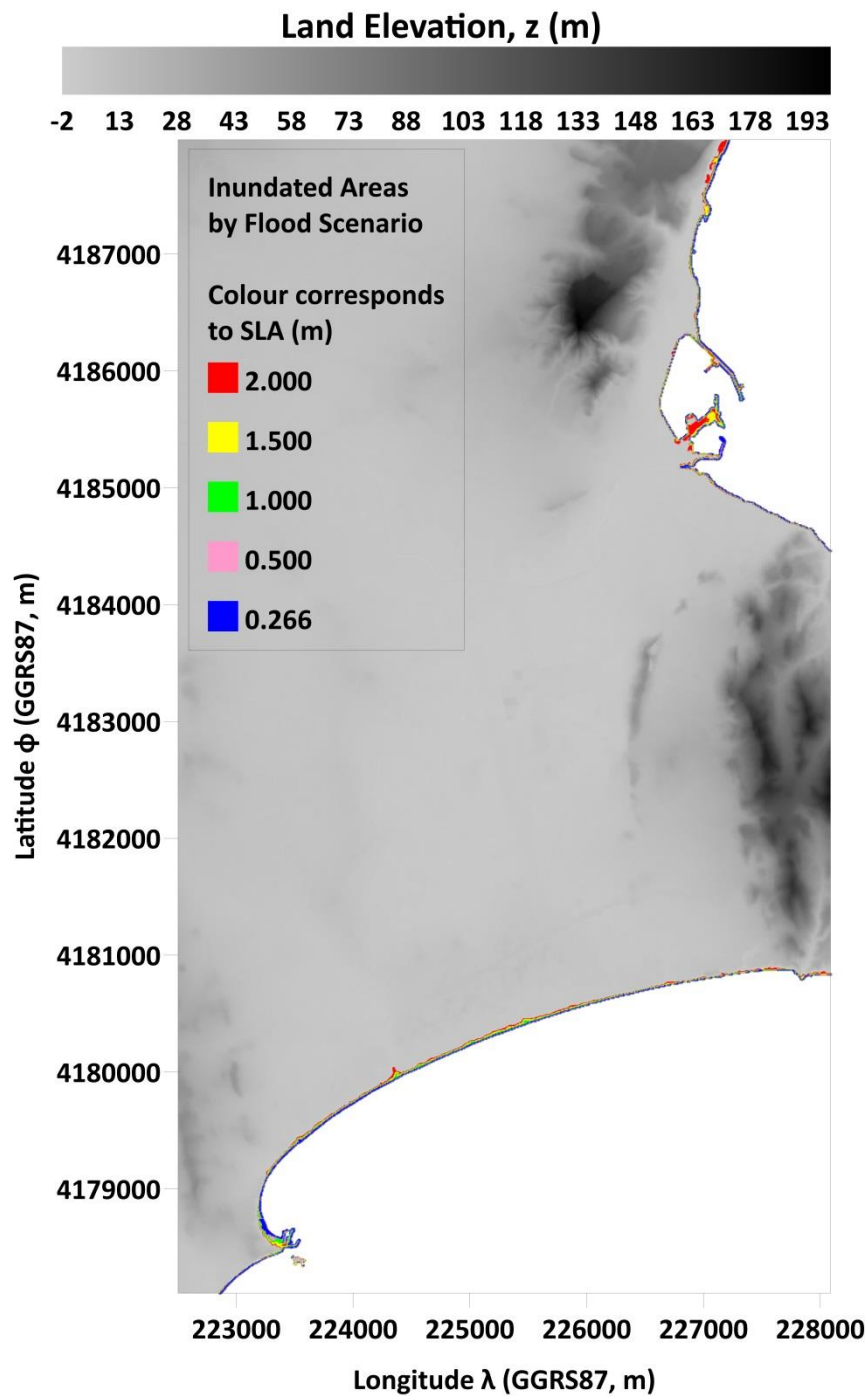


Figure S12 (a) Map of flooding coverage under the maximum Sea Level Anomaly (SLA) derived from the 1993-2021 period ($SLA_{max}=0.27$ m) and different SLA scenarios (0.5, 1, 1.5, 2 m) over Area 12 (Laganas).

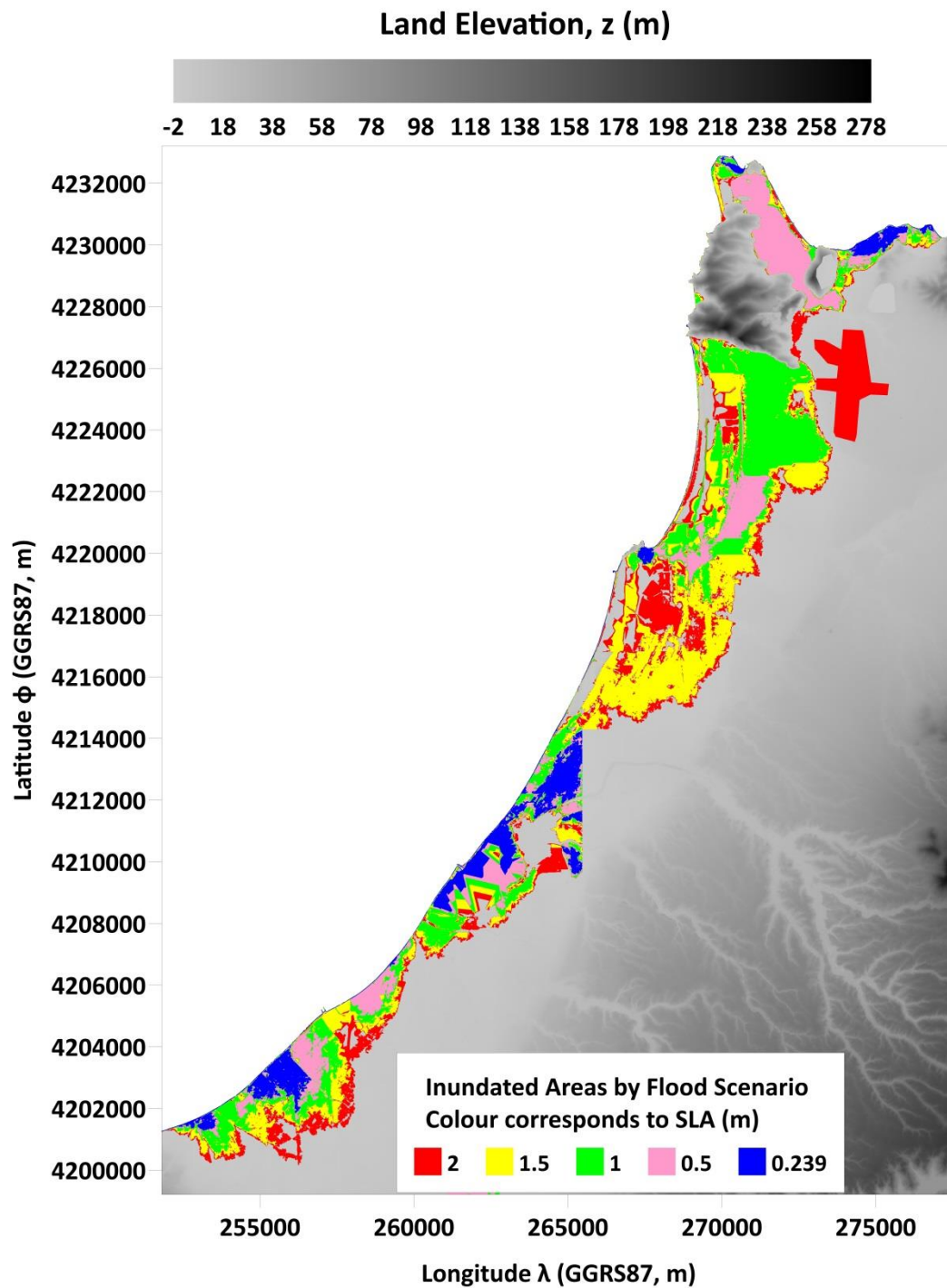


Figure S13 (a) Map of flooding coverage under the maximum Sea Level Anomaly (SLA) derived from the 1993-2021 period ($SLA_{max}=0.239$ m) and different SLA scenarios (0.5, 1, 1.5, 2 m) over Area 13 (Manolada).

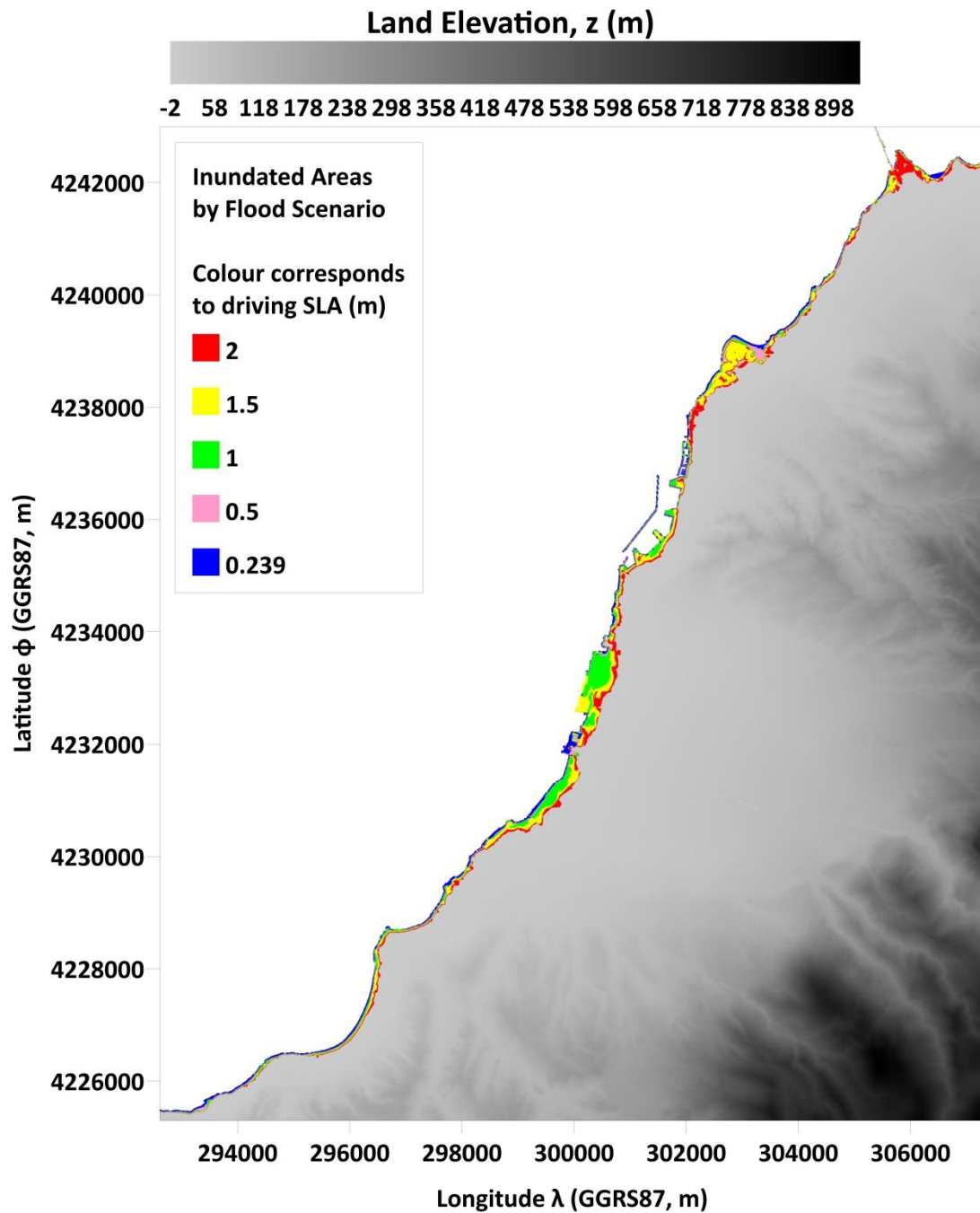


Figure S14 (a) Map of flooding coverage under the maximum Sea Level Anomaly (SLA) derived from the 1993-2021 period ($SLA_{max}=0.239$ m) and different SLA scenarios (0.5, 1, 1.5, 2 m) over Area 14 (Patra).

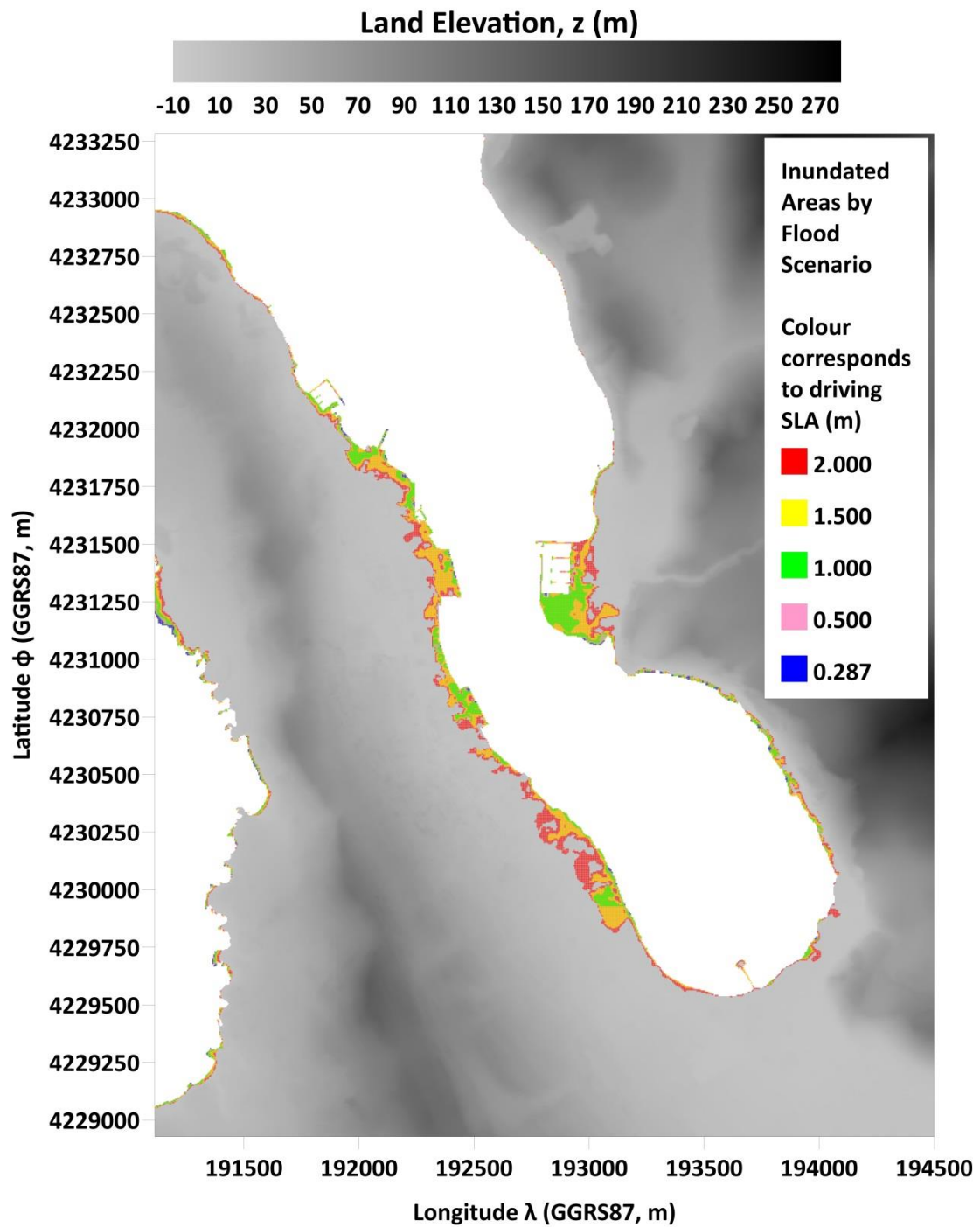


Figure S15 (a) Map of flooding coverage under the maximum Sea Level Anomaly (SLA) derived from the 1993-2021 period ($SLA_{max}=0.287$ m) and different SLA scenarios (0.5, 1, 1.5, 2 m) over Area 15 (Argostoli).

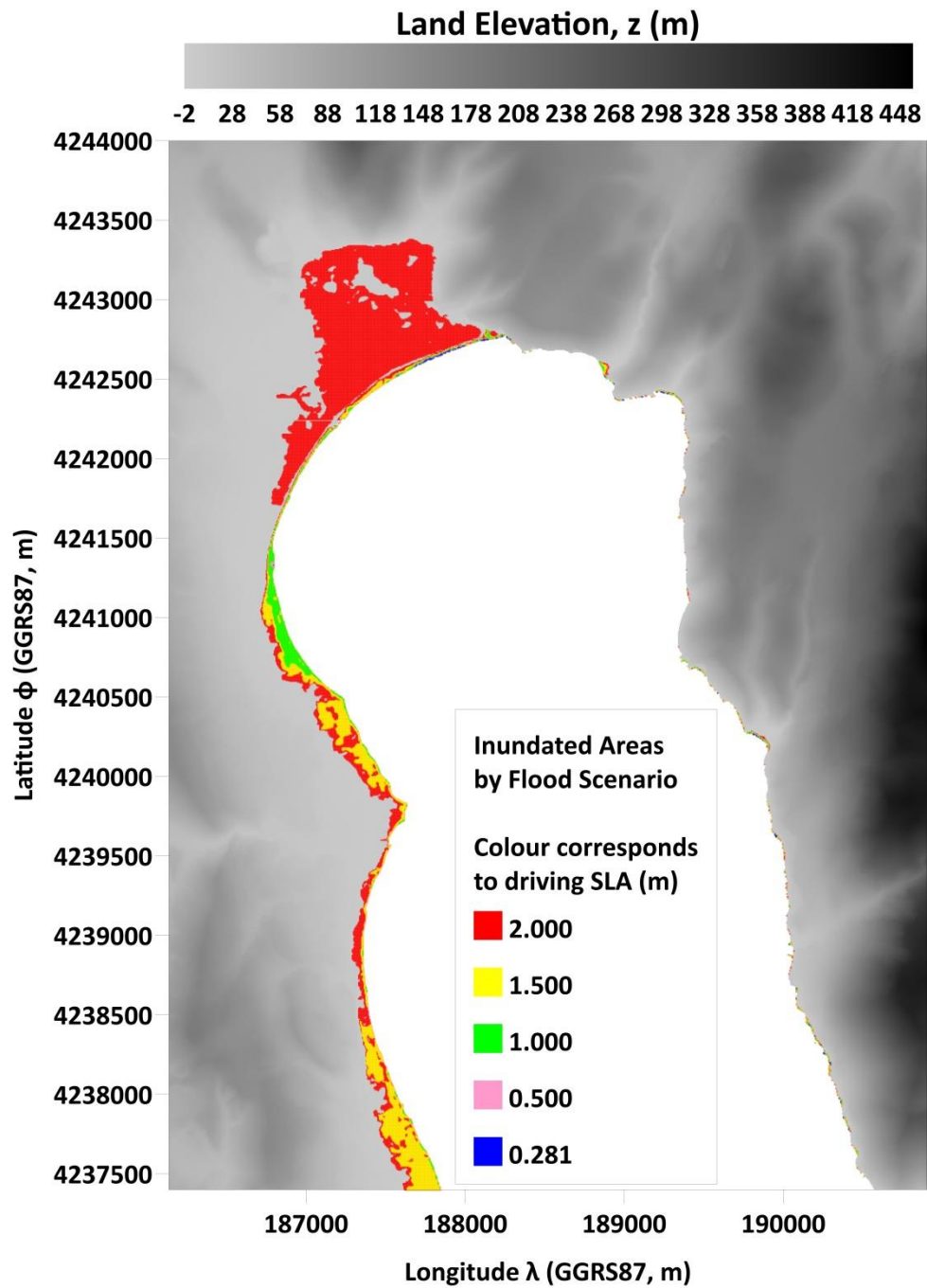


Figure S16 (a) Map of flooding coverage under the maximum Sea Level Anomaly (SLA) derived from the 1993-2021 period ($SLA_{max}=0.281$ m) and different SLA scenarios (0.5, 1, 1.5, 2 m) over Area 16 (Livadi).

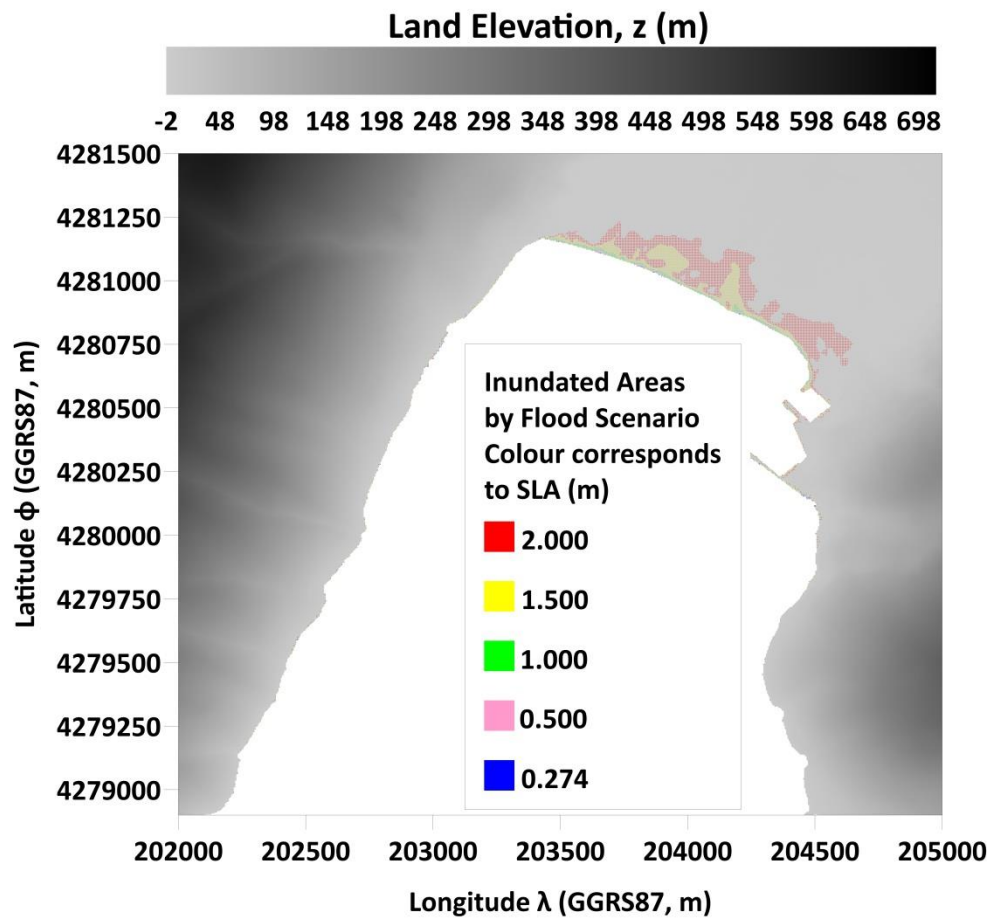


Figure S17 (a) Map of flooding coverage under the maximum Sea Level Anomaly (SLA) derived from the 1993-2021 period ($SLA_{max}=0.274$ m) and different SLA scenarios (0.5, 1, 1.5, 2 m) over Area 17 (Vassiliki).

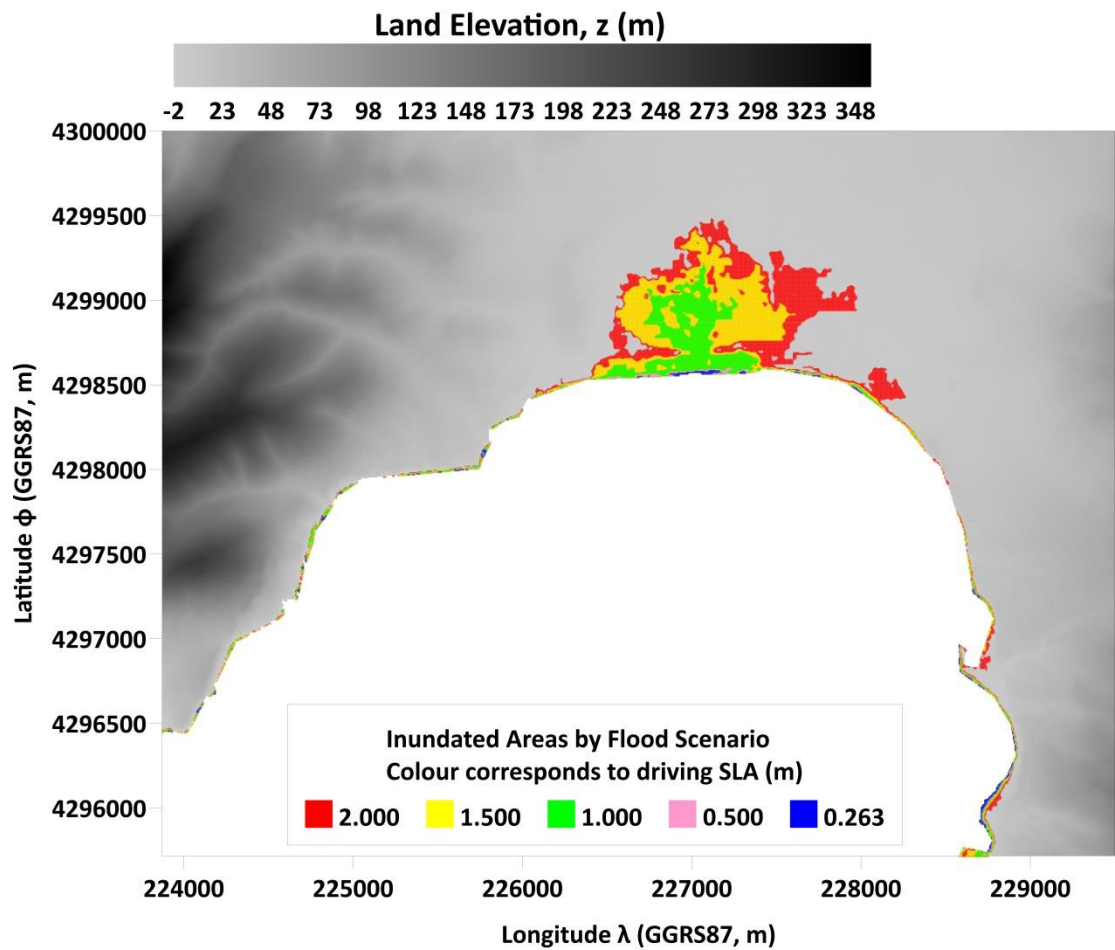
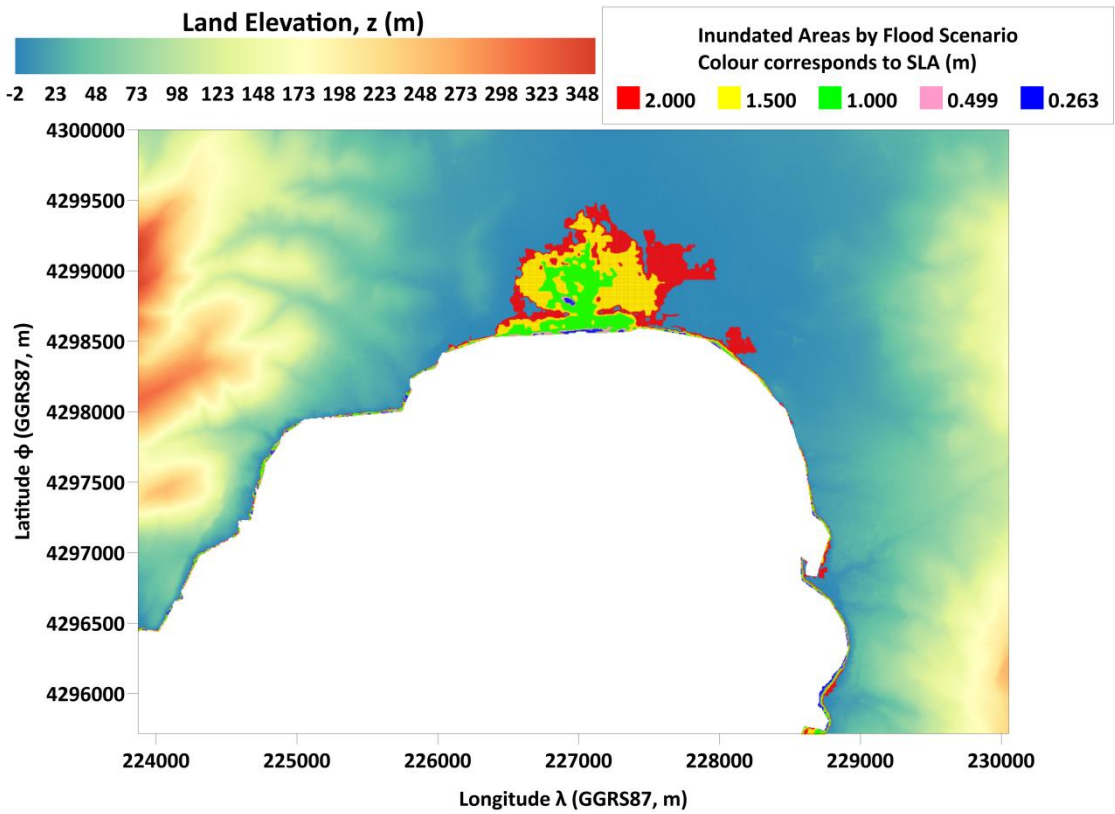


Figure S18 (a) Map of flooding coverage under the maximum Sea Level Anomaly (SLA) derived from the 1993-2021 period ($SLA_{max}=0.263$ m) and different SLA scenarios (0.5, 1, 1.5, 2 m) over Area 18 (Palairos).

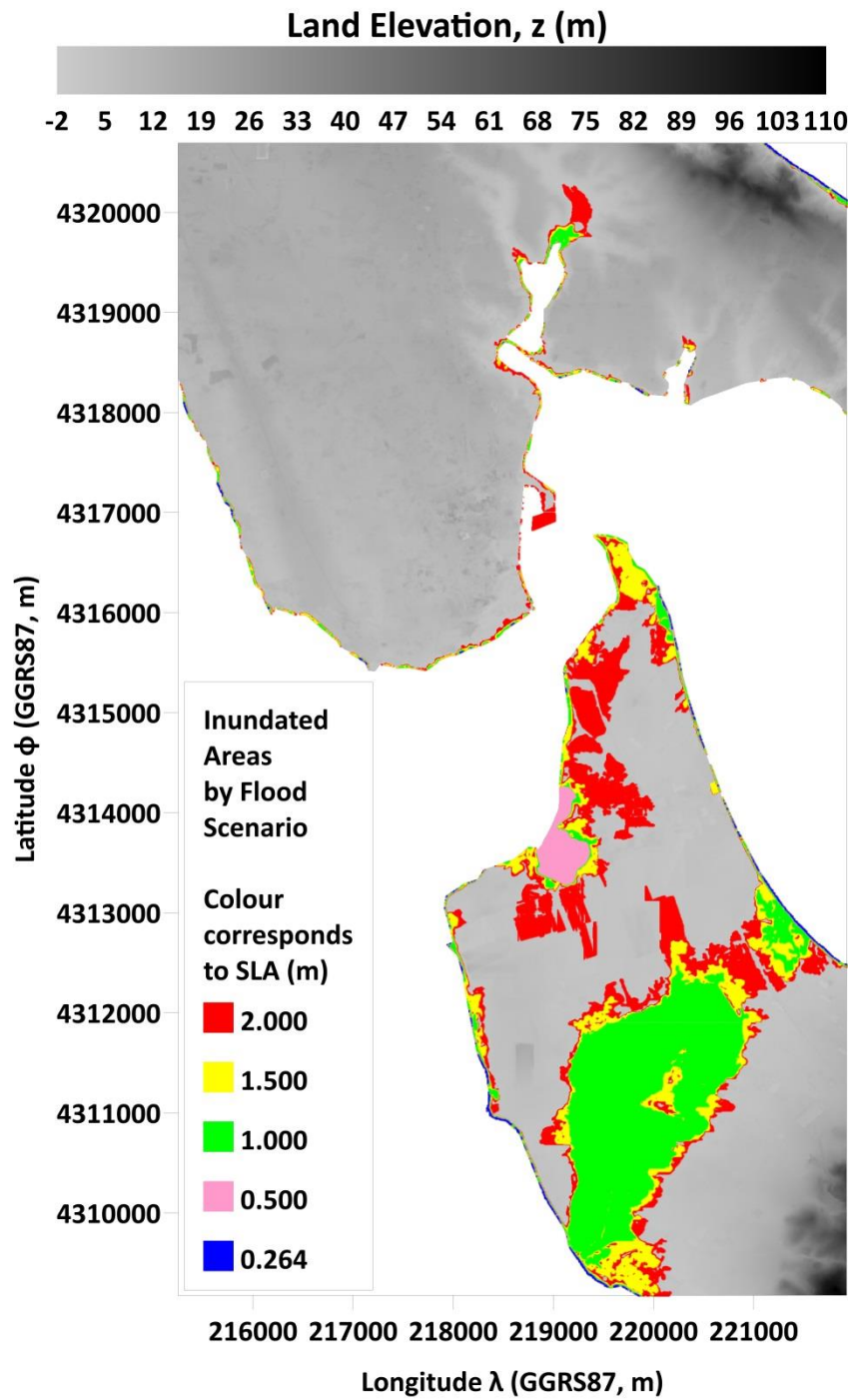


Figure S19 (a) Map of flooding coverage under the maximum Sea Level Anomaly (SLA) derived from the 1993-2021 period ($SLA_{max}=0.264$ m) and different SLA scenarios (0.5, 1, 1.5, 2 m) over Area 19 (Preveza).

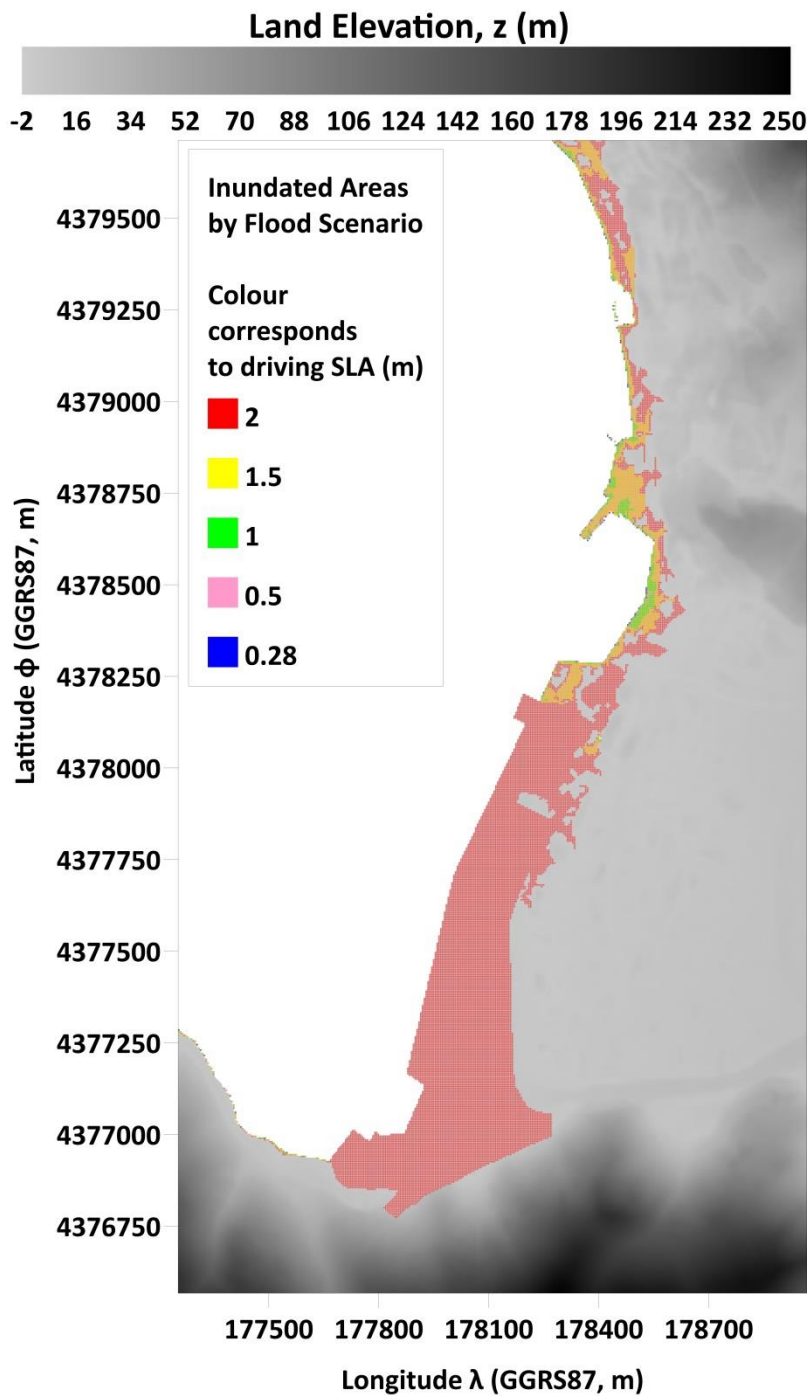


Figure S20 (a) Map of flooding coverage under the maximum Sea Level Anomaly (SLA) derived from the 1993-2021 period ($SLA_{max}=0.28$ m) and different SLA scenarios (0.5, 1, 1.5, 2 m) over Area 20 (Igoumenitsa).